NASA CR-112207

RESIDUAL STRESS ALLEVIATION OF AIRCRAFT METAL STRUCTURES REINFORCED WITH FILAMENTARY COMPOSITES

By. J. B. Kelly and R. R. June

January 1973

D6-60136-4

Prepared under contract NAS1-8858 by
THE BOEING COMMERCIAL AIRPLANE COMPANY
Seattle, Washington

for

Langley Research Center
NATIONAL AERONAUTICS AND SPACE ADMINISTRATION

DISCLAIMER NOTICE

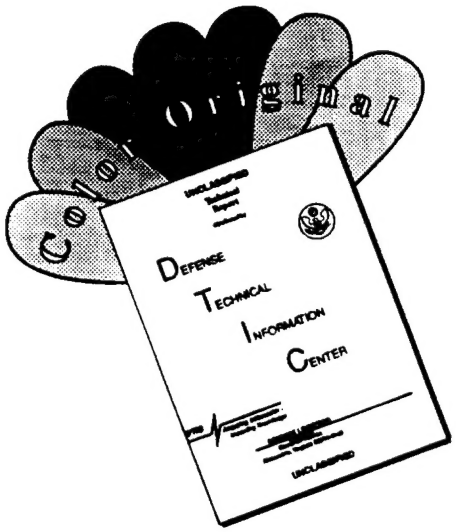

THIS DOCUMENT IS BEST QUALITY AVAILABLE. THE COPY FURNISHED TO DTIC CONTAINED A SIGNIFICANT NUMBER OF COLOR PAGES WHICH DO NOT REPRODUCE LEGIBLY ON BLACK AND WHITE MICROFICHE.

NASA CR-112207

RESIDUAL STRESS ALLEVIATION OF AIRCRAFT METAL STRUCTURES REINFORCED WITH FILAMENTARY COMPOSITES

By. J. B. Kelly and R. R. June

January 1973

D6-60136-4

Prepared under contract NAS1-8858 by
THE BOEING COMMERCIAL AIRPLANE COMPANY
Seattle, Washington

for

Langley Research Center
NATIONAL AERONAUTICS AND SPACE ADMINISTRATION

FOREWORD

This report was prepared by The Boeing Commercial Airplane Company under NASA contract NAS1-8858 (modification 10) and covers the work performed during the period of July 1971 through March 1972. The contract is being administered under the direction of Mr. R. A. Pride, head of the Composites Section, Materials Application Branch, NASA Langley Research Center.

The authors wish to acknowledge the contribution of R. N. Curran, of the Manufacturing Research and Development department of Boeing.

CONTENTS

TABLES

FIGURES

FIGURES (Concluded)

RESIDUAL STRESS ALLEVIATION OF AIRCRAFT METAL STRUCTURES REINFORCED WITH FILAMENTARY COMPOSITES

By J. B. Kelly and R. R. June

The Boeing Commercial Airplane Company

SUMMARY

Residual stresses occur in composite-reinforced metal structures as a result of the elevated temperatures employed to cure various structural adhesives and the differing coefficients of thermal expansion of the materials being bonded. Methods to eliminate or reduce residual stresses were explored during this program.

Residual stress level reductions were achieved in this program by modifying the manufacturing procedures used during adhesive bonding. The residual stress alleviation techniques involved various forms of mechanical constraint which were applied to the components during bonding. Nine methods were evaluated, covering a wide range in complexity. Some specimens were assembled with no tooling, while others employed complex tooling capable of generating preloads.

All methods investigated during this program affected the residual stress level. In general, residual stresses were reduced by 70% or more from the stress level produced by conventional adhesive bonding procedures. The most effective method used during this study employed a steel tool capable of loading the metal component in compression prior to the bonding cycle. The other methods were slightly less effective due to the presence of elastic deformations in the vicinity of mechanical fasteners. The bonded load transfer region between the fibers and the stepped titanium load transfer fittings experiences creep deformation which can lead to delamination at the higher bonding temperatures (450° K, 350° F) and high shear stress levels produced by some assembly techniques.

Compression creep deformation of 7075-T6 and 7178-T6 aluminum components was consistently observed when these elements were heated to 450° K during the cure cycle which established the adhesive bond. The 7178-T6 aluminum alloy apparently experiences more creep deformation than 7075-T6 at comparable stress levels. Creep deformation of aluminum at the cure temperature is an important consideration in development of residual stress alleviation techniques.

Developmental work is recommended to define the optimum stress-free temperature for subsonic airplane applications and the cost effectiveness of these methods. The methods examined in this study require scale-up to the production environment. Studies to define the creep behavior of the constituent materials and the effect of creep deformation on component strength and life are suggested.

INTRODUCTION

The weight saving potential of advanced-composite-reinforced metallic structural elements was explored during phases I, II, and III of NASA contract NAS1-8858, and the results are reported in references 1, 2, and 3. The structural concepts examined during these studies employed boron fibers supported in a polymeric matrix and adhesively bonded to aluminum and titanium metal details. During phase I of this program the occurrence of thermally induced residual stresses in the bonded assemblies was demonstrated.

Residual stresses occur when conventional elevated-temperature adhesive bonding procedures are employed and the materials being joined have unequal coefficients of thermal expansion. Elevated-temperature curing adhesives are commonly used to produce structurally satisfactory bonded assemblies. Typical curing temperatures are 394° K (250° F) and 450° K. The residual stresses occur because components of the assembly are brought together at room temperature, enclosed in a vacuum bag, and heated to the curing temperature in an oven or autoclave. During the heating process, thermal growth of each component proceeds without restriction. If the coefficients of linear thermal expansion are different, differing amounts of thermal growth occur. At the curing temperature the bond between the components is established. This, in general, becomes the "stress-free" temperature since the components were unstressed when the bonding occurred. Any subsequent temperature change, such as cooling to room temperature, will induce thermal stress since the components are mutually restrained from expanding or contracting at their individual rates. The residual stress level induced in this manner is a function of cross-sectional area, modulus of elasticity, and coefficient of thermal expansion of the components and the temperature change from the stress-free temperature.

Investigation suggested by NASA indicated that the stress-free temperature and, hence, the residual stresses could be altered through suitable modification of the manufacturing procedures used during the adhesive bonding process. This program was initiated to evaluate the potential capability to control the stress-free temperature and to explore several approaches to achieve this control.

SYMBOLS

The units used for physical quantities defined in this report are given in both the international system of units (SI) and in U.S. customary units.

A	area, square meters (square inches)
c	subscript designating composite
E	modulus of elasticity, Newtons per square meter (pounds force per square inch)
L	length, meters (inches)
m	subscript designating metal
SFT	stress-free temperature, degrees Kelvin (degrees Fahrenheit)
T	temperature, degrees Kelvin (degrees Fahrenheit)
t	thickness, meters (inches)
α	coefficient of linear thermal expansion, per degree Kelvin (per degree Fahrenheit)
ϵ	strain
σ	normal stress, Newtons per square meter (pounds force per square inch)

PROGRAM SCOPE

The residual stress alleviation techniques which were evaluated in this study involved various forms of mechanical constraint applied to the components during the adhesive bonding process. These constraints were selected to provide stress distributions which, when combined with the stress distribution that occurs due to the temperature change from bonding temperature to the desired stress-free temperatures, produce zero net stress.

A variety of manufacturing procedures may be postulated to develop the required stress distributions during the bonding process. Nine methods were examined during this study, as summarized in table 1. They range from the simplest concept, wherein the two components are mechanically fastened together at the desired stress-free temperature and subsequently bonded, to the more difficult concepts which require preloading one or both components to specified stress levels prior to the bonding process. The practical considerations of manufacturing ease and reproducibility are the major distinctions between methods.

To explore and demonstrate the concepts and methods, 46 metal-composite assemblies were fabricated. Hat and zee section stiffeners and flat sheets were reinforced with precured unidirectional composite details of boron- and graphite-epoxy. Only one of the manufacturing methods studied (method 4 of table 1) is suitable for co-cured reinforced assemblies, where matrix cure and the bond to the metal component are effected simultaneously. Specimen configurations are shown schematically in figures 1 and 2, and design parameters are given in table 2. Adhesive systems employed in this study were cured at 394° K and 450° K. Design stress-free temperatures were 272°, 294°, 339°, and 394° K (30°, 70°, 150°, and 250° F). Materials employed during this program are listed in appendix A. No material property measurements were made as a part of this study. The properties employed in the calculations are summarized in table 3.

Panel assemblies as shown in figure 3 were fabricated from completed details described above. These assemblies were made to determine the effect of subsequent bonding cycles on details which had stress-free temperatures differing from the secondary bonding temperature.

RESULTS

The stress alleviation techniques employed during the program required that the composite, the metal, or both components of the assemblies be stressed while the adhesive bonds were established. The component coefficients of thermal expansion were such that the composite details were stressed in tension and the metal details were stressed in compression to achieve a stress-free temperature lower than the bonding temperature. The magnitude of these stresses depends, in part, on the ratio of cross-sectional areas of the constituents, called area ratio.

Program results are summarized in figure 4, which shows the achieved reduction in residual thermal stress for the range of area ratios studied. Stress reduction is expressed as a percentage of the desired stress reduction, and area ratio is defined as the ratio of composite cross-sectional area to total cross-sectional area. Composite properties are normalized to 50% volume fraction (fiber area/composite area).

For most of the specimens, the residual stress was reduced by 70%, or more, from the stress level which would have occurred if no stress alleviation had been performed (fig. 4). The measured residual stresses of two specimens were substantially different from the objective stress levels, as shown in figure 4, where 171% and 198% of desired stress reduction was achieved. These specimens were designed to be stress free at 394° K after curing at 450° K. The method employed (method 7 of table 1) required a limited amount of free thermal expansion to occur prior to restraint of the metal component. This free thermal growth was prohibited, possibly by friction forces from the bolt pressure, resulting in excessive constraint which lowered the stress-free temperature to less than the design value. This method was used only for these two specimens and indicates that modifications to the method are required to obtain desired performance.

The results obtained with the nine assembly methods are summarized in figure 5. For each assembly method, the average achieved residual stress reduction is shown.

Program results are shown in further detail in figures 6 through 20, where specimen residual stress may be compared to the residual stress which would have been obtained had no stress alleviation been attempted. Data points are identified by specimen number, and specimen configuration details may be found in table 2. All results have been adjusted to reflect conditions at the design stress-free temperatures. Completely successful specimens would therefore have zero stress.

The results shown in figures 4 through 20 exclude eight of the 46 specimens fabricated during this program. Static failures were observed in these eight specimens. Six of these failures occurred at the bonded interface between the fibers and the stepped titanium load transfer region, which was employed on all composite components. Five of the six failures occurred during cure cycles at 450° K, and in all cases, load transfer region shear stress at the bonded fiber-to-titanium interface was 2.97 MN/m^2 (430 psi) or higher at the time of failure. One of these failures was caused by local deformation of both the metal and the composite components as a result of a tooling error.

One of the strap-reinforced skin panels failed because a group of tool pins used during preloading was inadvertently left in the assembly during curing. The tool pins were adequate for their intended use at room temperature, but due to the increased loads during the cure cycle the aluminum skin failed in bearing.

One zee section specimen failed during the bonding cycle due to buckling loads. The aluminum zee was preloaded to a level well in excess of its column buckling load, and was stabilized by a centrally located support attached to the tool. Due to the reduction of physical properties as the temperature was increased during the bond cycle (450° K for this assembly) the supported flange yielded, apparently allowing some buckling deflection. This failure emphasizes the need to provide adequate stabilizing elements in the design of tools.

Compression creep of the aluminum component was consistently observed in those specimens which were cured at 450° K. These results are summarized in figures 21 and 22, which show creep deformation as a function of predicted compression stress level during the bond cycle. Comparison of the figures indicates that 7178-T6 aluminum experiences more creep deformation than 7075-T6 aluminum at comparable stress levels. Since these results were rather unexpected and were inferred from measurements taken from composite-reinforced specimens, two additional tests were performed.

To demonstrate creep deformation, one specimen of each alloy was confined in a tool, simulating assembly method 4 of table 1, and subjected to a curing cycle which duplicated the 450° K bonding cycle conditions. The observed creep deformation from these tests is shown in figures 21 and 22. The results substantiate the analysis method employed and the conclusion that appreciable deformation occurs. No creep deformation trend was observed for specimens exposed to the 394° K cure cycle.

Bond line failures were observed in two of the three panel assemblies fabricated. Components for these assemblies, consisting of hat and zee sections and sheets, were reinforced by several of the methods listed in table 1. The reinforced components were then joined by secondary bond cycles. The assembly methods were selected to avoid protecting the previously established bond lines. Since the secondary bond was established at a temperature above the component stress-free temperature, shear stresses were thermally induced in the composite-to-metal bond lines.

Both of the observed failures occurred in panel assemblies designed to be stress free at room temperature. One panel employed components which were initially cured at 394° K, with subsequent panel assembly accomplished at the same temperature. During this assembly, the composite reinforcement on both zee stiffeners delaminated at the composite-to-metal interface, as shown in figure 23. The second observed failure, shown in figure 24, was a panel which was cured at 394° K from components which were cured at 450° K. The failure mode was quite different in that only one of the stiffener reinforcement elements failed and this failure was on the titanium stepped load transfer fitting shear plane, rather than on the composite-to-metal stiffener shear plane. It is likely that this failure initiated during the stiffener cure cycle and that the second, lower temperature, cure cycle merely enlarged the failed area, making it more visible.

The third panel assembly, which was successfully completed, was cured at 394° K from components which were bonded at 450° K. However, the design stress-free temperature was 339° K and, therefore, the stress level experienced by the established bond lines during the secondary cure cycle was somewhat lower than in the panels which failed.

DISCUSSION

As was shown in the preceding sections, most assembly methods were useful in reducing residual thermal stress. Some methods were found to be slightly more successful than others. Additionally, some methods appear more readily introduced into a production situation than others. In the following section, the manufacturing procedures will be described and the measurement and analysis techniques will be presented.

Specimen Fabrication

All composite details employed in this program were of unidirectional orientation. To minimize manufacturing cost a building block approach was selected. Four- and five-ply-thick sheets of graphite and boron, respectively, were laminated using a tape layup machine, as shown in figure 25. Because mechanical fasteners were to be employed in some manufacturing methods, titanium load transfer fittings with chemically milled steps were used to provide an adequate fastening area and a proven load introduction path for the fibers. The cured thickness of one ply of graphite-epoxy tape is approximately 0.203 mm (0.008 in.), while one ply of boron-epoxy tape is 0.140 mm (0.0055 in.). This difference in lamina thickness required the use of the two titanium fitting designs shown in figure 26. The four-ply graphite-epoxy and five-ply boron-epoxy building blocks had very nearly equal fiber area at a central cross section.

The laminated sheets were cured according to the material supplier's recommended cure cycle and then machined into strips of the desired width, depending on specimen type (see figs. 1, 2, and 3). The area of the reinforcement, and therefore the specimen area ratio, was varied by bonding the required number of composite building blocks together. The adhesive system used for this assembly was the same system which would subsequently be employed to bond the composite element to the metal detail. These details were then joined to the metal details as described in the following sections. Assembly method designation is taken from table 1.

Method 1: The most direct approach to developing a stress-free assembly is to join the component parts mechanically at the desired stress-free temperature. Any subsequent thermal growth will then be influenced by the mechanical constraint to maintain compatible strains at the interface of the details.

Three specimens (numbers 4, 13, and 18), shown in figures 27 through 30, were fabricated by this method. The components were assembled at room temperature using aluminum rivets, steel rivets, or steel bolts. Fastener material and size were selected on the basis of predicted load at the curing temperature. Throughout the program, force-interference fit, with 0.038 to 0.063 mm (0.0015 to 0.0025 in.) interference, was employed with the bolts, and rivets were installed to completely fill the holes.

The assembled details were enclosed in a vacuum bag, called an envelope bag since no additional restraining surface was in contact with the assembly. This is shown in figure 29. Using this method, residual stresses were reduced by 73 to 81%, as shown in figures 8, 16, and 18.

It is suspected that residual stresses were not completely eliminated due to joint flexibility effects in the region of the mechanical fasteners. This subject has been explored in references 4, 5, and 6, but the elastic deflections for these types of joints have not been developed. Extension of this theory to these joint configurations was beyond the scope of this program.

The specimen shown in figure 27 demonstrates a limitation of method 1. The specimen configuration was symmetric, having equal thicknesses of aluminum skin on both sides of the graphite composite. Due to the symmetry, the assembly curvature is not influenced by the residual stress level. The assembly is curved because it assumed the shape dictated by the stiffest member, in this case the composite. The composite detail was curved due to the residual stresses induced in the load transfer region during fabrication of those details. The autoclave pressure exerted during cure of the composite-to-metal bond joint acted uniformly on both sides of the assembly, producing no net force. This did not happen with the hat and zee section stiffeners, figures 28 and 30, because the metal component had sufficient stiffness to act as a tool for the assembly.

Method 2: This method is similar to method 1 in that the components are mechanically joined and the loads imposed on the components depend only on constituent properties. Equilibrium is maintained through mutual restraint. However, in method 2, a tool surface, or caul plate, was used to enforce flatness. Autoclave pressure was applied to one surface of the assembly, while the other surface was supported by a flat plane. Oversize holes were drilled in the caul plate at the fastener locations to ensure that it did not resist or apply any loads. Figure 31 shows two of the symmetric sheet-type specimens which were assembled by this method. In addition to these assemblies, unsymmetric sheets with both uniform reinforcement and with reinforcing straps, a zee section stiffener, and a hat section stiffener, were fabricated by method 2. The hat section stiffener and its support bar, specimen 14, are shown in figure 32. Specimens numbered 1, 5, 9, 14, 22, 25S, and 26S were fabricated by this method.

Achieved residual stress reductions ranged from 60% to 96% of the desired reduction. Residual stresses were reduced by larger percentages for those specimens bonded at 394° K than those cured at 450°K. Results are shown in figures 8, 13, 14, and 15. One of the load transfer region failures previously mentioned came from this group of specimens. The failure occurred on specimen 14, shown in figure 32. Load transfer region delamination occurred on both ends of the specimen but did not extend the entire width of the step. Both delaminations occurred on the same edge of the composite and may have been caused by the machining instead of during bonding.

Two panel assemblies, combining reinforced sheets and reinforced stiffeners, were fabricated by this approach. The composite reinforcement had been bonded to the metal elements in preceding operations, resulting in details which were stress free at temperatures close to room temperature. The panels were assembled by clamping the details flat and installing mechanical fasteners, as shown in figure 33. These fasteners did not secure the composite. The bolted assemblies were then placed in a vacuum bag, shown in figure 34, and the bond between the details was cured. The completed assemblies are shown in figures 23 and 24.

Delaminations occurred in both panel assemblies. The delaminations on panel 25 (fig. 24) occurred in a fiber ply to titanium stepped fitting interface, similar to the failure discussed above. The first-stage bond, which assembled the details, had been cured at 450° K. The second-stage bond, assembling the panel, was cured at 394° K and no failure was anticipated. It is possible that the failure began during the initial cure cycle, when stress levels were highest, and was only completed by the second cure cycle.

Gross delamination of the composite details which had been bonded to the zee stiffeners was observed after assembly of panel 26, shown in figure 23. As before, the stiffeners were attached to the reinforced skin in a manner that required the first-stage bond line to resist the thermal stresses induced while curing the second-stage bond. The curing temperature for both bond cycles was 394° K. The extent of the delamination, as determined by nondestructive testing, is shown in figure 23 by the cross-hatched area on each stiffener, and the plane of the failures is shown by the thin metal shims which have been placed into the delamination.

Method 3: Methods 1 and 2 permitted part geometry to determine the loads applied during the cure cycle. If the assembly contained a large cross-sectional area of aluminum compared to the composite area, the thermal growth of the aluminum would dictate the specimen growth. This, then, would induce high stresses in the composite and in the bonded load transfer region and relatively low stresses in the metal. Failure in the composite component might result.

For assembly method 3, a tool was used to which both components were mechanically fastened. The cross section of the tool was made sufficiently large so that its thermal expansion determined the length of the components. Steel tooling was selected for these assemblies because the coefficient of expansion of steel is approximately midway between the component expansion coefficients. This approach makes it possible to reduce the stress level in one component, providing some protection from failure during the cure cycle.

Nine specimens, identified as specimen numbers 3, 6, 8, 15, 17, 20, 24, 25H, and 25H-1, were fabricated using this approach. For these assemblies, the residual stress was reduced by 64% to 87%. As before, the greatest percentage reduction in residual stress was obtained with specimens cured at 394° K. Three delamination failures were observed, all in specimens cured at 450° K. Of these, two were reinforced with graphite composite and one with boron. Results are shown on figures 13, 14, 15, 16, and 20.

The two hat section stiffeners which become components of the panel assembly discussed in the preceding section (see fig. 24) were assembled by this method. As mentioned above, the failure which was observed after panel assembly may have begun during this cure cycle.

Figure 35 shows a zee section stiffener (specimen 20) attached to the steel tool. In this case the tool was quite simple. Notice that more fastening capability was required to restrain the aluminum component than was required for the composite element. An example of a more complex tool is shown in figure 36 (specimen 25H). This tool has steel plates symmetrically located above and below the specimen. Without this symmetry, the expanding aluminum would introduce a bending moment which would deflect the steel tool, permitting undesirable movement of the components being assembled.

In this method, as in methods 1 and 2, mechanical fasteners were used to join the components, either together or to the tool. As was mentioned, joint flexibility due to elastic deformations around the bolts probably prevented complete elimination of residual stresses. Additional developmental effort on this aspect of the problem seems warranted.

Method 4: Assembly method 4 was the first of several techniques which used mechanical preloading of the components to achieve residual stress control. The preload was applied to the metal detail, as shown in figures 37 and 38. Preload level was selected to completely compensate for the thermal expansion of both components, permitting the composite detail to be installed with no restraint.

Eight specimens (numbers 10, 12, 16, 19, 21, 27S, 27H, and 27H-1) with design stress-free temperature equal to 294° K were fabricated by this method. As a group, these specimens were the most successful of the program. Residual stress level reductions ranging from 93% to 102% were obtained in six of the eight assemblies. The achieved residual stress levels are shown in figures 6, 10, 15, and 18. Due to the preload application method, the metal details were restrained by a uniform pressure on a bearing plate in the tool rather than by mechanical fasteners through the metal detail. Bolted joint flexibility was therefore eliminated. The remaining two of the eight specimens experienced metal failure.

Tool pins, used during the preloading of specimen 27S, were inadvertently left in the assembly during the cure cycle. The aluminum detail was able to sustain the preload stress on the tool pins at room temperature but, upon heating, the restricted expansion increased the stress level while the bearing stress capability was reduced at the higher temperature. The aluminum failed in bearing at the tool pin locations. In spite of this failure, 83% of the desired stress reduction was achieved.

The other failed specimen from this group was the zee section assembly (number 21) shown in figure 38. This specimen was preloaded to a compressive stress somewhat in excess of the column buckling stress. Stability was obtained by supporting the zee at midlength, as shown in the illustration. The induced lateral forces, combined with the reduced zee section strength at the curing temperature, yielded the supported flange, producing a shape very much like a joggle.

This assembly method was also the first method capable of producing assemblies having stress-free temperatures which were different from the assembly temperature. Four assemblies, identified as specimens 34, 35S, 35H, and 35H-1, were made for which the design stress-free temperature was 339° K. Residual stress reductions ranging from 105% to 116% were achieved. These results are shown in figures 7 and 19.

This prestress assembly method achieved a high degree of success in terms of residual stress reduction and an absence of delaminations. The latter benefit was achieved by eliminating the stress in the composite load transfer joint plane, but did so at the expense of the metal details. Large amounts of creep deformation were observed in the aluminum components as a result of the high compression stresses, as shown in figures 21 and 22.

Method 5: This method was a modification of method 4 in which the metal component was preloaded and then both the metal detail and the composite detail were mechanically fastened to the steel tool. The assembly technique is capable of producing assemblies with stress-free temperatures which are either above or below the assembly temperature, depending on the preload level and direction (tension or compression).

Three specimens were built by this technique. Residual stress reductions of 83%, 89%, and 103% of desired reductions were achieved. These specimens were identified as numbers 23, 28, and 33, and results are shown in figures 11, 12, and 17. Design stress-free temperatures were 272° K and 339° K. Figure 39 shows a zee stiffener being preloaded in tension. Notice that the chords of the zee were removed in the load application area. This was necessary to permit access to the web so that preload could be applied and the tool bolts fastened with no induced bending moment. The completed assembly, still in the tool, is shown in figure 40. Figure 41 shows an unsymmetric skin assembly and the tooling used to build it.

One panel assembly was also completed using this assembly technique. The detail components were bonded using other methods. The panel assembly was designed to be stress free at 339° K, as were the detail parts. The expansion characteristics of the reinforced details were such that the hat section details had to be loaded in tension prior to establishing the secondary bond line. The preloading method is shown in figure 42.

After the preload was established, the details were bolted to a steel tool plate. The bolts went through the unreinforced legs of the hat sections, and through an unreinforced portion of the skin detail. The composite straps on all details were restrained only by the previously established bond lines, which had been cured at 450° K. The secondary bond, joining the hats to the skin, was cured at 394° K. The assembly was successfully fabricated, with no observed delaminations. The reinforced hat stiffeners were located directly over the composite straps, which reinforced the skin detail. Strain measurements on these concealed straps could not be made, preventing a complete force balance analysis of the panel assembly. From those measurements which were made there was no significant increase in residual stress indicated.

Method 6: A further extension of methods 4 and 5 involved preloading both the metal and the composite component prior to assembly. This method might prove attractive considering the potential creep limitation on the aluminum components. The stress level in the aluminum can be reduced during bonding by increasing the stress level in the composite.

Two components were fabricated by this method. Figure 43 shows specimen 32, a hat section stiffener, being loaded in tension. After the desired strain level was obtained the hat was bolted to the steel tool and the composite detail was loaded in compression, as shown in figure 44. Restraints to prevent column buckling of the composite are shown. After preloading, the assembly was cured in a conventional manner at 394° K. The design stress-free temperature was 339° K. Achieved residual stress reduction, shown in figure 17, was 76% of the objective. Joint flexibility effects could account for a portion of the unobtained reduction. In addition, there is some tolerance associated with each preload application, which also influences results.

The second component fabricated by this method was specimen 30, an aluminum skin reinforced by composite straps. The skin was first preloaded in tension, as shown in figure 45. The composite was then loaded in compression, as shown in figure 46, by placing it in the slot shown in the tool and then tightening the screws to advance pressure blocks against the ends of the straps. Stability was provided by the slot-filling elements which were retained in the tool by overhanging washers. This design was required to permit pressure transmission to the bond line within the tool.

One of the composite straps failed, and the metal skin was locally deformed in the vicinity of the load transfer fittings. The failure was induced by a design detail of the tool. Access holes had been drilled in the tool to permit strain measurements of the metal skin during preloading. These holes were plugged by rubber pieces during the cure cycle. However, there was insufficient space provided for the contraction of the rubber plugs due to autoclave pressure, and they deformed the metal and the composite straps. The deformed areas, shown in figure 47, rendered measurements on this assembly meaningless. The failed area of the composite strap is under one of these deformations and was probably caused by it.

From a manufacturing viewpoint, this was the most cumbersome method used during the program. However, a greater range of design stress-free temperature can be realized through this method since both components can be stressed to their limit during cure. When bolt flexibility effects are fully defined, this method offers the capability to compensate for them through adjustment of preload levels.

Method 7: Another approach to obtain assemblies which are stress free at temperatures above room temperature was attempted. The components were assembled on a steel tool which was to govern expansion during heating. However, oversized holes were drilled at the attachment of the aluminum detail so that a predetermined amount of free thermal growth, or limited slip, would occur before the metal was stopped by the bolts.

Specimens 29 and 31 were made by this method. The residual stress reductions, shown in figure 9, were 171% and 198% of the desired reduction. Instead of the desired 394° K stress-free temperature (after cure at 450° K), the achieved stress-free temperature was close to 339° K. This indicates that insufficient free thermal expansion occurred. The desired expansion was restricted due to bolt clamp-up forces and transmitted pressure. A tool design modification would improve the performance of this method.

Method 8: Assembly method 8 utilized thermal rather than mechanical means to accomplish preloading. The aluminum components to be preloaded were cooled and then placed in a cavity-type tool. The amount of preload was adjusted by using a shim pack at one end of the tool to control the length of the cavity. Subsequent expansion of the aluminum parts would proceed freely until the part contacted the ends of the tool. Continued warming to room temperature induced compressive stress in the aluminum. The composite detail was then added to the assembly and bonded in a normal manner.

Two parts (specimens 26Z and 26Z-1) were fabricated wherein the composite details were unrestrained in the tool. This required high preload levels in the aluminum zee sections which were obtained by cooling the zees in a combination of dry ice and liquid nitrogen.

The aluminum was cooled to approximately 105° K (-270° F) and then placed in the tool, as shown in figure 48. The achieved residual stress reductions on these assemblies were 122% and 123%, indicating excessive preload. Residual stress levels are shown in figure 13.

Specimen 11, a reinforced hat section, was fabricated with the aluminum detail preloaded and both the aluminum and the composite detail fastened to the steel tool. A smaller amount of preload was desired for this assembly because the composite was loaded by the expanding tool. The preloading was accomplished with dry ice alone. The assembly was cured at 450° K, and during the cure cycle the composite strap delaminated at the interface with the titanium load transfer fitting. This failure, induced by high bondline stress, had nothing to do with the preload technique, which was judged the most convenient approach employed for preloading in the entire program.

Method 9: The final assembly method to be explored during this program was designed to provide thermal growth control of the aluminum through continuous support rather than at discrete points at the extremity of the part. Fiberglass-reinforced polyester laminate was selected as the tooling material due to its relatively low coefficient of expansion (4.1 x 10^{-6}/°K). The precured tool was bonded to the aluminum component of the assembly using a room temperature curing adhesive,* as shown in figure 49. After this bond had cured, the composite detail was mechanically fastened to the aluminum sheet. Clearance holes were provided on the tool side. This assembly was then cured as before and, after cure, the fiberglass tool was separated from the assembly by peeling the tool laminations off the assembly.

Two assemblies were fabricated by this method. Figure 50 shows specimen 2, an unsymmetric skin assembly. Residual thermal stress, shown in figure 6, was reduced 72% in this assembly, which was cured at 450° K. The second assembly, shown during fabrication in figure 51, was cured at 394° K. Residual stresses in this specimen, identified as number 7, were reduced by 68%, as indicated in figure 8.

The results obtained with this method were surprisingly good considering the limitations of most room temperature curing adhesives. However, the technique does not look promising as employed in these assemblies. The continuous restraint concept, if combined with a perimeter restraint, may prove useful for reinforcing large-size sheet structure where the stresses could induce local instability. Additional development would be required to develop a tool removal method.

Measurement Technique

The measurement technique selected for this program to determine residual stress was to measure the strain induced in the components as a result of the bonding cycle. Strain was determined by measuring the distance between two scribed lines spaced approximately 25.4 cm (10 in.) along the length of the component. This approach, rather than the use of strain gages, was selected both to minimize cost and because strain gages are affected by exposure to elevated temperature.

*Permabond 747 contact cement, available from Rexco Corporation, New York

Reference lines were scribed on the surfaces of all details which would be visible after the bonding cycle. The lines were transverse to the fiber direction of the assembly and were centered on the detail to avoid load transfer fitting influences. Scribing surfaces were provided on the precured composite details by bonding small patches of titanium to the exposed surface. For an example, see figure 28.

The measuring equipment is shown in figure 52. The equipment was assembled on a surface plate to provide a flat reference. Principal elements of the measuring equipment are a low-power microscope, a supporting platform, ways, and a Vernac* reading head and scale. The scale is rigidly attached to the surface plate by the structure which supports the ways. The microscope and Vernac reading head are mounted to the platform, which rides on the ways. Components are aligned to place the scale below the Vernac reading head. The scale is subdivided into 0.635-mm (0.025-in.) increments, which are labelled on the scale. The scale increment, which is below the Vernac reading head, is projected onto the face of the dial. The scale is read directly to the nearest 0.635 mm (0.025 in.) and a spiral, printed on the face of the dial, is aligned with the projected mark to subdivide the increment by rotating the dial. The device is direct reading to 0.0025 mm (0.0001 in.)

Components and assemblies were secured to the surface plate before and after the bonding cycle and clamped in a flat position. The microscope, which contained a hairline, was aligned over one of the scribed lines on the piece being measured, and the Vernac scale reading was recorded. The platform, including the microscope and the reading head, was then translated along the ways until the second scribed line aligned with the hairline. The second reading was recorded, and the difference between these readings was the desired length measurement. Measurements before and after bonding were compared to determine the length change which had occurred during bonding. These measurements are summarized in tables 4 and 5.

As mentioned above, the part to be measured was clamped in a flat position. This requirement was fundamental to the applicability of the analysis employed, as described in the following section, and necessitated complex and time-consuming clamping methods. An example is shown in figure 53, where a panel assembly is being measured. The inability to consistently clamp the various parts in exactly the same flat position undoubtedly led to some errors in the measurements.

Based upon the least count of the instrument, implied accuracy was ±0.0025 mm (±0.0001 in.). At the beginning of the program a rectangular bar made of invar and certified as a secondary standard was measured and, based on these results, instrument accuracy was estimated to be ±0.0125 mm (±0.0005 in.). However, this was a simple shape to clamp in a flat position. During the course of the program, a few parts were measured two and three times to verify the values which were being reported. In some instances, successive measurements disagreed by ±0.05 mm (±0.002 in.). Other successive measurements agreed within ±0.0025 mm (±0.0001 in.). Clamping variations and operator error are the most likely explanations for these discrepancies.

*Simpson Optical Company, Chicago, Illinois

The problems encountered in obtaining the measurements for this program indicate that the adaptation of any of the techniques to a production situation will require considerable developmental effort to obtain a reliable and accurate monitoring system for fabrication of large quantities of stress-controlled assemblies.

Analysis

Thermally induced stresses occur when two or more materials, having differing thermal expansion characteristics, are joined at one temperature and subsequently heated or cooled to any other temperature. The stresses occur because the individual components of the assembly are restrained from expanding or contracting at their individual rates. Assuming there are no external constraints upon the assembly, the internal forces must be self-equilibrating. These internal forces act at the centroid of the individual elements and, if the specimen is not symmetric, an internal bending moment is produced in addition to the axial force. This internal bending moment results in out-of-plane deflection, altering the internal stress distribution to maintain force and bending moment equilibrium. These relationships are developed in reference 7.

For the condition that the assembly remains flat, either due to symmetry or external constraint, the internal stress becomes uniform over the thickness of each element provided that the external constraint only reacts the internal bending moment. In this case, the analysis becomes somewhat simplified in that bending stiffness parameters need not be evaluated. This condition was achieved in this program by making all measurements on specimens while they were held flat.

The distance between scribed marks was measured for each component of an assembly before and after the adhesive bonding cycle. Part temperature during measurement was 294° K ± 2.8° K. The residual strain in each component was computed from the change in distance between scribe marks divided by the nominal distance between scribe marks.

$$\epsilon = (L_2 - L_1)/L_n$$

where

ϵ = strain

L_2 = measured distance after bonding

L_1 = measured distance before bonding

L_n = nominal distance between scribed lines (25.4 cm or 10.0 in.)

Assuming all intermediate stress states were elastic, the residual stress induced by the adhesive bonding cycles becomes

$$\sigma = E\epsilon$$

where

E = elastic modulus (N/m^2 or psi)

σ = stress (N/m^2 or psi)

For the unsymmetric specimens, which contained one metal element and exposed composite elements, measurements were obtained on both materials. This provided a means to verify the computed residual stress through a check of force equilibrium, and led to the discovery of the creep deformations which occurred.

The measured strains for many of the specimens indicated that both components of the assembly were stressed in tension, which was clearly impossible since there were no external axial loads applied.

The high-modulus fibers used in this program are almost perfectly elastic and are not significantly influenced by exposure to temperature levels employed during this program. Since the length measurements obtained from the composite element of the assembly did not extend into the load transfer region bond line (which may be affected by temperature), the measured strain and computed stress from the composite element was assumed to be a true measure of the specimen condition.

Based upon composite stress level, internal force was computed as the product of stress and area. A force equal in magnitude and opposite in sign is required in the metal component to satisfy equilibrium. The metal stress level was computed from this force by dividing force by the metal area. This is the residual stress level in the metal component of the assembly. For those assemblies where design stress-free temperature was the same as the measurement temperature (294° K), this computation was made directly from the data. For specimens having other design stress-free temperatures, equilibrium conditions were computed for the assembly existing at 294° K and then the stress level was adjusted to the design stress-free temperature. The results of these computations are included in tables 4 and 5.

To verify the presumed creep model, two tests were performed as previously described. The analysis in these cases required only the observation of length change and the inferred strain, combined with the computation of exposure stress during the simulated bonding cycle. The excellent agreement between the test part results and the creep model results, shown in figures 21 and 22, verified the use of this approach.

Six symmetric specimens were fabricated during the study. These specimens had metallic face skins completely covering both sides of the composite element, making it impossible to obtain composite strain and stress values. Residual stress levels for these specimens were developed using the best estimate of strain based on measurements and corrected for creep deformation for those specimens exposed to 450° K. Creep deformation was not demonstrated at 394° K, and so no correction was applied in those cases.

The achieved reduction in residual stress was evaluated by comparing the measured results to the residual stress level which would have occurred if standard adhesive bonding techniques had been used. The stress level in the metallic portion of the assembly is used in these comparisons because this component experiences residual tension stresses, which are presumed to be detrimental to fatigue life.

The residual stress level in the metallic component under standard bonding conditions is found from

$$\sigma_m = \frac{(\alpha_m - \alpha_c)\,(\Delta T)\,E_m}{1 + (A_m E_m)/(A_c E_c)}$$

where

σ_m = metal stress level (N/m^2 or psi)

α = coefficient of linear thermal expansion ($°K^{-1}$ or $°F^{-1}$)

E = elastic modulus (N/m^2 or psi)

A = cross-sectional area (m^2 or $in.^2$)

The subscripts c and m refer to composite and metal, respectively, and the term ΔT is the difference between the stress-free temperature and the temperature at which the residual stress is desired. In the case of standard bonding conditions, the stress-free temperature is the curing temperature. This relationship is developed in reference 1.

CONCLUSIONS AND RECOMMENDATIONS

Based upon the results obtained during this study, the following conclusions are drawn:

- Residual thermal stresses induced during bonding reinforcing composite to metal structural elements can be reduced or eliminated through suitable modification of the manufacturing procedures employed to establish the adhesive bond.

- The most successful method employed during this study used a steel tool capable of mechanically loading the metal component in compression prior to the bonding cycle.

- Compression loading and subsequent heating to 450° K during the bond cycle can result in permanent creep deformation in aluminum components. The magnitude of the deformation increases with increasing stress level.

- Achieved residual stress alleviation is reduced by elastic deformations in the vicinity of mechanical fasteners used to restrain the components during the bonding. Careful attention to bearing stresses and bolt sizing is required.

- The bonded load transfer region between the fibers and the stepped titanium end fittings is subject to failure during exposure to high temperatures (450° K) and high shear stress levels during establishment of the composite-metal element bond line.

- The adhesive bond line of composite-reinforced metal details is not capable of sustaining the stresses imposed during reheating to the original cure temperature in all cases, depending upon the adhesive system, the stress-free temperature, the exposure temperature, and the area ratio.

As indicated above, residual stress alleviation has been achieved in a laboratory environment, and several significant factors have been identified. The following recommendations are offered to permit transition to a production environment.

- The selection of an assembly method for fabrication of residual-stress-controlled assemblies should be made on the basis of predicted stress levels and limitations imposed by the constituent materials.

- Additional development work is required to:

  - Define the desired stress-free temperature for subsonic aircraft and other applications.

  - Determine the cost effectiveness of introducing stress control methods to reinforced component fabrication.

- Extend the laboratory methods into a production environment, i.e., scale-up.
- Define the creep behavior of the constituent materials.
- Define the effect of creep deformation during fabrication on component strength and life.
- Develop load deflection relationships for mechanically fastened joints of the configurations employed in stress relief techniques.
- Develop a strain measurement technique suitable for use in production situations.
- Define adhesive system capabilities and limitations pertinent to the fabrication of assemblies which employ composite-reinforced elements.

APPENDIX A

TEST SPECIMEN MATERIAL

Aluminum sheet and formed (hat) sections were alloy 7075-T6 per QQ-A-283. Aluminum extrusions (zees) were alloy 7178-T6 per MIL-A-9180. Titanium sheet was alloy 6Al-4V per MIL-T-9046F, type III, composition C, annealed.

Boron composite was SP-272, obtained from Minnesota Mining and Manufacturing Company. This is a unidirectional, preimpregnated tape containing 84 fibers per centimeter of tape width (212 fibers per inch). Boron filaments are 0.010 cm (0.004 in.) in diameter and consist of boron vapor deposited onto a tungsten substrate. The matrix material, designated PR-279, is an epoxy resin system designed to cure at 450° K.

Graphite composite was SP-286, obtained from Minnesota Mining and Manufacturing Company. This is a unidirectional, preimpregnated tape containing approximately 55% (by volume) graphite fibers. The graphite fibers used in this program were Whitaker-Morgan's Modmor type II, containing 10,000 filaments per tow. The matrix system was a modified epoxy designed to cure at 450° K.

Adhesive systems employed for composite-to-metal bonding were:

AF-126, obtained from Minnesota Mining and Manufacturing Company. This is a film adhesive of epoxy resin impregnated onto a dacron fiber mat. The material thickness was 0.026 cm (0.010 in.) and cure was accomplished at 394° K.

AF-30, obtained from Minnesota Mining and Manufacturing Company. This is an unsupported film adhesive of nitrile-phenolic resin. The film thickness was 0.026 cm, and cure was accomplished at 450° K.

All metal surfaces were primed with BR-127, a corrosion-inhibitive primer available from Bloomingdale Department of American Cyanamid Company.

Tooling materials used in this program were:

Aluminum alloy 6061-T6 per QQ-A-270
Cold-rolled steel; AISI-C-1018 per QQ-S-633
Cold-rolled steel; AISI-4340 annealed per MIL-S-5000
Fiberglass-polyester resin laminates made from U.S. Polymeric, Inc., 1581/P-604C preimpregnated cloth

Fiberglass-polyester laminated tools were bonded to the metal details with Permabond 747 contact cement, a methyl cyanoacrylate adhesive available from Rexco Corporation, New York.

REFERENCES

1. Oken, S. and June, R. R.: Analytical and Experimental Investigation of Aircraft Metal Structures Reinforced with Filamentary Composites; Phase I: Concept Development and Feasibility. NASA CR-1859, December 1971.

2. Blichfeldt, B. and McCarty, J. E.: Analytical and Experimental Investigation of Aircraft Metal Structures Reinforced with Filamentary Composites; Phase II: Structural Fatigue, Thermal Cycling, Creep, and Residual Strength. NASA CR-2039, June 1972.

3. Bryson, L. L. and McCarty, J. E.: Analytical and Experimental Investigation of Aircraft Metal Structures Reinforced with Filamentary Composites; Phase III: Major Component Development. NASA CR-2122, 1972.

4. Tate, M. B. and Rosenfeld, S. J.: Preliminary Investigation of the Loads Carried by Individual Bolts in Bolted Joints. NACA TN 1051, 1946.

5. Rosenfeld, S. J.: Analytical and Experimental Investigation of Bolted Joints. NACA TN 1458, 1947.

6. Peravali, R.: Bolt Constant Determination by the Method of Beam on Elastic Foundation. Boeing document D6-24521, July 1970.

7. Timoshenko, S.: Analysis of Bi-Metal Thermostats. Journal of The Optical Society of America, Vol. II, 1925, pp. 233-255.

TABLE 1.—ASSEMBLY METHODS

Method	Description
1	Mechanically join components—no supporting tool
2	Mechanically join components—support on tool or caul plate
3	Mechanically join components to tool
4	Preload metal detail and constrain by tool—composite component not restrained
5	Preload metal detail and mechanically fasten all components to tool
6	Preload all components and mechanically fasten all components to tool
7	Mechanically fasten components to tool but allow for limited free thermal growth of metal component
8	Preload metal detail by cooling and retaining in tool
9	Bond metal detail to tool having low coefficient of expansion; mechanically fasten composite details to metal detail

TABLE 2.—DESIGN PARAMETERS

Specimen	Type[a]	Temperature, °K		Material[c]				Fiber plies	Metal t, mm	A_c/A_t	Assembly method	Tool material	Conditions during adhesive bonding operation					
													Preload, Newtons		Strain x 10^6		Load, Newtons		Metal stress, MN/m^2	Bondline stress,[d] kN/m^2
		Cure	SFT[b]	Al	Ti	Bo	Gr						Metal	Fibers	Metal	Fibers	Metal	Fibers		
1	S1S	394	294	x			x	8	1.27	0.583	2	–	–	–	-1 795	724	- 7 750	7 750	-120.	1 500
2	S1S	450	294	x			x	8	3.18	0.358	9	GRP[e]	–	–	-3 000	910	- 29 600	9 890	-183.5	1 910
3	S1S	450	294		x	x		10	0.813	0.628	3	Steel	–	–	589	1 090	2 520	15 200	60.9	2 940
4	S2S	394	294	x			x	4	0.381	0.537	1	–	–	–	-1 710	815	- 4 430	4 430	-114.	1 710
5	S2S	450	294	x		x		5	1.27	0.213	2	–	–	–	-1 395	1 580	- 11 030	11 030	- 85.5	4 260
6	S2S	450	294		x		x	8	0.406	0.687	3	Steel	–	–	589	2 030	2 520	22 000	60.9	4 250
7	Strap	394	294	x			x	12	1.27	0.281	9	GRP[e]	–	–	-1 930	585	- 33 300	7 150	-129.	1 230
8	Strap	450	294	x			x	12	3.18	0.136	3	Steel	–	–	-1 875	2 030	- 74 500	24 800	-115.	4 250
9	Strap	450	294		x		x	16	0.813	0.449	2	–	–	–	- 704	739	- 12 000	12 000	- 72.7	1 550
10	Hat	450	294	x		x		10	1.63	0.111	4	Steel	-14 300	0	-2 971	0	- 33 000	› 0	-175.	0
11	Hat	450	272	x		x		20	1.63	0.197	8	Steel	- 7 170	0	-2 423	1 091	- 26 950	9 700	-149.	2 950
12	Hat	450	294	x		x		30	1.63	0.271	4	Steel	-14 250	0	-2 961	0	- 32 800	0	-175.	0
13	Hat	394	294	x		x		10	1.63	0.111	1	–	–	–	- 520	1 390	- 6 280	6 280	- 34.7	3 750
14	Hat	394	294	x		x		20	1.63	0.197	2	–	–	–	- 810	1 155	- 9 800	9 800	- 54.0	3 110
15	Hat	394	294	x		x		30	1.63	0.271	3	Steel	–	–	-1 208	702	- 14 600	9 440	- 80.8	1 890
16	Zee	450	294	x		x		20	3.18	0.157	4	Steel	-32 400	0	-3 131	0	- 73 700	0	-201.	0
17	Zee	450	294	x		x		30	3.18	0.220	3	Steel	–	–	-2 040	1 091	- 48 100	22,550	-131.	2,940
18	Zee	450	294	x		x		40	3.18	0.271	1	–	–	–	-1 681	1 325	- 39 700	39,700	-108.	3,570
19	Zee	450	294	x			x	16	3.18	0.245	4	Steel	-55,000	0	-4 060	0	- 95 700	0	-261.	0
20	Zee	450	294	x			x	24	3.18	0.269	3	Steel	–	–	-2 045	2 030	- 48 100	33,000	-131.	4,250
21	Zee	450	294	x			x	32	3.18	0.328	4	Aluminum	-106 400	0	-4 070	0	- 95 700	0	-261.	0
22	Zee	394	294	x			x	16	3.18	0.245	2	–	–	–	- 789	1 850	- 19 950	19 950	- 54.4	3 850
23	Zee	394	272	x			x	24	3.18	0.269	5	Steel	-15,700	0	-1 895	1 305	- 48 000	21 300	-131.	2 740
24	Zee	394	294	x			x	32	3.18	0.328	3	Steel	–	–	-1 315	1 305	- 33 300	28 300	- 90.6	2 740
25S	S2S	450	294	x		x		5	1.27	0.212	2	–	–	–	-1 390	1 580	- 44 100	44 100	- 85.3	4 260
25H	Hat	450	294	x		x		20	1.63	0.179	3	Steel	–	–	-1 875	1 091	- 22 800	9 700	-115.	2 940
26S	S2S	394	294	x			x	4	0.381	0.537	2	–	–	–	-1 755	812	- 17 600	17 600	-114.	1 710
26Z	Zee	394	294	x			x	24	3.18	0.270	8	Steel	-35 400	0	-3 870	0	- 98 000	0	-267.	0
27S	Strap	450	294	x			x	12	3.18	0.136	4	Steel	-94 900	0	-3 905	0	-155 000	0	-240.	0
27H	Hat	450	294	x			x	12	1.63	0.330	4	Steel	-30 100	0	-3 905	0	- 49 200	0	-240.	0
28	S1S	394	339	x		x		10	0.813	0.620	5	Steel	2 540	0	- 670	390	- 1 810	5 250	- 43.9	1 010
29	S2S	450	394	x			x	4	0.381	0.538	7	Steel	–	–	- 670	2 030	- 1 595	11 000	- 42.4	4 250
30	Strap	450	339	x			x	12	0.813	0.379	6	Steel	5,860	-12 540	-1 376	1 414	- 14 160	28 700	- 84.5	2 960
31	Hat	450	394	x			x	24	1.63	0.326	7	Steel	–	–	- 670	2 030	- 7 440	21 400	- 41.1	4 260
32	Hat	394	339	x		x		30	1.63	0.267	6	Steel	5 880	- 5 250	- 758	303	- 9 000	3 990	- 49.6	793
33	Zee	450	339	x			x	16	3.18	0.197	5	Steel	31 500	0	- 878	2 030	- 20 700	22 000	- 56.4	4 260
34	Zee	394	339	x		x		20	3.18	0.162	4	Steel	5 150	0	-1 120	0	- 28 400	0	- 77.1	0
35S	Strap	450	339	x			x	8	0.813	0.290	4	Steel	-10 930	0	-2 790	0	- 28 300	0	-171.	0
35H	Hat	450	339	x			x	12	1.63	0.195	4	Steel	-11 980	0	-2 790	0	- 30 900	0	-171.	0
25	Panel	394	294								2									
26	Panel	394	294								2									
27	Panel	450	294								3									
35	Panel	394	339								5									

[a] S1S: Sheet on one side
S2S: Sheet on two sides

[b] Stress-free temperature

[c] Al: 7075-T6 except zees are 7178-T6
Ti: 6Al-4V titanium
Bo: SP-272 boron-epoxy prepreg
Gr: SP-386 graphite-epoxy prepreg

[d] Average shear stress at bonded interface between fibers and titanium load transfer fitting

[e] Fiberglass

TABLE 2A.—DESIGN PARAMETERS (ENGLISH UNITS)

Specimen	Type[a]	Temperature, °F		Material[c]				Fiber plies	Metal t, in.	A_c/A_t	Assembly method	Tool material	Conditions during adhesive bonding operation						
		Cure	SFT[b]	Al	Ti	Bo	Gr						Preload, lb		Strain x 10^6		Load, lb		Metal stress, psi	Bondline stress,[d] psi
													Metal	Fibers	Metal	Fibers	Metal	Fibers		
1	S1S	250	70	x			x	8	0.050	0.583	2	–	–	–	-1 795	724	- 1 740	1 740	-17 400	218
2	S1S	350	70	x			x	8	0.125	0.358	9	GRP[e]	–	–	-3 000	910	- 6 660	2 220	-26 600	277
3	S1S	350	70		x	x		10	0.032	0.628	3	Steel	–	–	589	1 090	565	3 420	8 830	427
4	S2S	250	70	x			x	4	0.015	0.537	1	–	–	–	-1 710	815	- 995	995	-16 550	248
5	S2S	350	70	x		x		5	0.050	0.213	2	–	–	–	-1 395	1 580	- 2 480	2 480	-12 400	619
6	S2S	350	70		x		x	8	0.016	0.687	3	Steel	–	–	589	2,030	565	4 950	8 830	617
7	Strap	250	70	x			x	12	0.050	0.281	9	GRP[e]	–	–	-1 930	585	- 7 480	1 605	-18 700	178
8	Strap	350	70	x			x	12	0.125	0.136	3	Steel	–	–	-1 875	2 030	-16 700	5 560	-16 700	617
9	Strap	350	70		x		x	16	0.032	0.449	2	–	–	–	- 704	739	- 2 700	2 700	-10 550	225
10	Hat	350	70	x		x		10	0.064	0.111	4	Steel	-3 210	0	-2 971	0	- 7 410	0	-26 400	0
11	Hat	350	30	x		x		20	0.064	0.197	8	Steel	-1 610	0	-2 423	1 091	- 6 050	2 180	-21 600	428
12	Hat	350	70	x		x		30	0.064	0.271	4	Steel	-3 200	0	-2 961	0	- 7 390	0	-26 400	0
13	Hat	250	70	x		x		10	0.064	0.111	1	–	–	–	- 520	1 390	- 1 410	1 410	- 5 040	545
14	Hat	250	70	x		x		20	0.064	0.197	2	–	–	–	- 810	1 155	- 2 200	2 200	- 7 850	451
15	Hat	250	70	x		x		30	0.064	0.271	3	Steel	–	–	-1,208	702	- 3 280	2 120	-11 710	274
16	Zee	350	70	x		x		20	0.125	0.157	4	Steel	-7 260	0	-3 131	0	-16 550	0	-29 100	0
17	Zee	350	70	x		x		30	0.125	0.220	3	Steel	–	–	-2 040	**1 091**	-10 800	5,060	-19 050	427
18	Zee	350	70	x		x		40	0.125	0.271	1	–	–	–	-1 681	1 325	- 8 910	8,910	-15 650	519
19	Zee	350	70	x			x	16	0.125	0.245	4	Steel	-12 340	0	-4 060	0	-21 500	0	-37 800	0
20	Zee	350	70	x			x	24	0.125	0.269	3	Steel	–	–	-2 045	2 030	-10 800	7 410	-19 000	618
21	Zee	350	70	x			x	32	0.125	0.328	4	Aluminum	-23 900	0	-4 070	0	-21 500	0	-37 800	0
22	Zee	250	70	x			x	16	0.125	0.245	2	–	–	–	- 789	1 850	- 4 480	4 480	- 7 890	559
23	Zee	250	30	x			x	24	0.125	0.269	5	Steel	-3 530	0	-1 895	1 305	-10 780	4 790	-18 950	398
24	Zee	250	70	x			x	32	0.125	0.328	3	Steel	–	–	-1 315	1 305	- 7 490	6 350	-13 150	398
25S	S2S	350	70	x		x		5	0.050	0.212	2	–	–	–	-1 390	1 580	- 9 900	9 900	-12 380	620
25H	Hat	350	70	x		x		20	0.064	0.179	3	Steel	–	–	-1 875	1,091	- 5 140	2 180	-16 700	427
26S	S2S	250	70	x			x	4	0.015	0.537	2	–	–	–	-1 755	812	- 3 960	3 960	-16 550	248
26Z	Zee	250	70	x			x	24	0.125	0.270	8	Steel	-7 950	0	-3 870	0	-22 000	0	-38 700	0
27S	Strap	350	70	x			x	12	0.125	0.136	4	Steel	-21 300	0	-3 905	0	-34 800	0	-34 800	0
27H	Hat	350	70	x			x	12	0.064	0.330	4	Steel	-6 750	0	-3 905	0	-11 040	0	-34 800	0
28	S1S	250	150	x		x		10	0.032	0.620	5	Steel	570	0	- 670	390	- 407	1 178	- 6 360	147
29	S2S	**250**	250	x			x	4	0.015	0.538	7	Steel	–	–	- 670	2 030	- 358	2 470	- 6 150	618
30	Strap	350	150	x			x	12	0.032	0.379	6	Steel	1 318	-2 820	-1 376	1 414	- 3 140	6 450	-12 280	430
31	Hat	350	250	x			x	24	0.064	0.326	7	Steel	–	–	- 670	2 030	- 1 670	4 810	- 5 960	619
32	Hat	250	150	x		x		30	0.064	0.267	6	Steel	1 320	-1 180	- 758	303	- 2 020	896	- 7 200	115
33	Zee	350	150	x			x	16	0.125	0.197	5	Steel	7 090	0	- 878	2 030	- 4 650	4 950	- 8 170	619
34	Zee	**250**	150	x		x		20	0.125	0.162	4	Steel	1 158	0	-1 120	0	- 6 370	0	-11 200	0
35S	Strap	350	150	x			x	8	0.032	0.290	4	Steel	-2 455	0	-2 790	0	- 6 350	0	-24 800	0
35H	Hat	350	150	x			x	12	0.064	0.195	4	Steel	-2 690	0	-2 790	0	- 6 950	0	-24 800	0
25	Panel	250	70								2									
26	Panel	250	70								2									
27	Panel	350	70								3									
35	Panel	250	150								5									

[a]S1S: Sheet on one side
S2S: Sheet on two sides

[b]Stress-free temperature

[c]Al: 7075-T6 except zees are 7178-T6
Ti: 6Al-4V titanium
Bo: SP-272 boron-epoxy prepreg
Gr: SP-386 graphite-epoxy prepreg

[d]Average shear stress at bonded interface between fibers and titanium load transfer fitting

[e]Fiberglass

TABLE 3.–MATERIAL PROPERTIES

Material	Coefficient of expansion x 10^6		Modulus of elasticity					
			294° K(70° F)		394° K(250° F)		450° K(350° F)	
	$°K^{-1}$	$°F^{-1}$	GN/m^2	psi x 10^{-6}	GN/m^2	psi x 10^{-6}	GN/m^2	psi x 10^{-6}
Component materials								
Boron fiber	5.6	3.1	400	58	---	---	---	---
Graphite fiber	-0.45	-0.25	242	35	---	---	---	---
7075-T6 aluminum	24.7	13.7	71	10.3	65.5	9.5	60.7	8.8
7178-T6 aluminum	25.6	14.2	72.5	10.5	67.6	9.8	62.8	9.1
6Al-4V titanium	8.8	4.9	110	16	108	15.6	104	15.0
Tooling materials								
6061-T6 aluminum	24.7	13.7	68	9.9	---	---	---	---
1018 & 4340 steel	12.6	7.0	200	29	---	---	---	---
Fiberglass-polyester laminate	4.1	2.3	24.2	3.5	---	---	---	---

TABLE 4.–MEASUREMENTS AND RESULTS FOR SPECIMENS STRESS FREE AT ROOM TEMPERATURE

Spec	Measured surface	Strain x 10^6		Stiffness ratio A_cE_c/A_mE_m	Strain x 10^6		Residual stress			
		After preload	After bonding		Equilibrium	Metal creep	Metal		Fiber	
							MN/m^2	psi	MN/m^2	psi
1	Aluminum Graphite	– –	+ 470 - 51	2.36	+120 - 51	(a)	+ 8.55	+1 240	- 12.3	- 1 780
2	Aluminum Graphite	– –	+ 107 - 572	0.946	+540 -572	-433	+39.0	+5 560	-138	- 2 000
3	Titanium Boron	– –	+ 260 - 45	3.07	+138 - 45	0	+15.2	+2 210	- 18.1	- 2 620
4	Alum. -1[b] Alum. -2	– –	+ 477 - 331	1.97	+477 +477	(a)	+33.8	+4 900	- 40.1	- 5 810
5	Alum. -1 Alum. -2	– –	+ 239 + 81	0.760	+160 +160	-210[c]	+26.2	+3 800	-194.5	-28 200
6	Titan. -1 Titan. -2	– –	+ 426 + 167	2.38	+297 +297	0	+32.8	+4 750	- 30.0	- 4 350
7	Alum. -A Alum. -B Alum. -D Graph. -1 Graph. -2	– – – – –	+ 203 + 230 + 283 - 511 - 475	0.665	+328 +328 +328 -493 -493	(a)	+23.3	+3 380	-119.0	-17 250
8	Alum. -A Alum. -B Alum. -C Graph. -1 Graph. -2	– – – – –	- 153 - 148 - 211 - 928[d] - 435	0.266	+116 +116 +116 (b) -435	-287	+ 8.29	+ 1 200	-105	-15 220
9	Titan. -A Titan. -B Titan. -C Graph. -1 Graph. -2	– – – – –	+ 380 + 133 + 87 - 148 - 154	0.895	+135 +135 +135 -151 -151	0	+14.9	+2 160	- 36.5	- 5 290
10	Aluminum Boron	– –	- 263 - 69	0.352	+ 24 - 69	-287	+ 1.72	+ 250	- 27.6	- 4 000
12	Aluminum Boron	-1 077 0	- 489 - 101	1.05	+106 -101	-595	+ 7.51	+1 090	- 40.5	- 5 870
13	Aluminum Boron	– –	+ 307 - 347	0.352	+122 -347	(a)	+ 8.70	+1 260	-139.2	-20 200
14	Aluminum Boron	– –	+ 367 - 77[d]	0.695	+ 54 - 77	(a)	+ 3.86	+ 560	- 30.8	- 4 460
15	Aluminum Boron	– –	+ 96 - 116	1.05	+122 -116	(a)	+ 8.70	+1 260	- 46.5	- 6 740
16	Aluminum Boron	-1 110 0	- 539 - 150	0.517	+ 78 -150	-617	+ 5.65	+ 820	- 60.1	- 8 710
17	Aluminum Boron	– –	- 532 - 362[d]	0.778	+282 -362	-820	+20.4	+2 960	-145	-21 000
18	Aluminum Boron	– –	- 49 - 283	1.03	+292 -283	-341	+21.1	+3 060	-113	-16 400
19	Aluminum Graphite	-2 049 0	- 898 - 8	0.410	+ 3 - 8	-901	+ 0.21	+ 31	- 1.93	- 280
20	Aluminum Graphite	– –	+ 51 - 402[d]	0.615	+247 -402	-196	+17.9	+2 600	- 97.3	-14 100
21	Aluminum Graphite	-3 994 0	-1 623[d] + 434	0.816	-354 +434	-1 269	-25.6	-3 720	+105	+15 200
22	Aluminum Graphite	– –	+ 3 - 361	0.410	+148 -361	(a)	+10.7	+1 550	- 87.0	-12 600
24	Aluminum Graphite	0 0	+ 133 - 215	0.816	+175 -215	(a)	+12.7	+1 840	- 52.0	- 7 530
25S	Alum. -1 Alum. -2	0 0	+ 245 + 145	0.761	+395 +395	-200[c]	+28.1	+4 070	-208	-30 200

Note: See following page for footnotes

TABLE 4.—Concluded

Spec	Measured surface	Strain x 10^6		Stiffness ratio A_cE_c/A_mE_m	Strain x 10^6		Residual stress			
		After preload	After bonding		Equilibrium	Metal creep	Metal		Fiber	
							MN/m^2	psi	MN/m^2	psi
25H	Aluminum Boron	— —	- 192 - 362	0.611	+221 -362	-413	+15.7	+2 280	-145	- 2 100
25H-1	Aluminum Boron	— —	- 225 - 281	0.611	+172 -281	-397	+12.2	+1 770	-112.5	-16 300
26S	Alum.-1 Alum.-2	— —	+ 34 + 70	1.97	+ 52 + 52	(a)	+ 3.69	+ 535	- 6.35	- 921
26Z	Aluminum Graphite	-1 265 0	- 262 + 370	0.615	-228 +370	(a)	-16.6	-2 400	+ 89.4	+12 950
26Z-1	Aluminum Graphite	-1 364 0	- 420 + 354	0.615	-218 +354	(a)	-15.8	-2 290	+ 85.6	+12 400
27S	Alum.-A Alum.-C Alum.-D Graph.-1 Graph.-2	— — — — —	- 413 - 587 - 471 - 507 - 393[d]	0.265	+119 +119 +119 -450 -450	-609	+ 8.50	+1 230	-108.8	-15 750
27H	Aluminum Graphite	-2 003 0	- 634 - 36	0.840	+ 30 - 36	-664	+ 2.14	+ 310	- 8.70	- 1 260
27H-1	Aluminum Graphite	-1 960 0	- 554 + 50	0.840	- 42 + 50	-513	- 2.96	- 430	+ 12.2	+ 1 750

[a]Creep deformation was not demonstrated with assemblies cured at 394° K (250° F)

[b]Letter or numeral designates measurement position

[c]Estimate based on behavior of other specimens

[d]Static failure

TABLE 5.—MEASUREMENTS AND RESULTS FOR SPECIMENS HAVING DESIGN STRESS-FREE TEMPERATURE OTHER THAN ROOM TEMPERATURE

Spec	Measured surface	Room temp strain x 10^6		Stiffness ratio A_cE_c/A_mE_m	Room temp strain x 10^6		Design SFT equilibrium strain x 10^6	Residual stress at design SFT			
								Metal		Fiber	
		After preload	After bonding		Equilibrium	Metal creep		MN/m^2	psi	MN/m^2	psi
11	Aluminum Boron	- 609 0	- 419 + 133[b]	0.695	- 93 +133	-329	+ 80 -118	+ 5.70	+ 825	- 47.2	- 6 850
23	Aluminum Graphite	- 543 0	+ 62 + 50	0.615	- 31 + 50	(a)	+183 -318	+13.25	+1 920	- 76.5	-11 100
28	Aluminum Boron	+ 851 0	+ 962 - 173	4.58	+792 -173	(a)	+ 96 -21	+ 6.83	+ 990	- 8.42	- 1 220
29	Alum.-1 Alum.-2	— —	(c) + 915	1.97	+915	(c)	-690	-46.2	-6 700	+ 79.4	+11 500
30	Alum.-A Alum.-B Alum.-C Alum.-D Graph.-1 Graph.-2	+ 563 + 563 + 563 + 563 - 634 - 577	+ 476 + 433 + 504 + 500 - 830 -1 021[b]	1.04	+964 -926	-486	+394 -379	+27.2	+3 940	- 91.9	-13 300
31	Aluminum Graphite	— —	+ 283 - 584	0.824	+480 -584	-197	-654 +796	-43.8	-6 350	+192	+27 900
32	Aluminum Boron	+ 542 - 413	+ 683 - 549	1.025	+562 -549	(a)	+132 -132	+ 9.11	+1 320	- 52.9	- 7 660
33	Aluminum Graphite	+1 187 0	+ 94 - 766	0.410	+314 -766	-220	- 24 + 62	- 1.70	- 247	+ 15.0	+ 2 170
34	Aluminum Boron	+ 234 0	+ 541 - 339	0.535	+181 -339	(a)	-131 +246	- 9.31	-1 350	+ 98.7	+14 300
35S	Alum.-A Alum.-C Alum.-D Graph.-1 Graph.-2	- 854 - 969 (c) 0 0	+ 74 - 166 - 41 - 576 - 557	0.694	+392 -566	-438	- 65 + 83	- 4.48	- 650	+ 20.1	+ 2 910
35H	Aluminum Graphite	- 897 0	- 257 - 695	0.415	+288 -695	-545	- 38 + 95	- 2.62	- 380	+ 23.0	+ 3 330
35H-1	Aluminum Graphite	- 963 0	- 244 - 473	0.415	+196 -473	-440	-130 +317	- 8.97	-1 300	+ 76.5	+11 100

[a]Creep deformation was not demonstrated wtih assemblies cured at 394° K (250° F)

[b]Static failure

[c]Not available

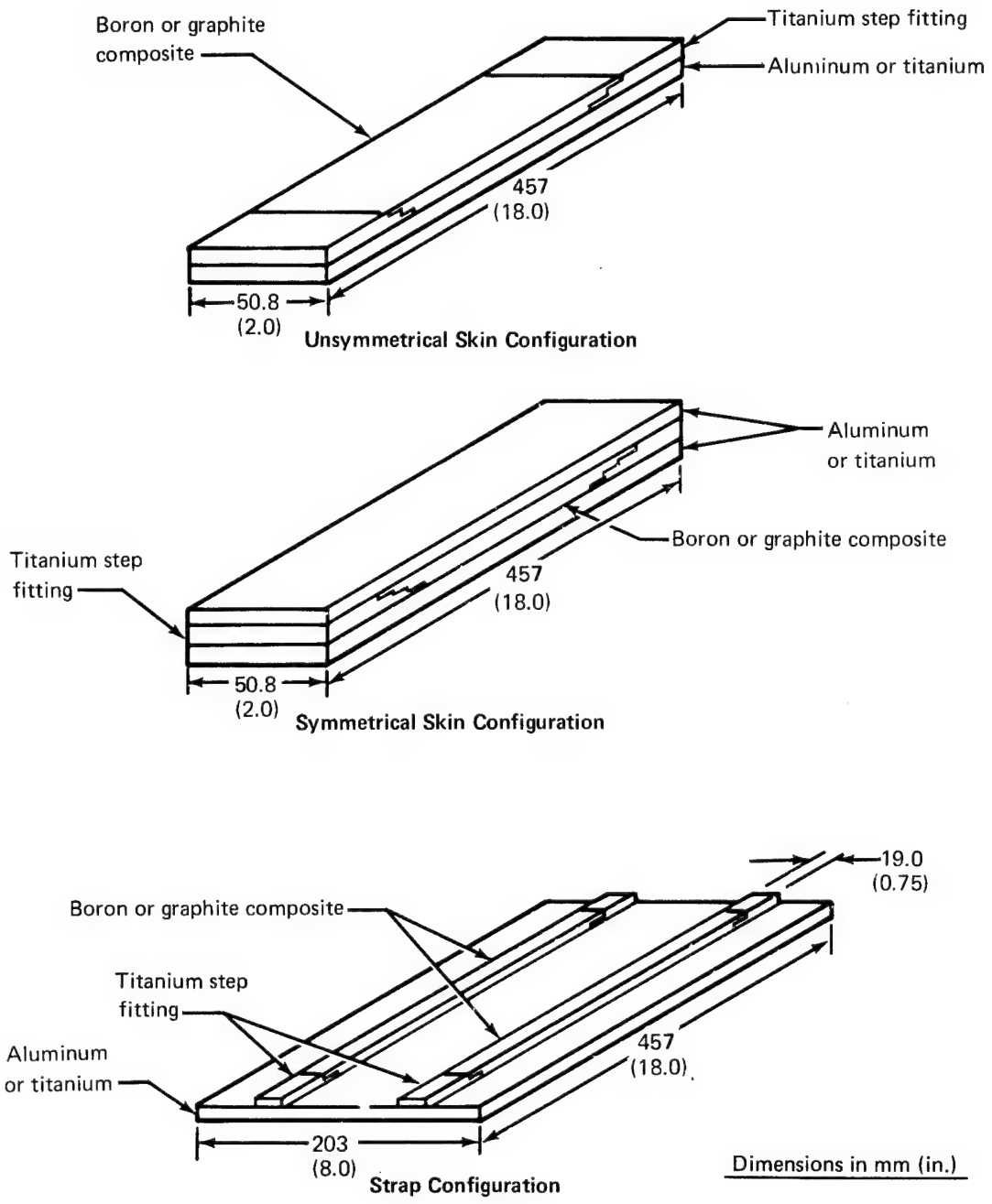

FIGURE 1.—SHEET-TYPE SPECIMEN CONFIGURATIONS

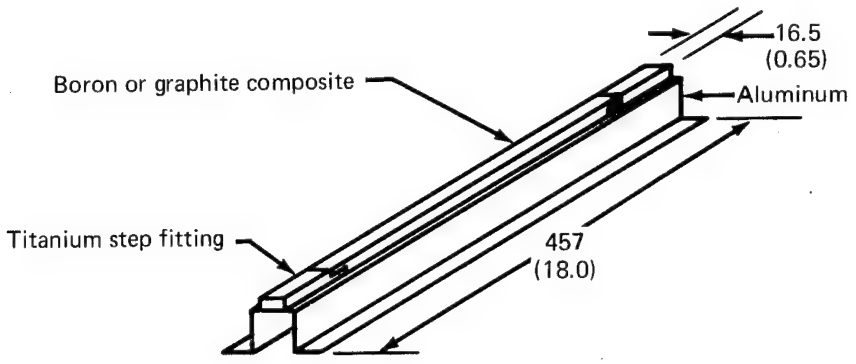

Hat Configuration

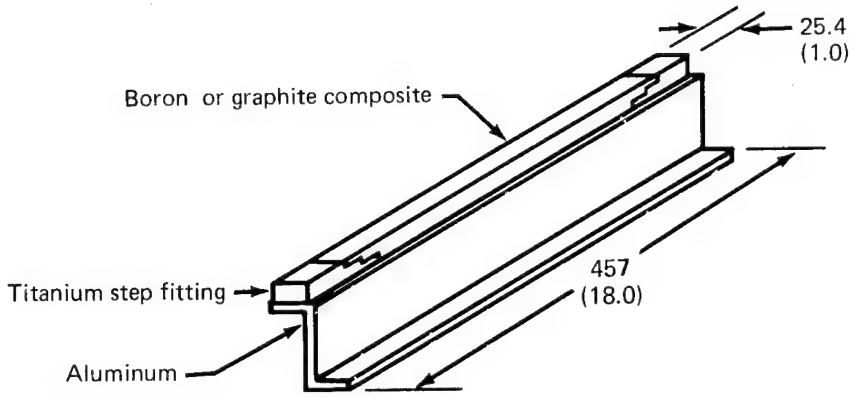

Zee Configuration

Dimensions in mm (inches)

FIGURE 2.–STIFFENER SPECIMEN CONFIGURATIONS

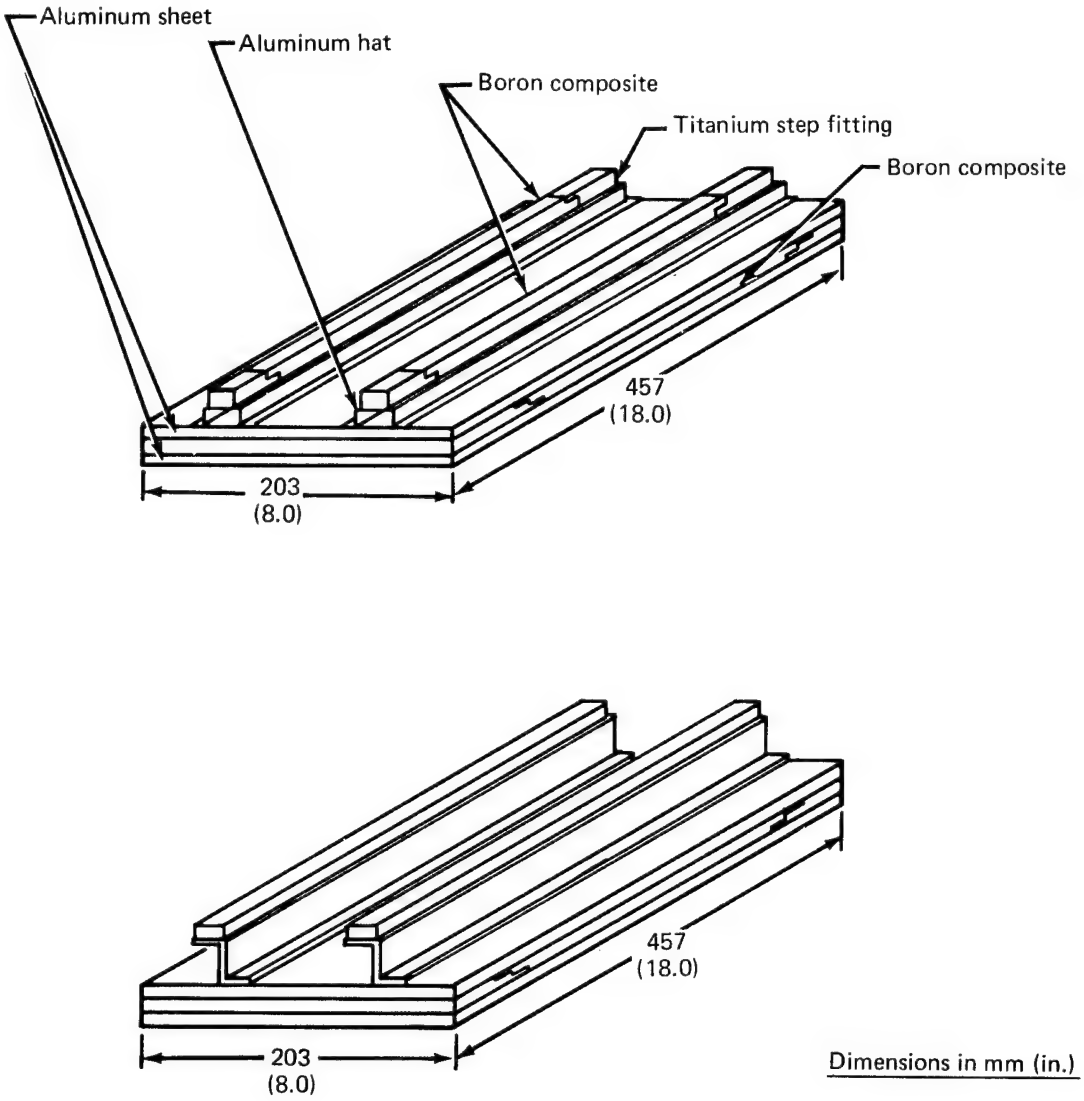

FIGURE 3.–PANEL ASSEMBLY CONFIGURATIONS

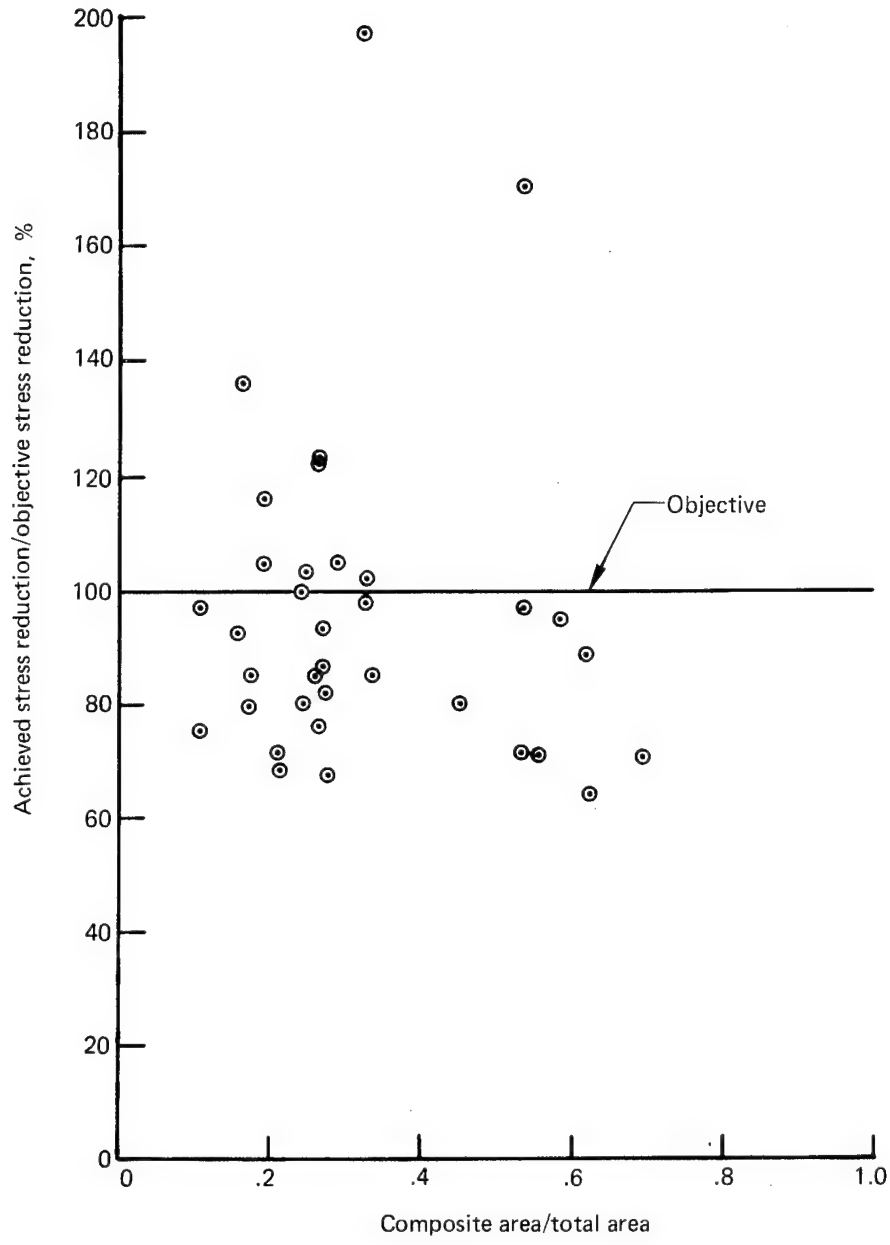

FIGURE 4.–SUMMARY OF STRESS REDUCTION RESULTS

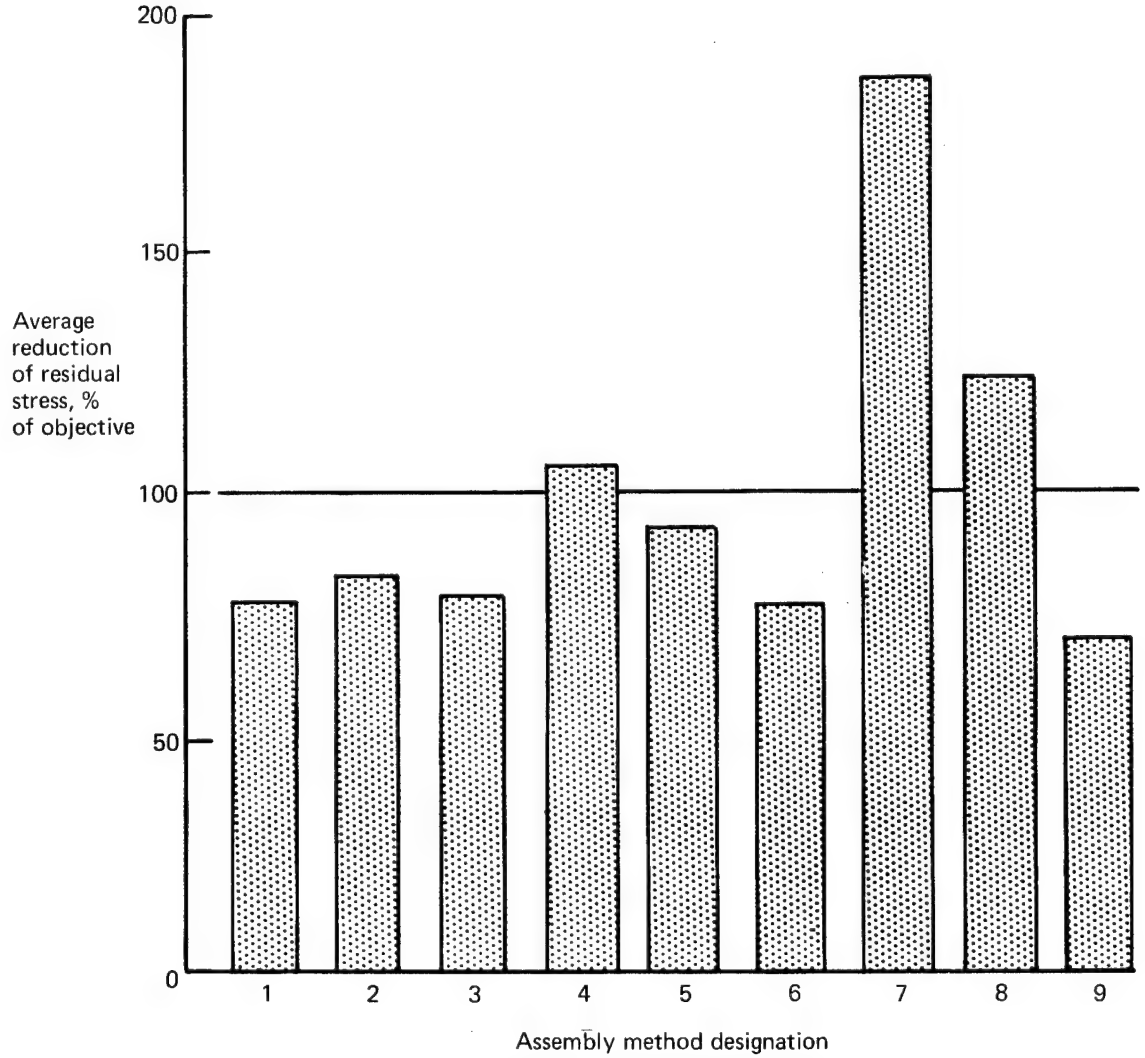

FIGURE 5.—COMPARISON OF ASSEMBLY METHOD RESULTS

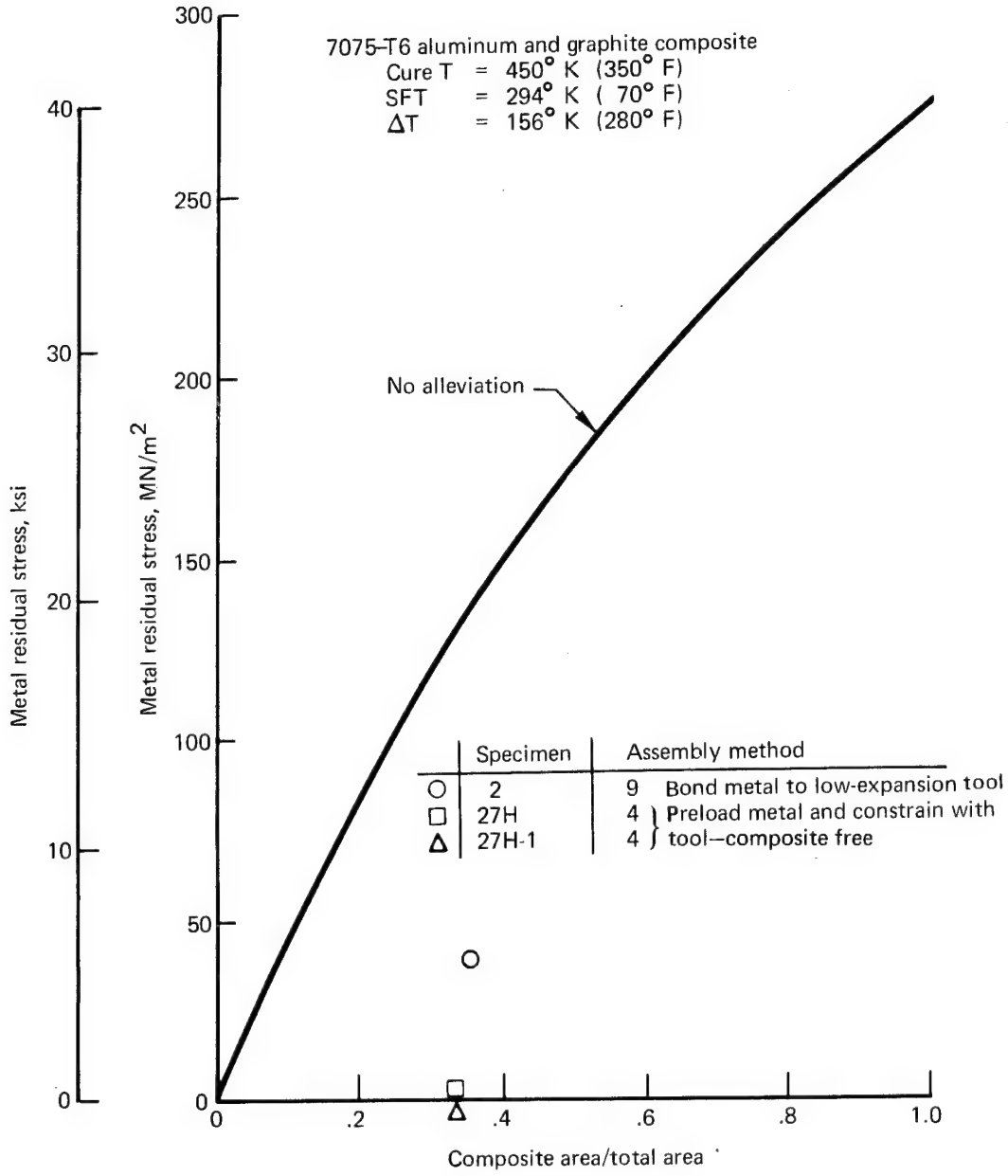

FIGURE 6.—SPECIFIC RESULTS—SPECIMENS 2, 27H, AND 27H-1

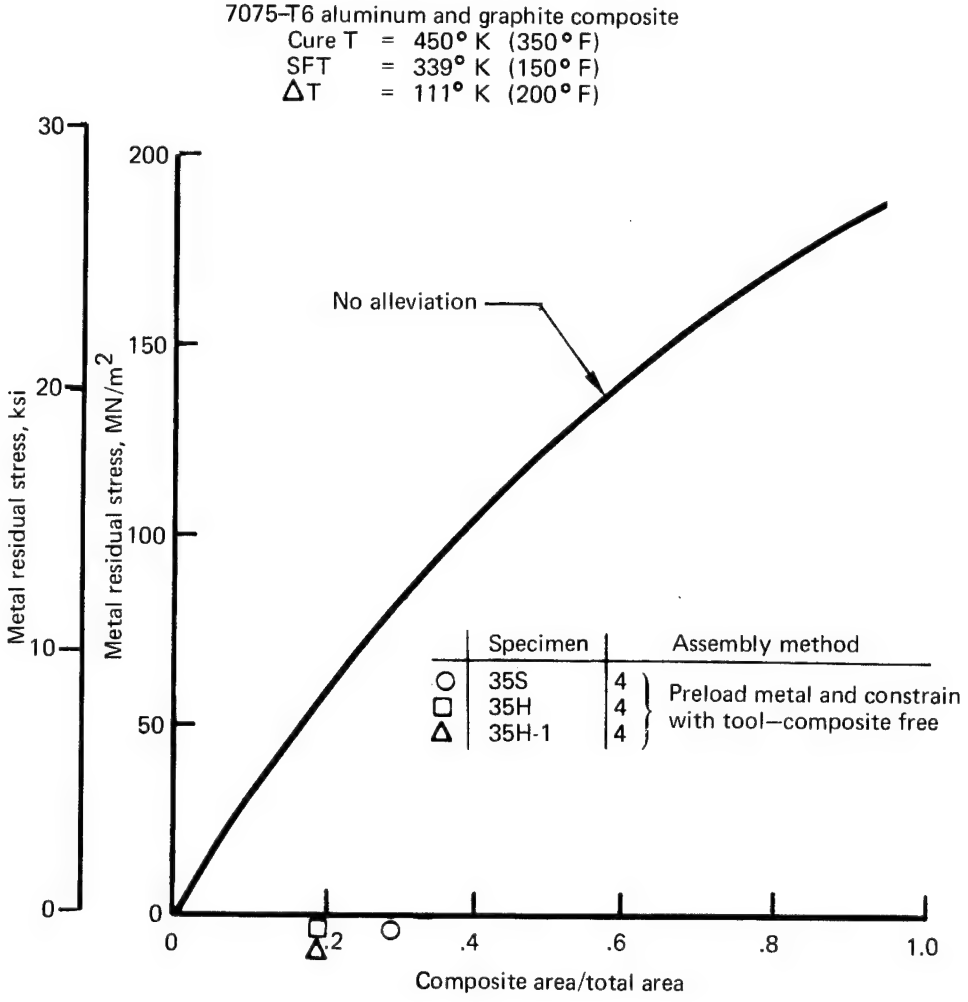

FIGURE 7.–SPECIFIC RESULTS–SPECIMENS 35S, 35H, AND 35H-1

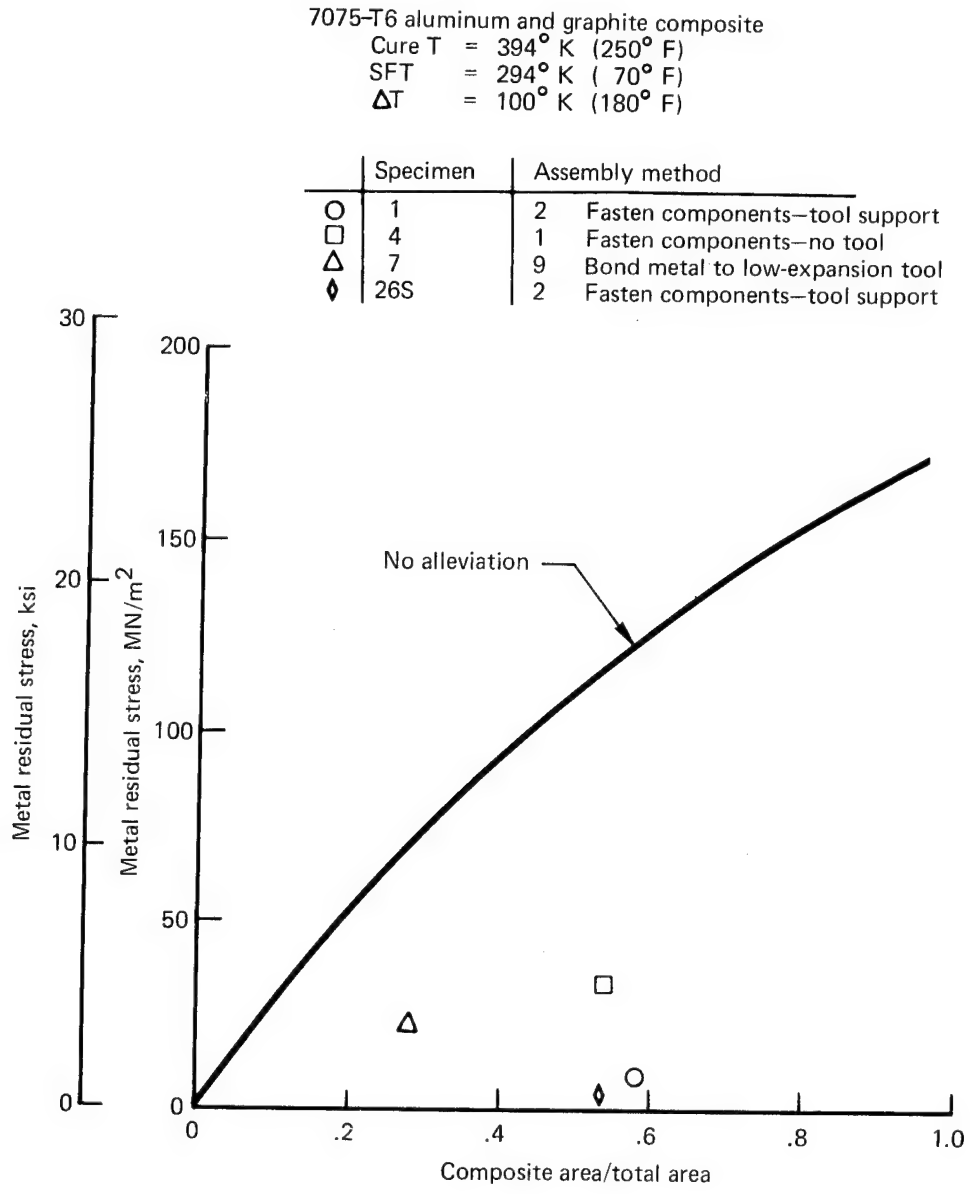

FIGURE 8.—SPECIFIC RESULTS—SPECIMENS 1, 4, 7, AND 26S

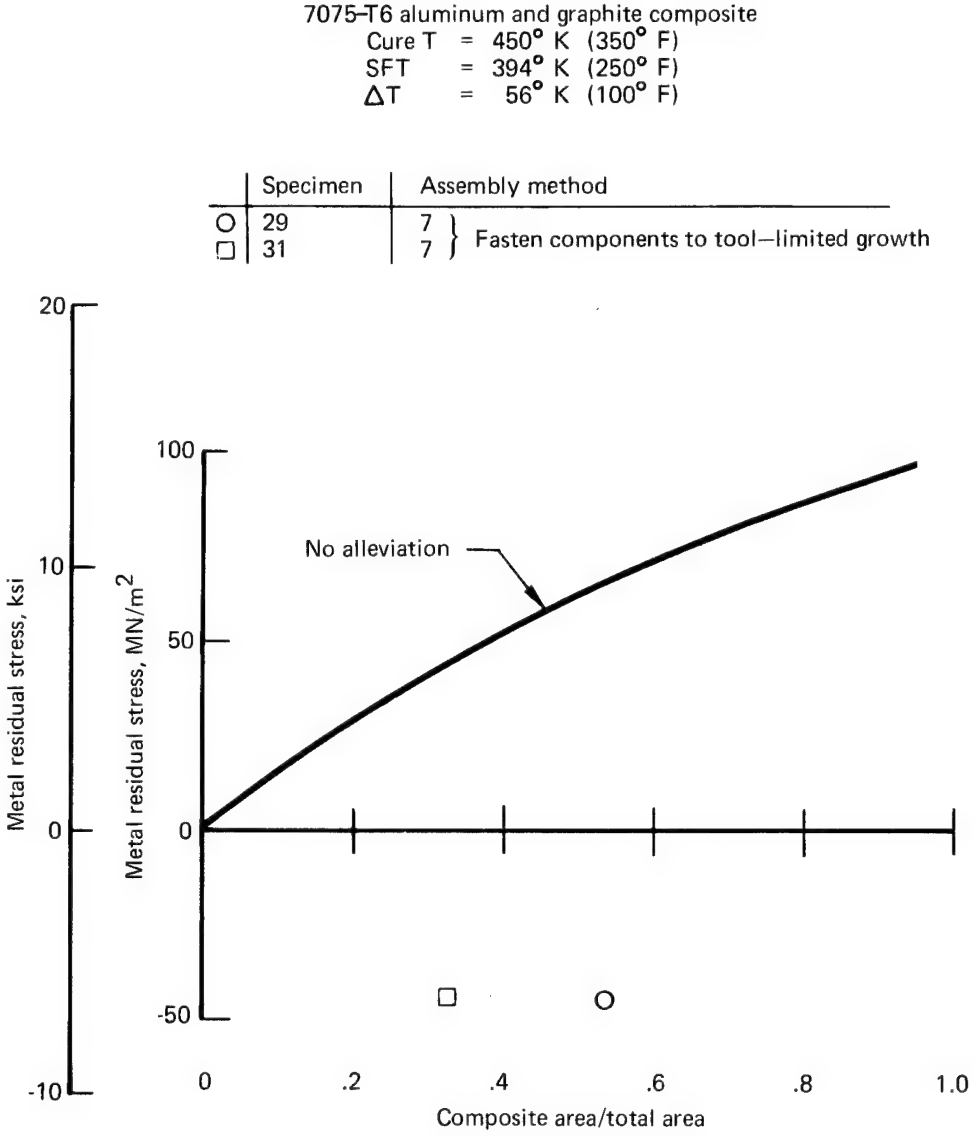

FIGURE 9.—SPECIFIC RESULTS—SPECIMENS 29 AND 31

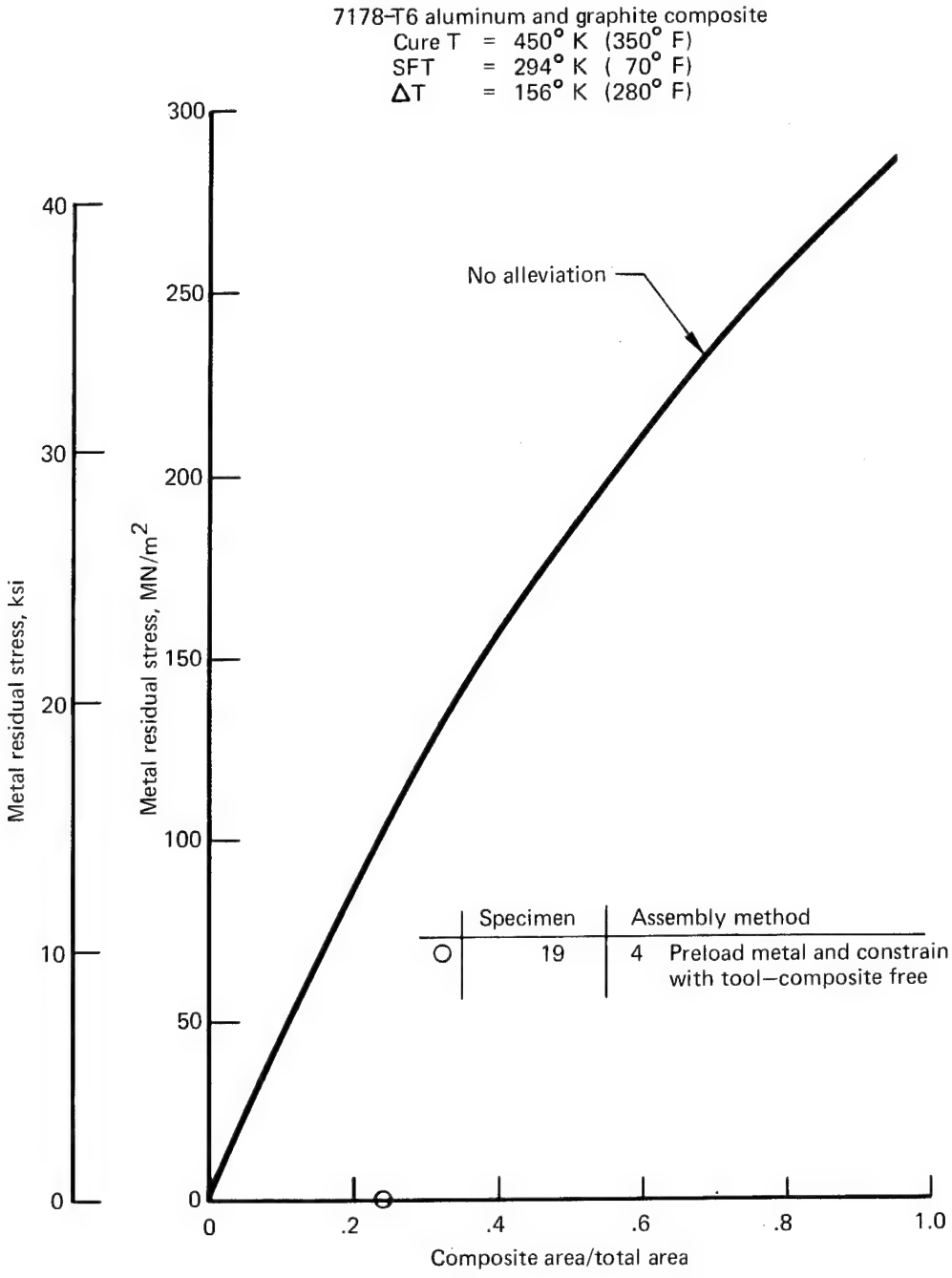

FIGURE 10.–SPECIFIC RESULTS–SPECIMEN 19

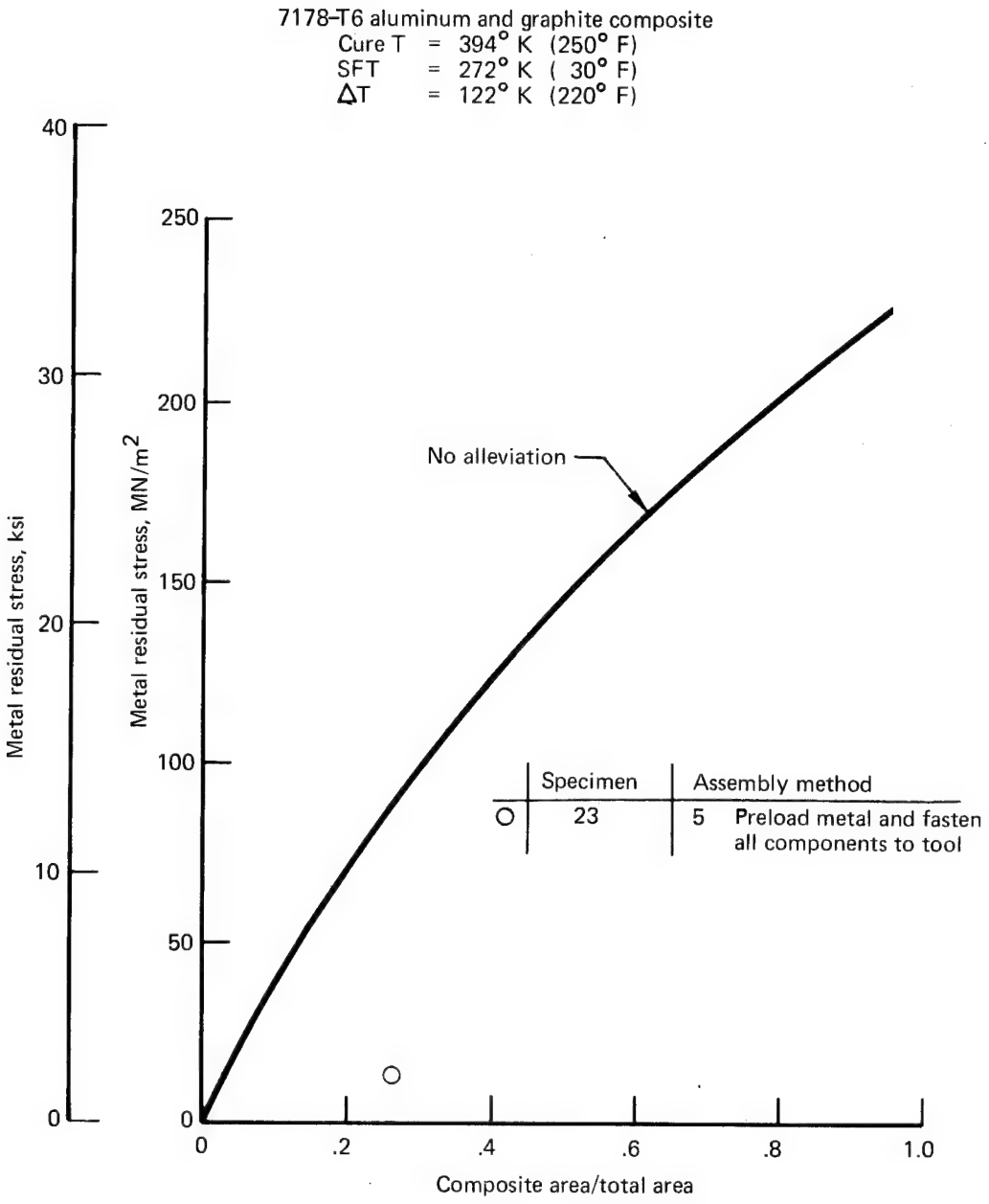

FIGURE 11.–SPECIFIC RESULTS–SPECIMEN 23

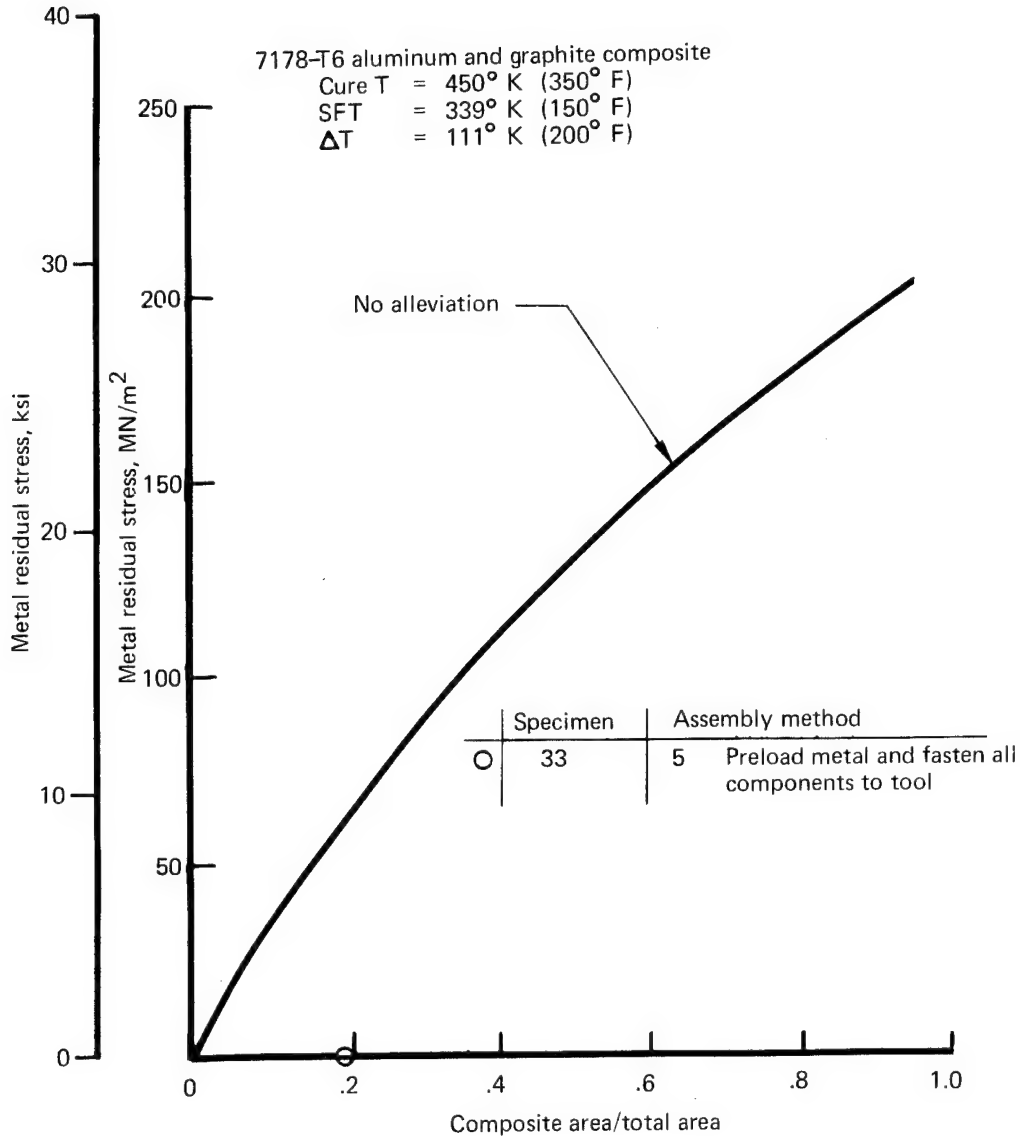

FIGURE 12.–SPECIFIC RESULTS–SPECIMEN 33

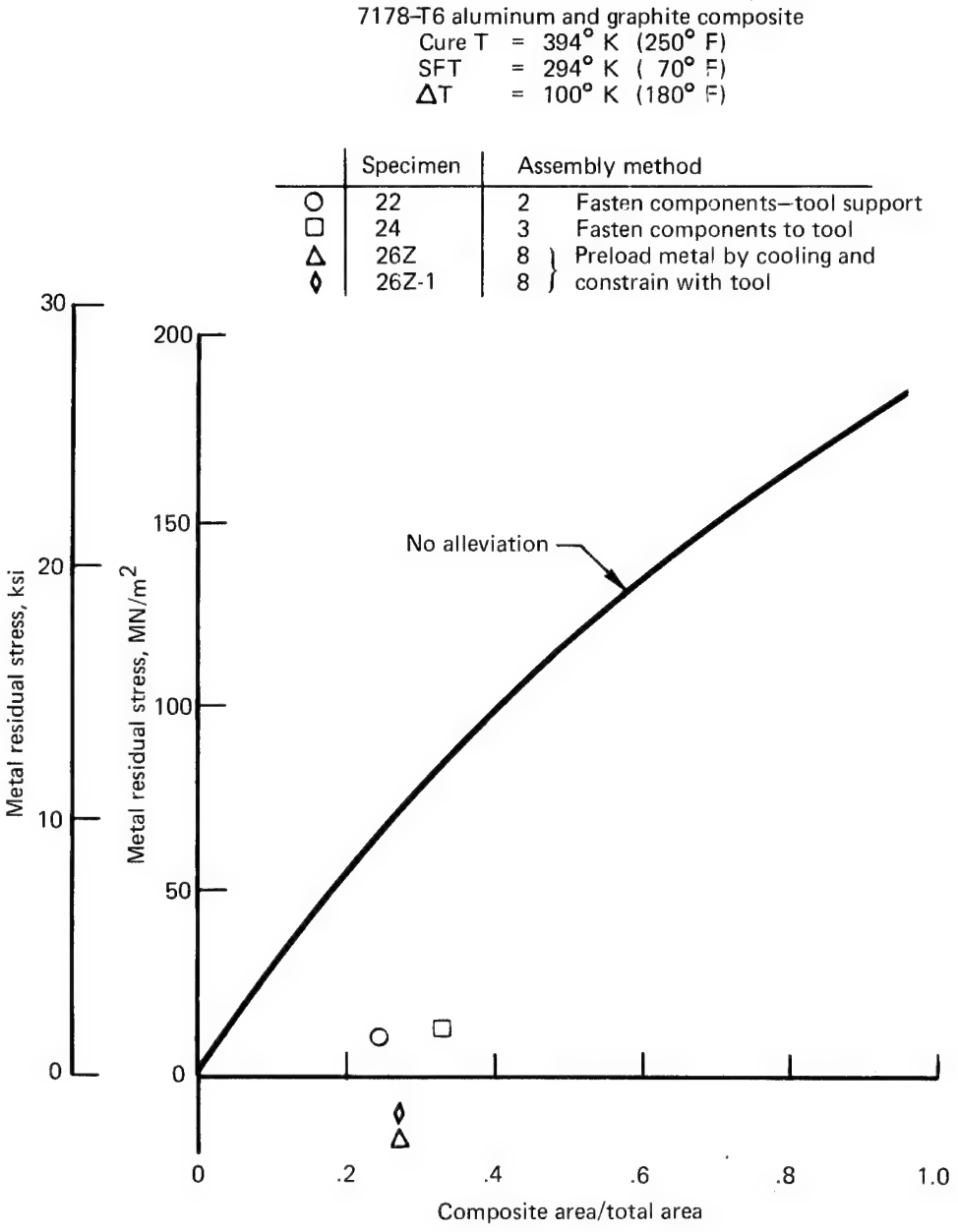

FIGURE 13.—SPECIFIC RESULTS—SPECIMENS 22, 24, 26Z, AND 26Z-1

6Al-4V titanium and graphite composite
Cure T = 450° K (350° F)
SFT = 294° K (70° F)
ΔT = 156° K (280° F)

	Specimen	Assembly method	
○	6	3	Fasten components to tool
□	9	2	Fasten components—tool support

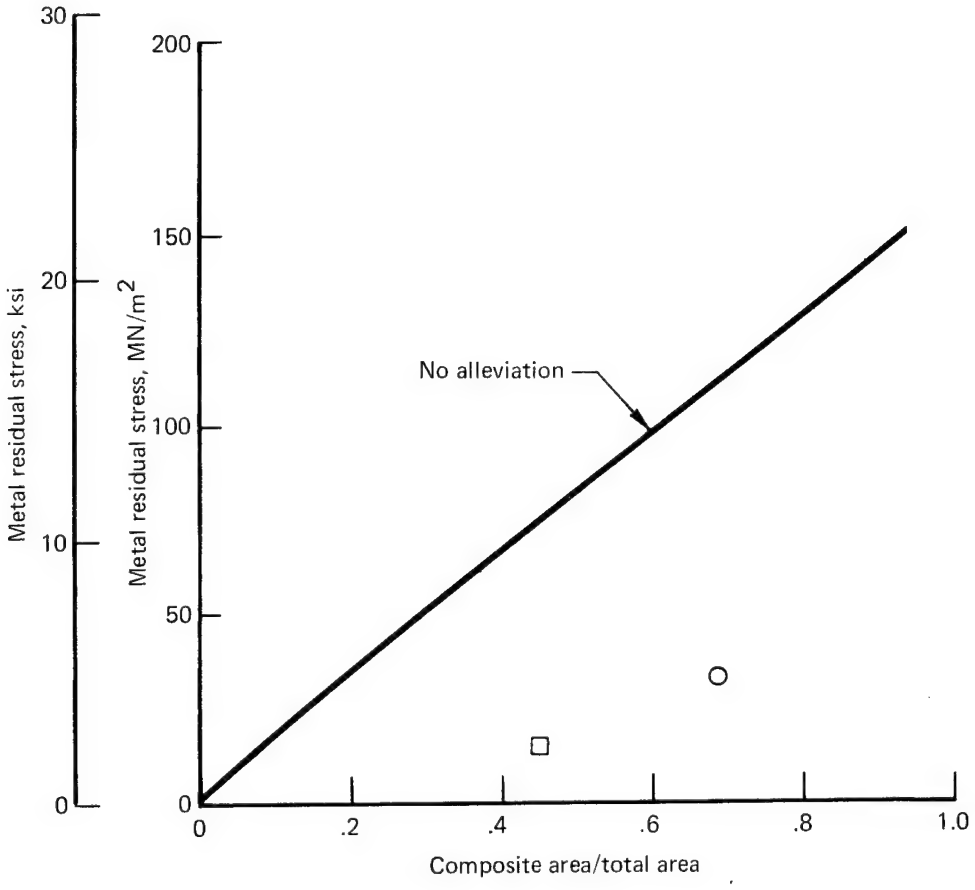

FIGURE 14.–SPECIFIC RESULTS–SPECIMENS 6 AND 9

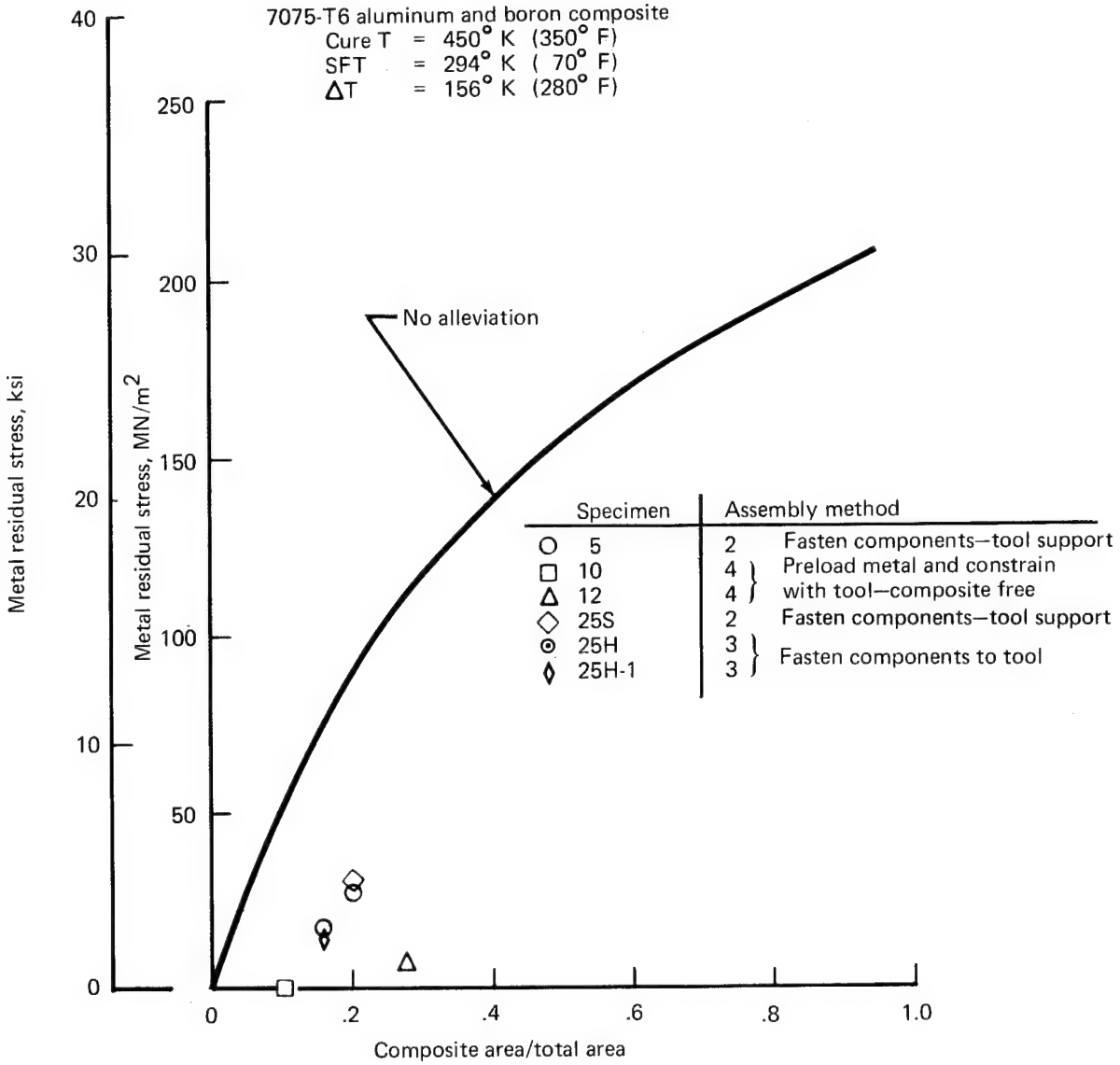

FIGURE 15.—SPECIFIC RESULTS—SPECIMENS 5, 10, 12, 25S, 25H, AND 25H-1

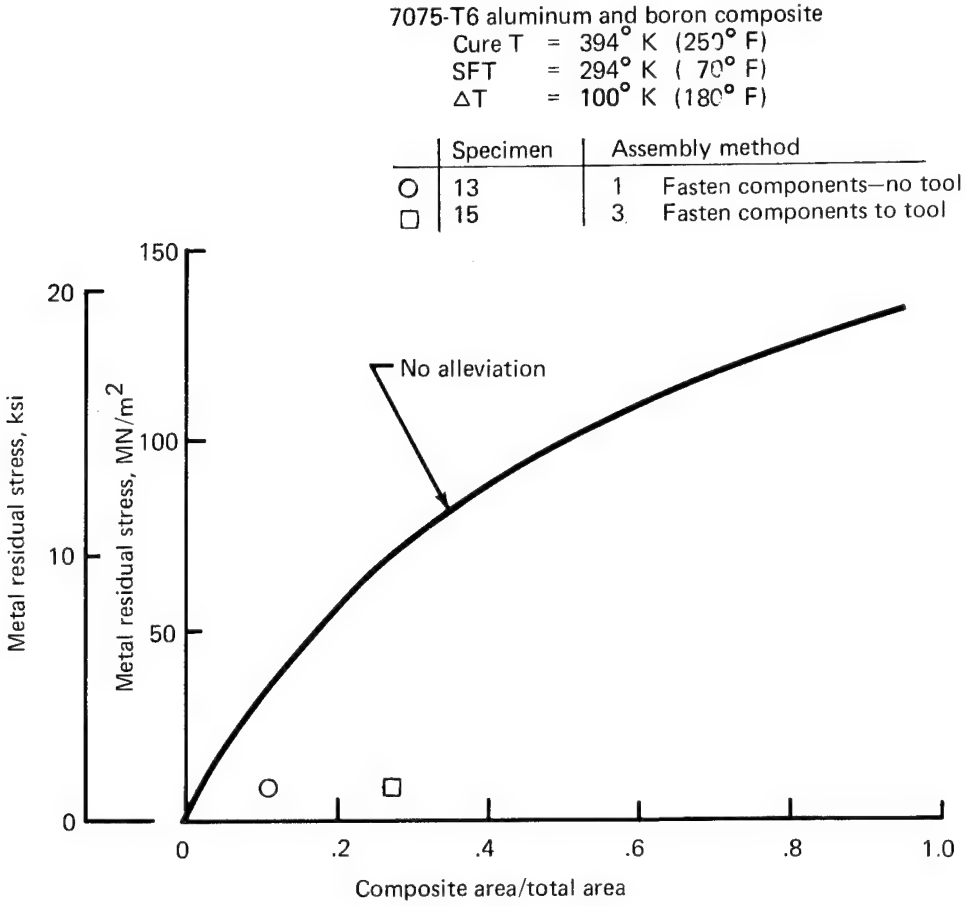

FIGURE 16.—SPECIFIC RESULTS—SPECIMENS 13 AND 15

7075-T6 aluminum and boron composite
Cure T = 394° K (250° F)
SFT = 339° K (150° F)
ΔT = 55° K (100° F)

	Specimen		Assembly methods
○	28	5	Preload metal and fasten all components to tool
□	32	6	Preload all components and fasten to tool

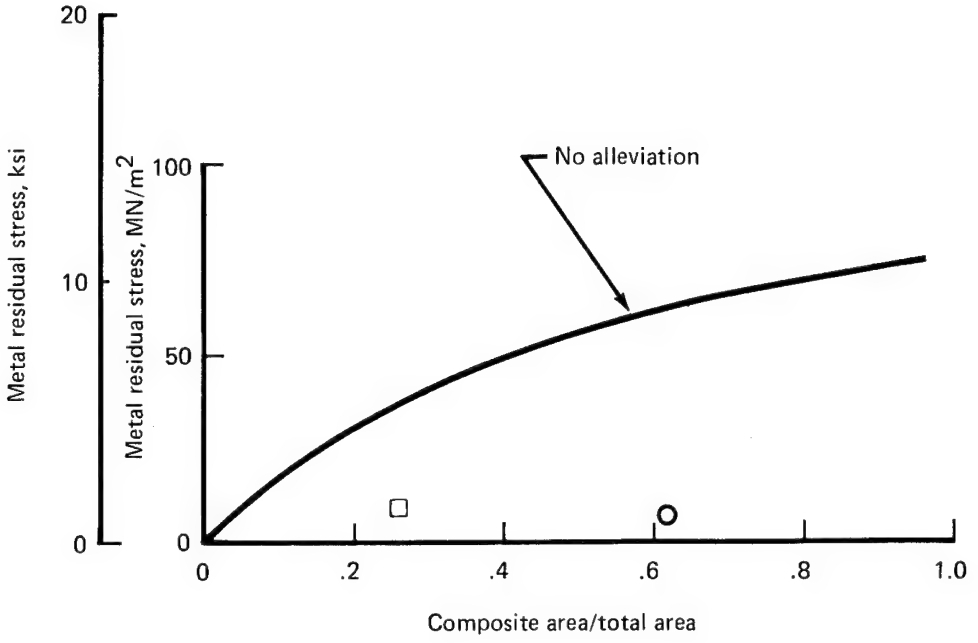

FIGURE 17.—SPECIFIC RESULTS—SPECIMENS 28 AND 32

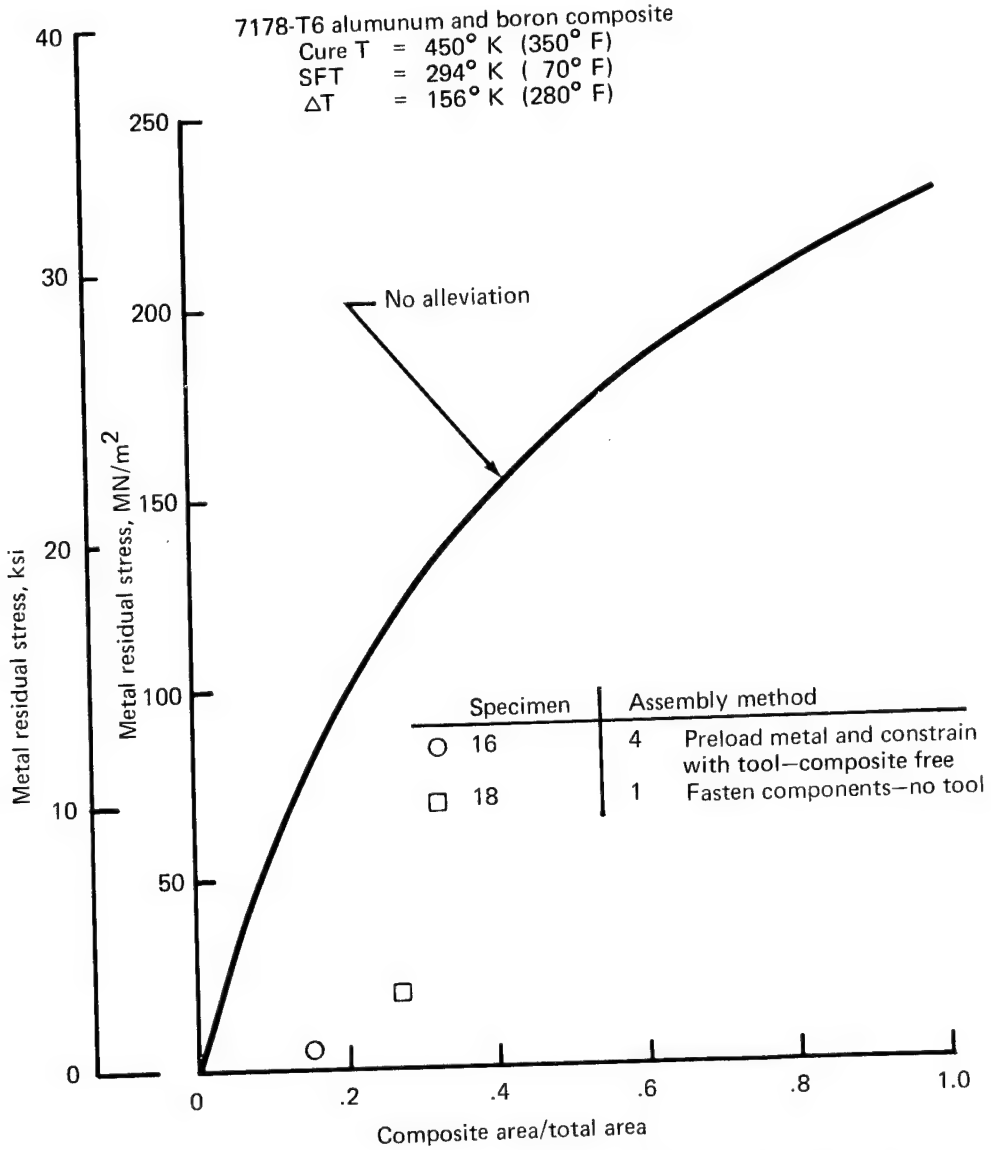

FIGURE 18.–SPECIFIC RESULTS–SPECIMENS 16 AND 18

7178-T6 aluminum and boron composite
Cure T = 394° K (250° F)
SFT = 339° K (150° F)
ΔT = 55° K (100° F)

	Specimen	Assembly method	
O	34	4	Preload metal and constrain with tool—composite free

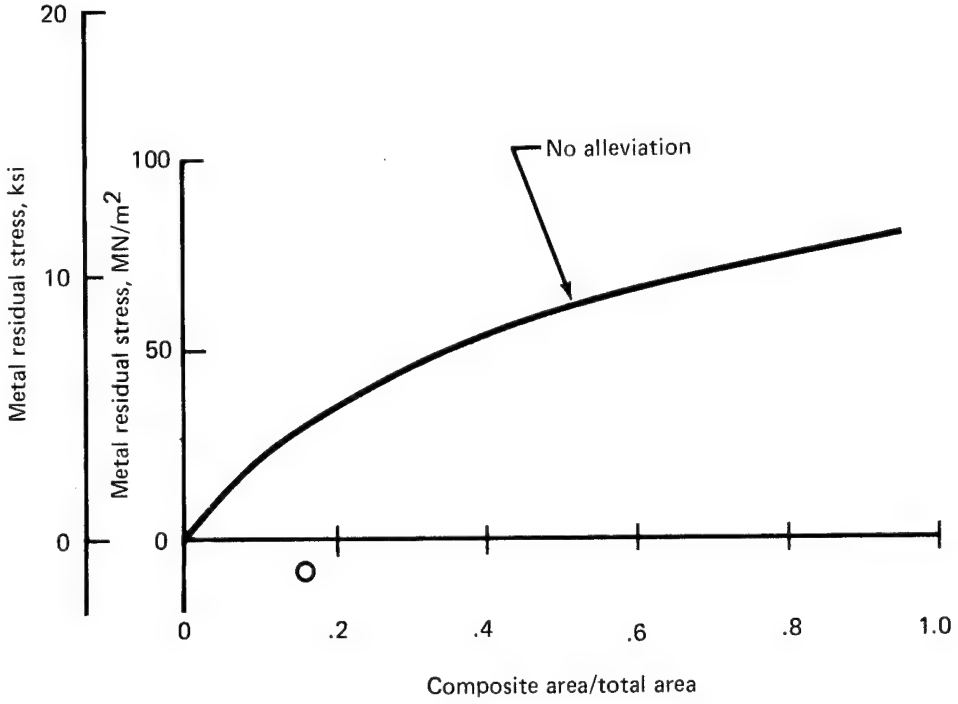

FIGURE 19.—SPECIFIC RESULTS—SPECIMEN 34

6Al-4V titanium and boron composite
Cure T = 450° K (350° F)
SFT = 294° K (70° F)
ΔT = 156° K (280° F)

	Specimen	Assembly method	
O	3	3	Fasten components to tool

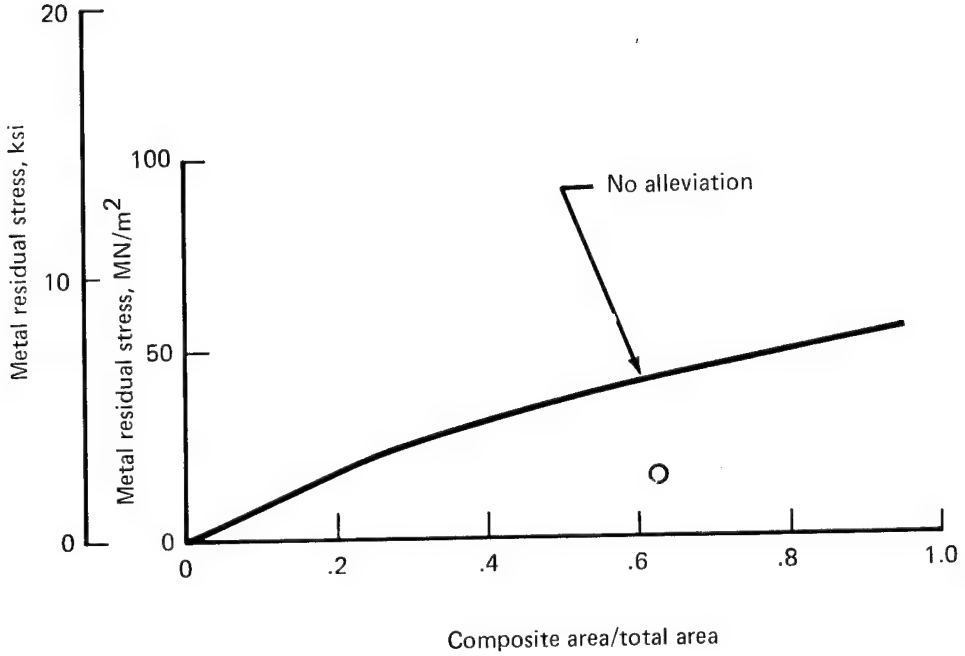

FIGURE 20.–SPECIFIC RESULTS–SPECIMEN 3

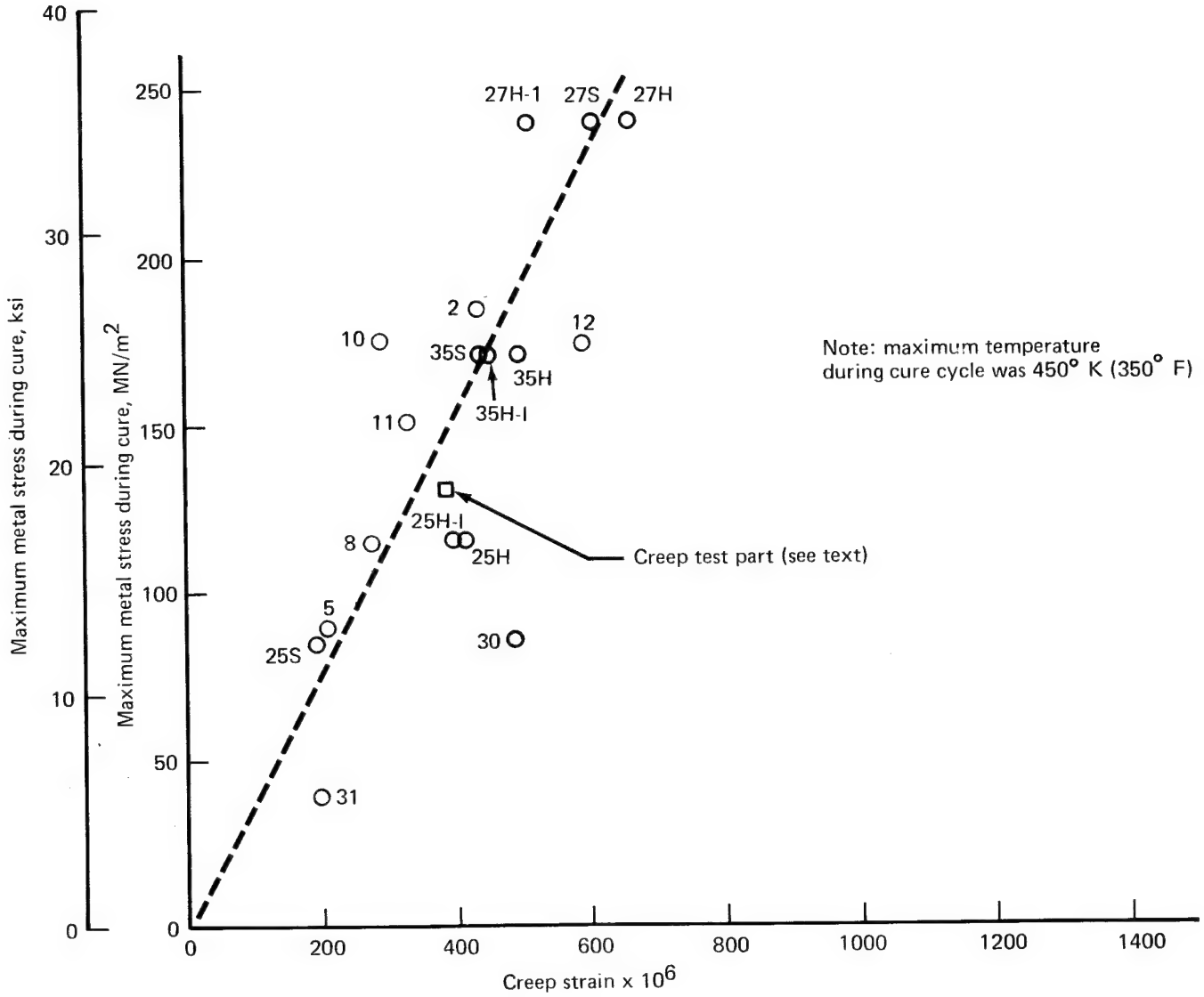

FIGURE 21.–CREEP DEFORMATION OF ALLOY 7075-T6

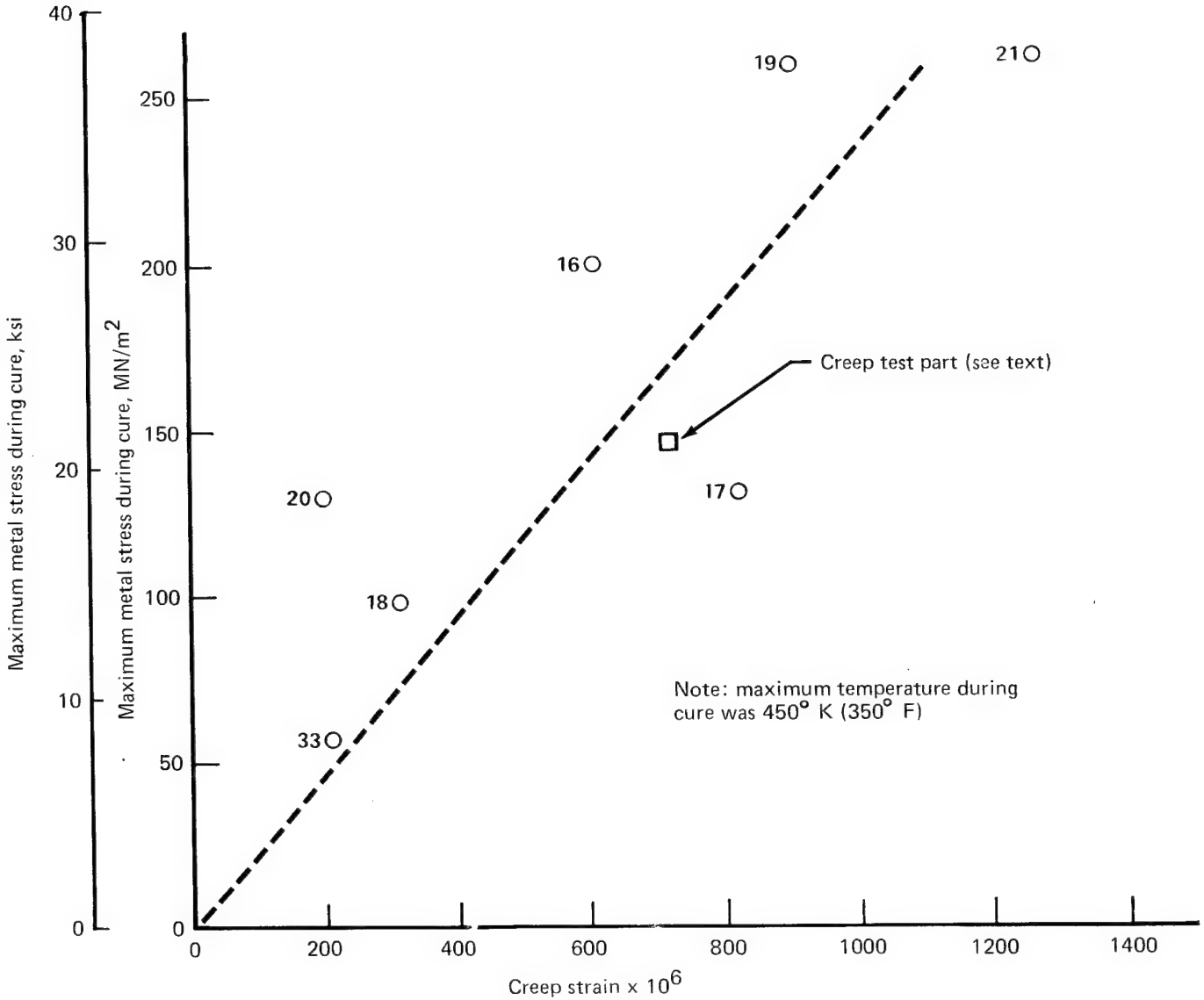

FIGURE 22.–CREEP DEFORMATION OF ALLOY 7178-T6

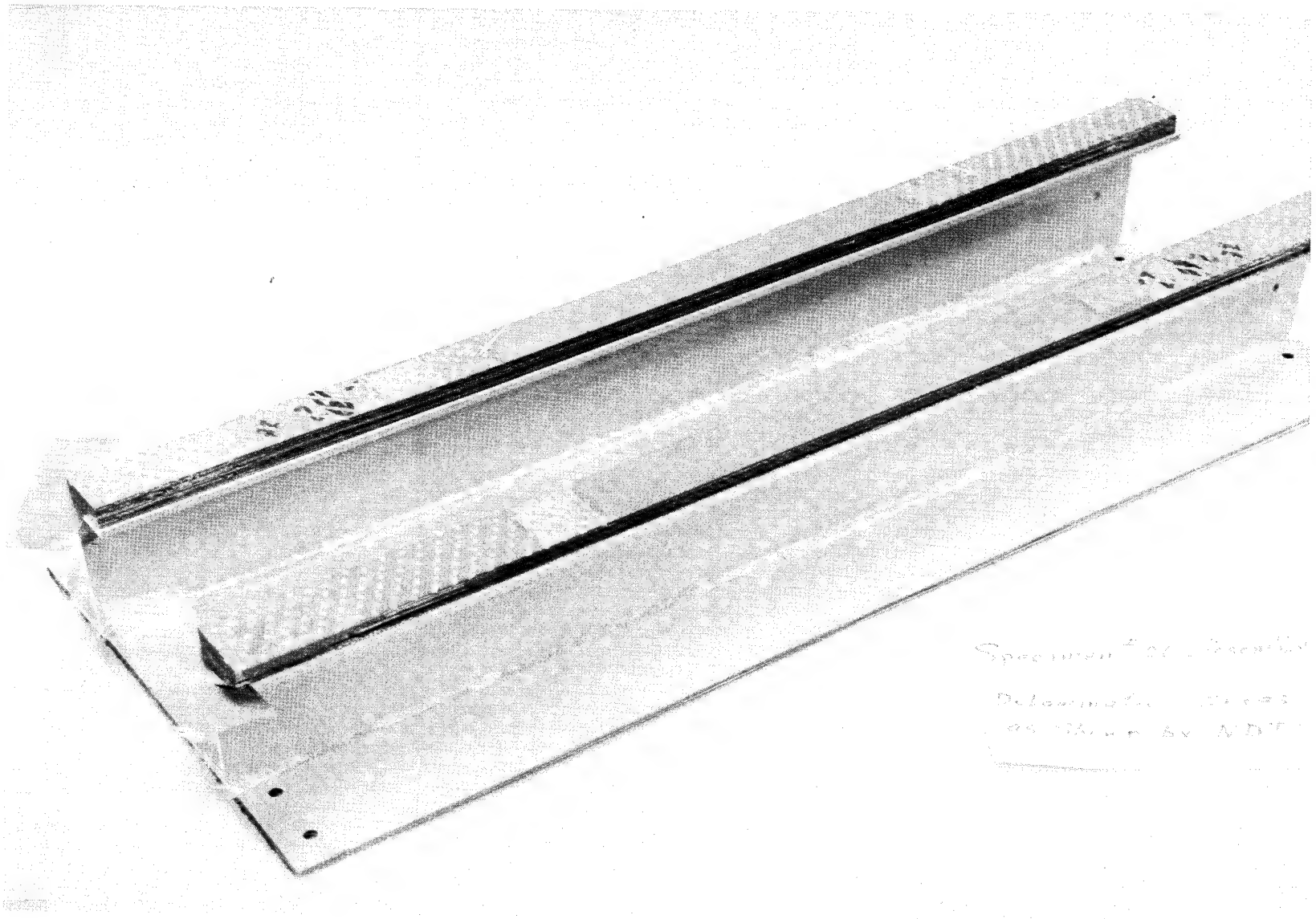

FIGURE 23.–PANEL ASSEMBLY WITH GROSS DELAMINATION

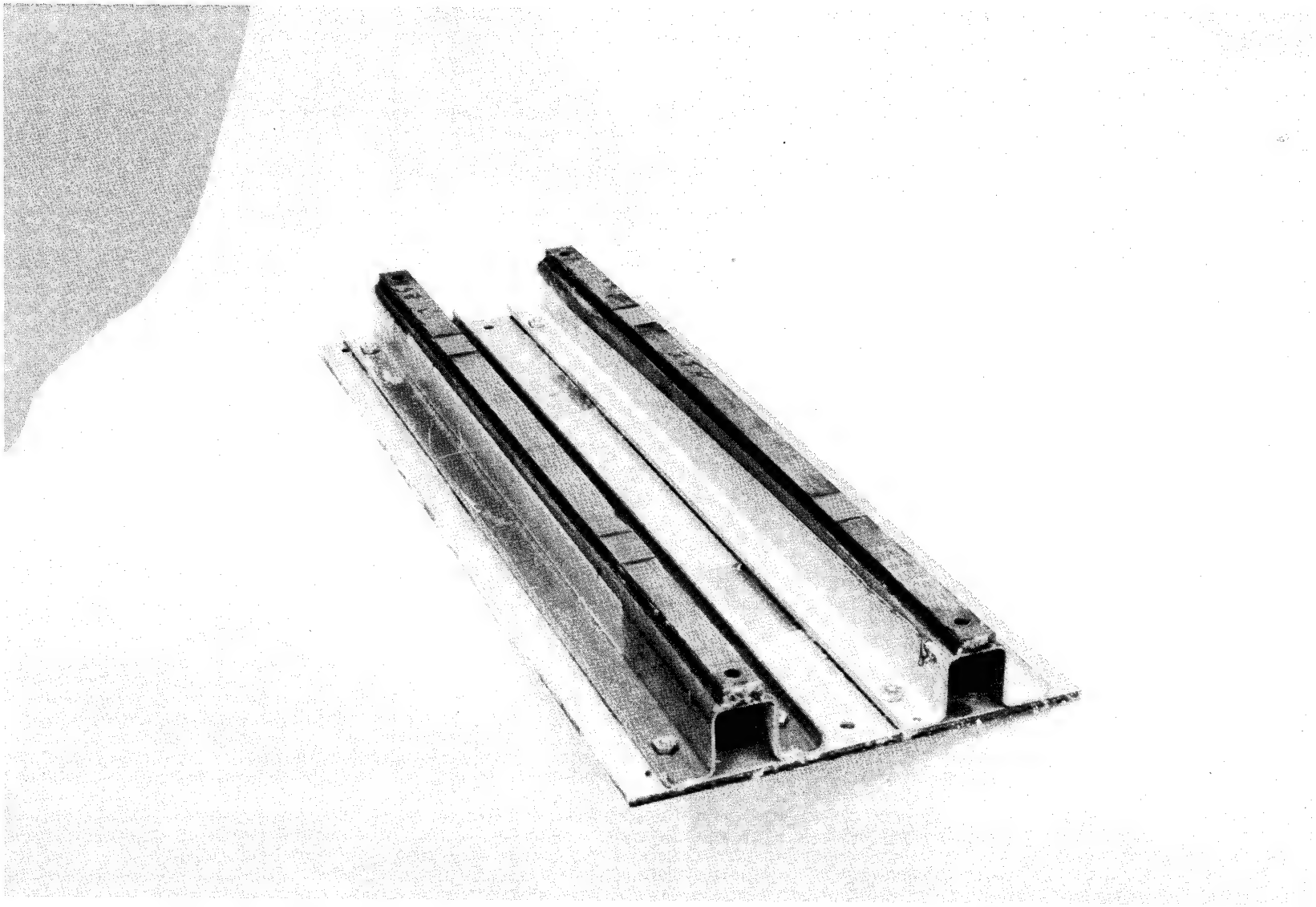

FIGURE 24.—PANEL ASSEMBLY WITH STEP FITTING DELAMINATION

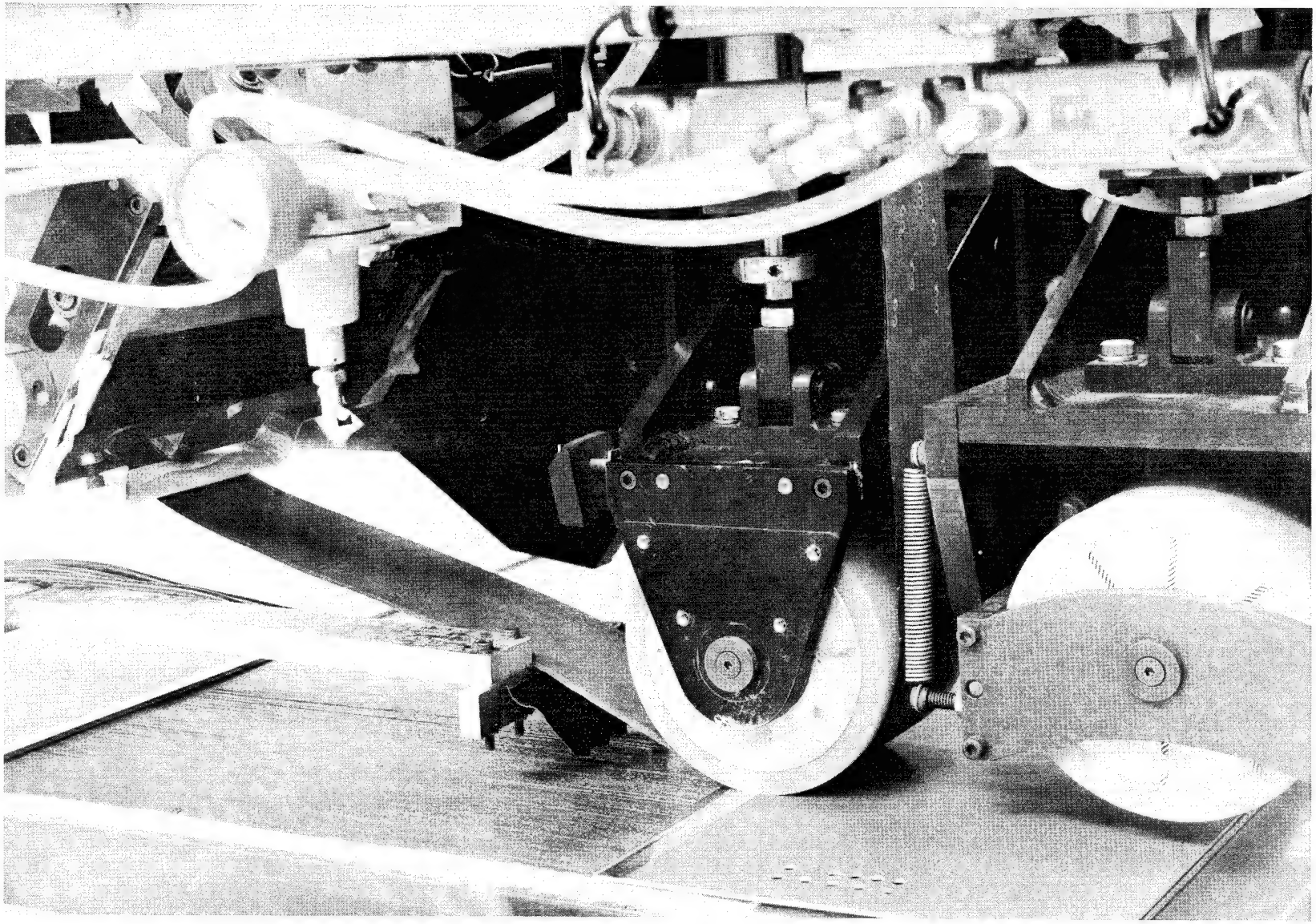

FIGURE 25.—TAPE LAYUP MACHINE

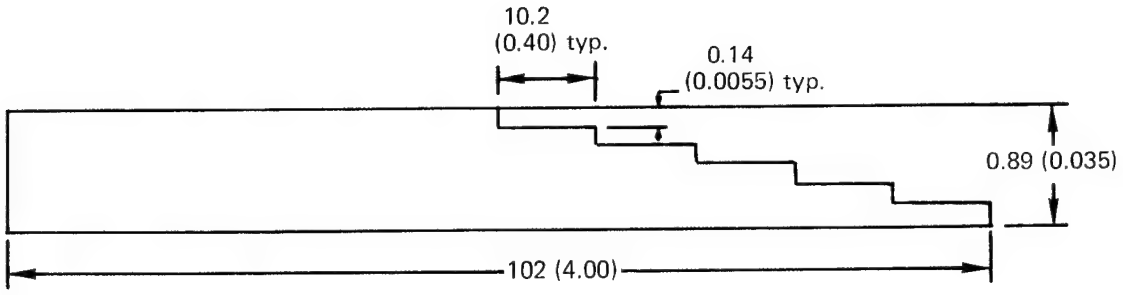

Titanium End Fitting For Boron Composite

Dimensions in mm (inches)

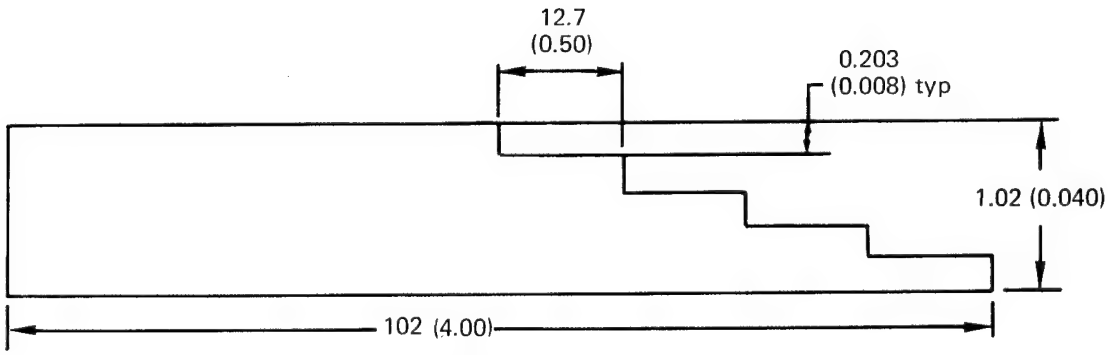

Titanium End Fitting For Graphite Composite

FIGURE 26.—TITANIUM STEPPED FITTING DESIGN

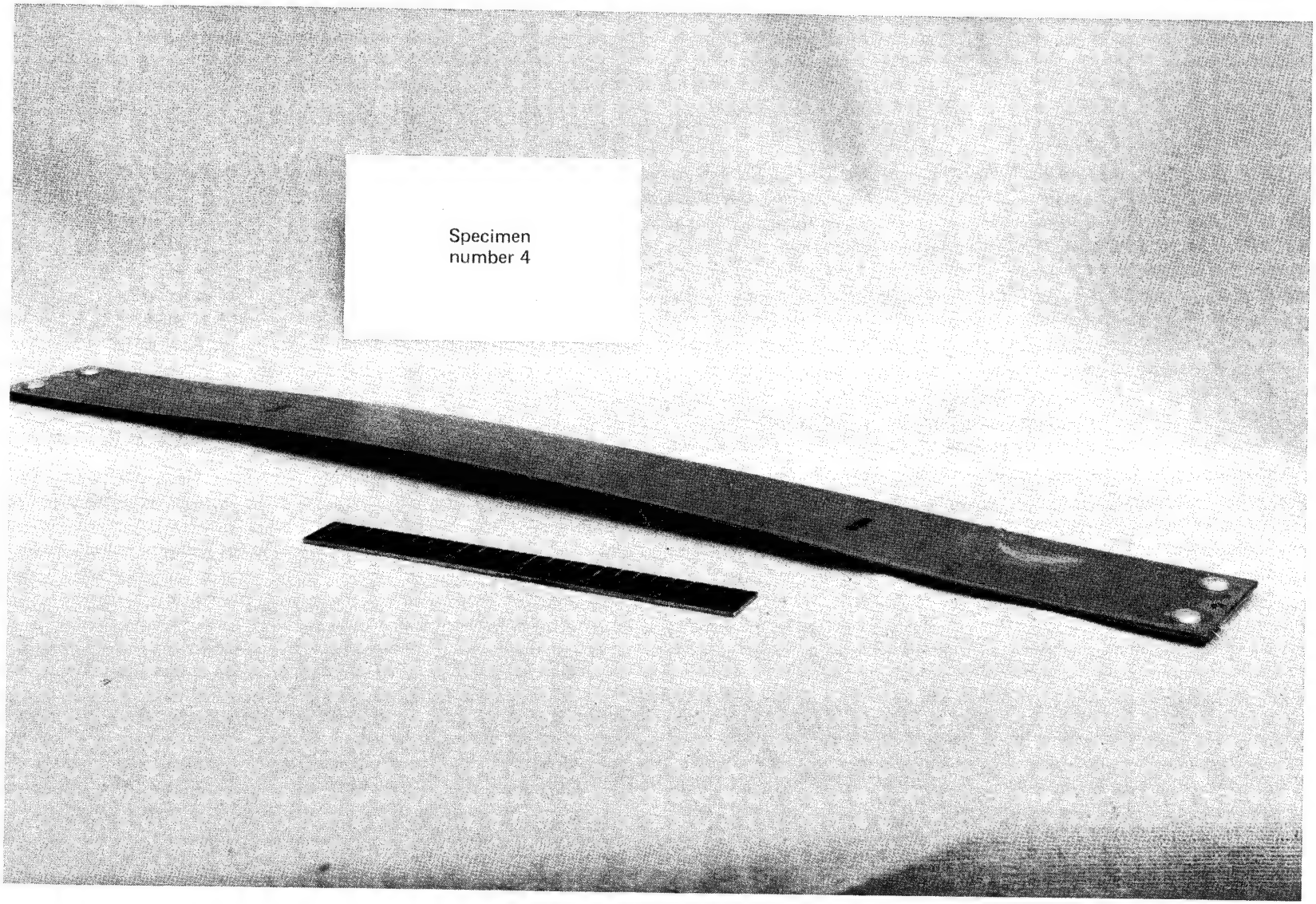

FIGURE 27.—SHEET SPECIMEN FABRICATED BY METHOD 1

FIGURE 28.—HAT STIFFENER FABRICATED BY METHOD 1

FIGURE 29.–METHOD 1 PART IN ENVELOPE BAG

FIGURE 30.—ZEE STIFFENER FABRICATED BY METHOD 1

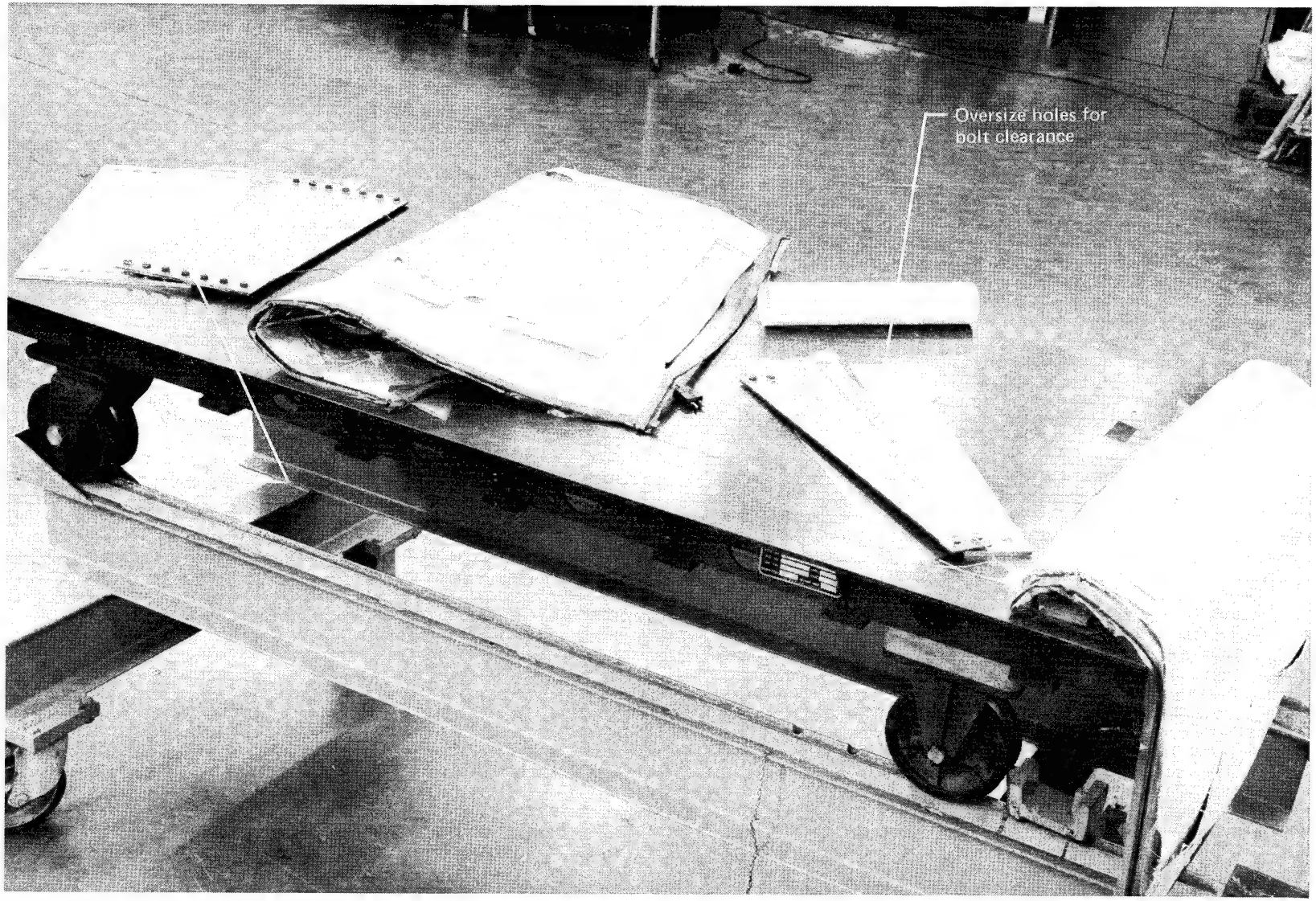

FIGURE 31.–SHEET SPECIMENS FABRICATED BY METHOD 2

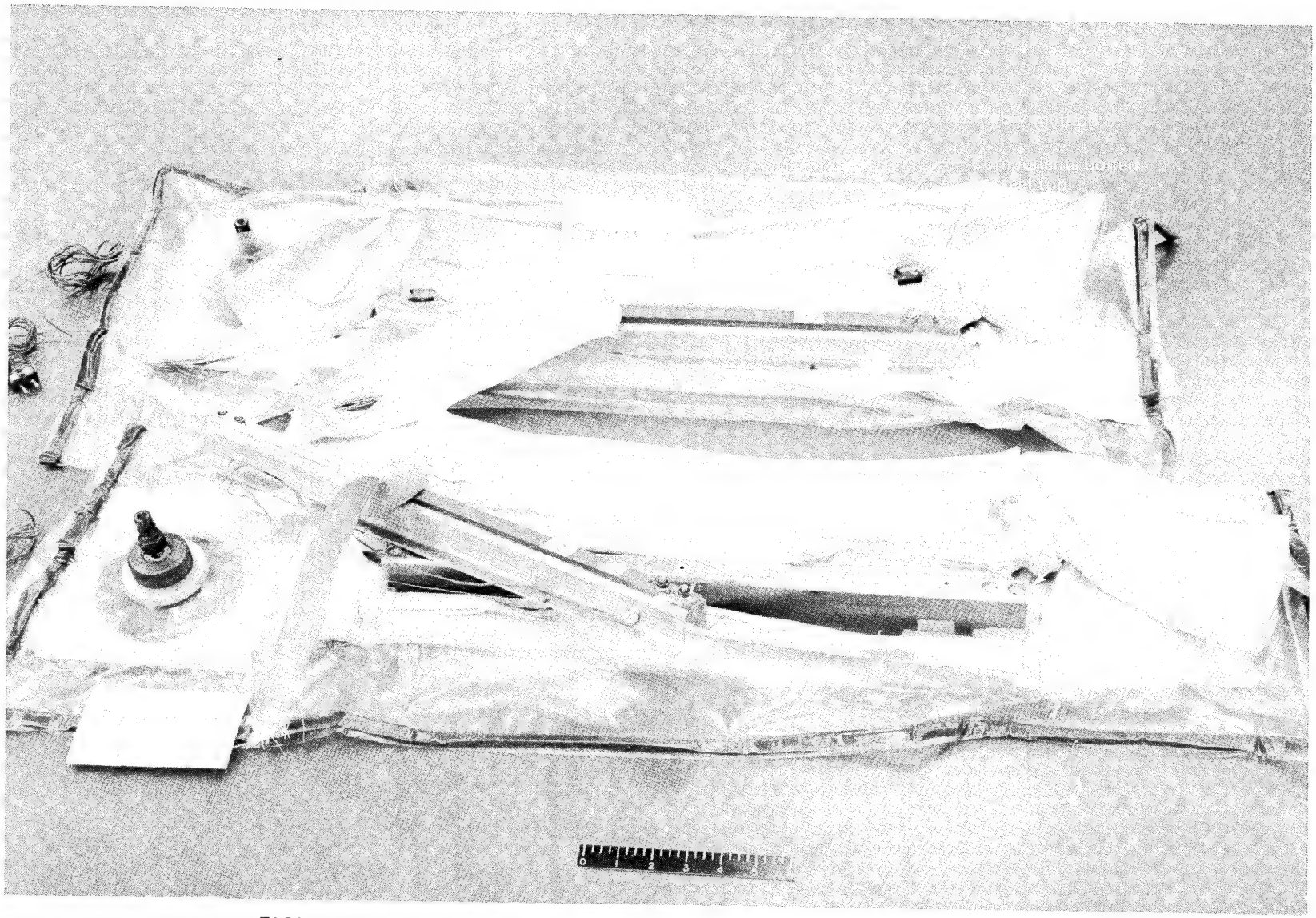

FIGURE 32.—HAT STIFFENERS FABRICATED BY METHODS 2 AND 3

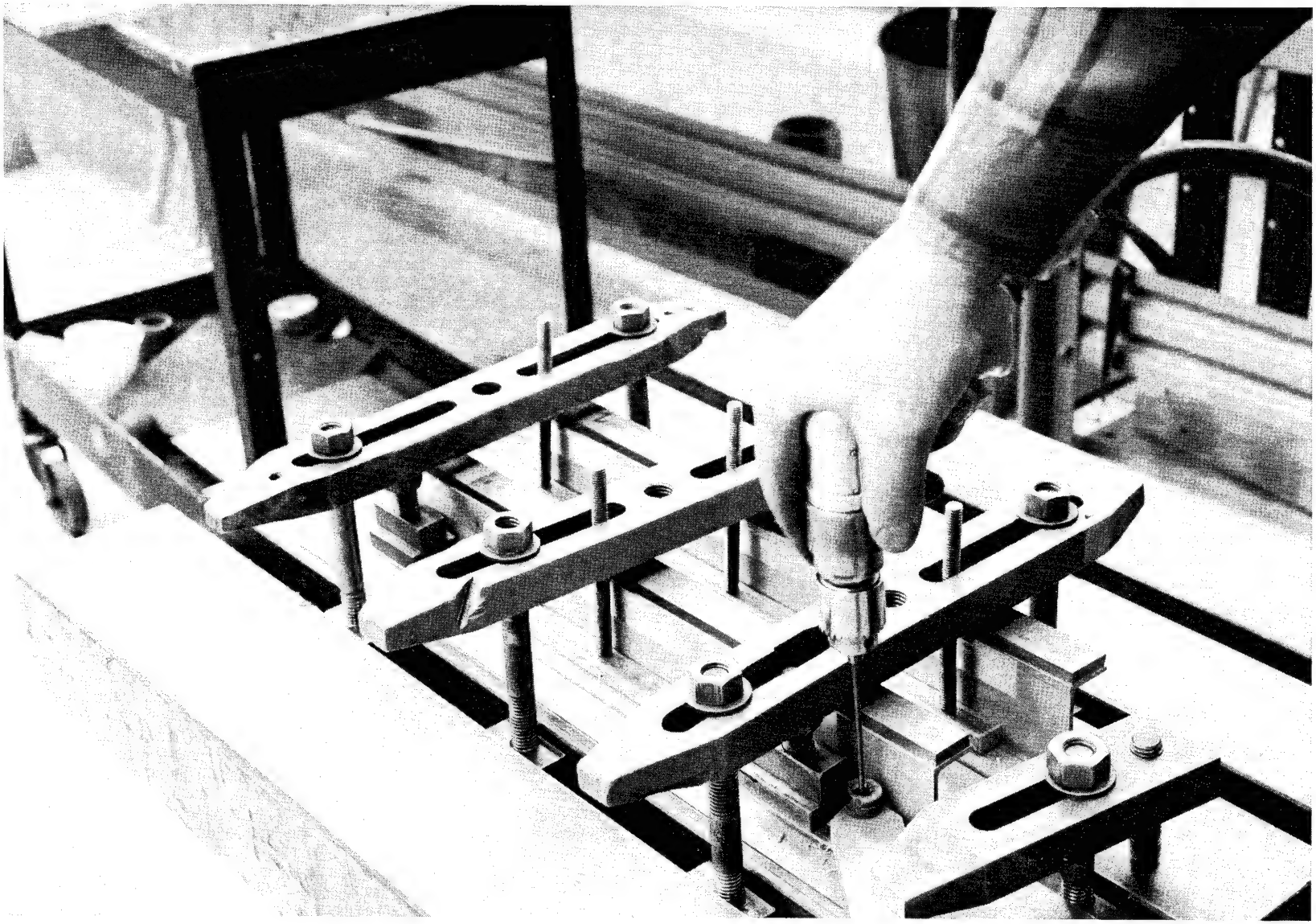

FIGURE 33.—CLAMPING TECHNIQUE

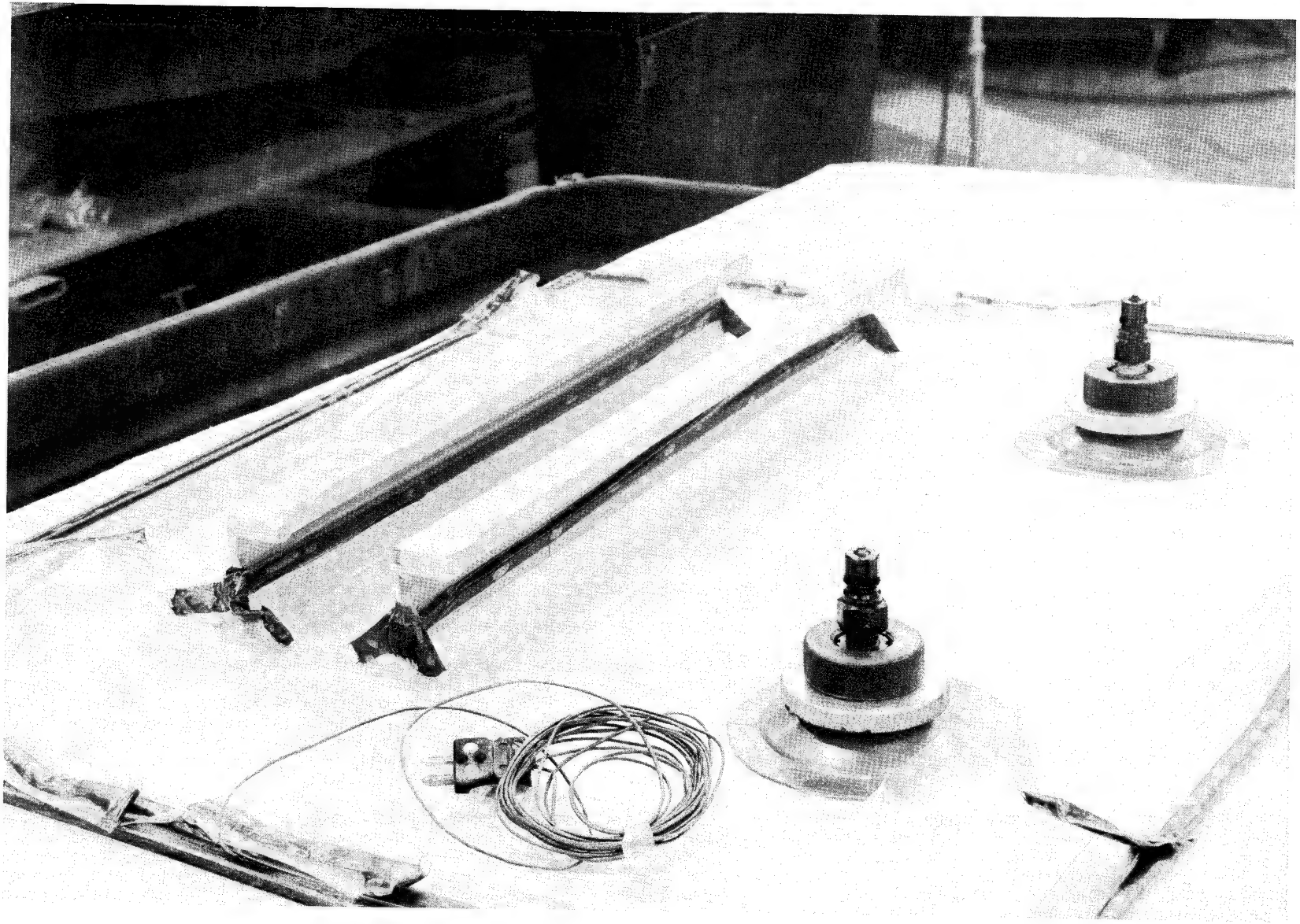

FIGURE 34.—PANEL ASSEMBLY READY FOR CURING

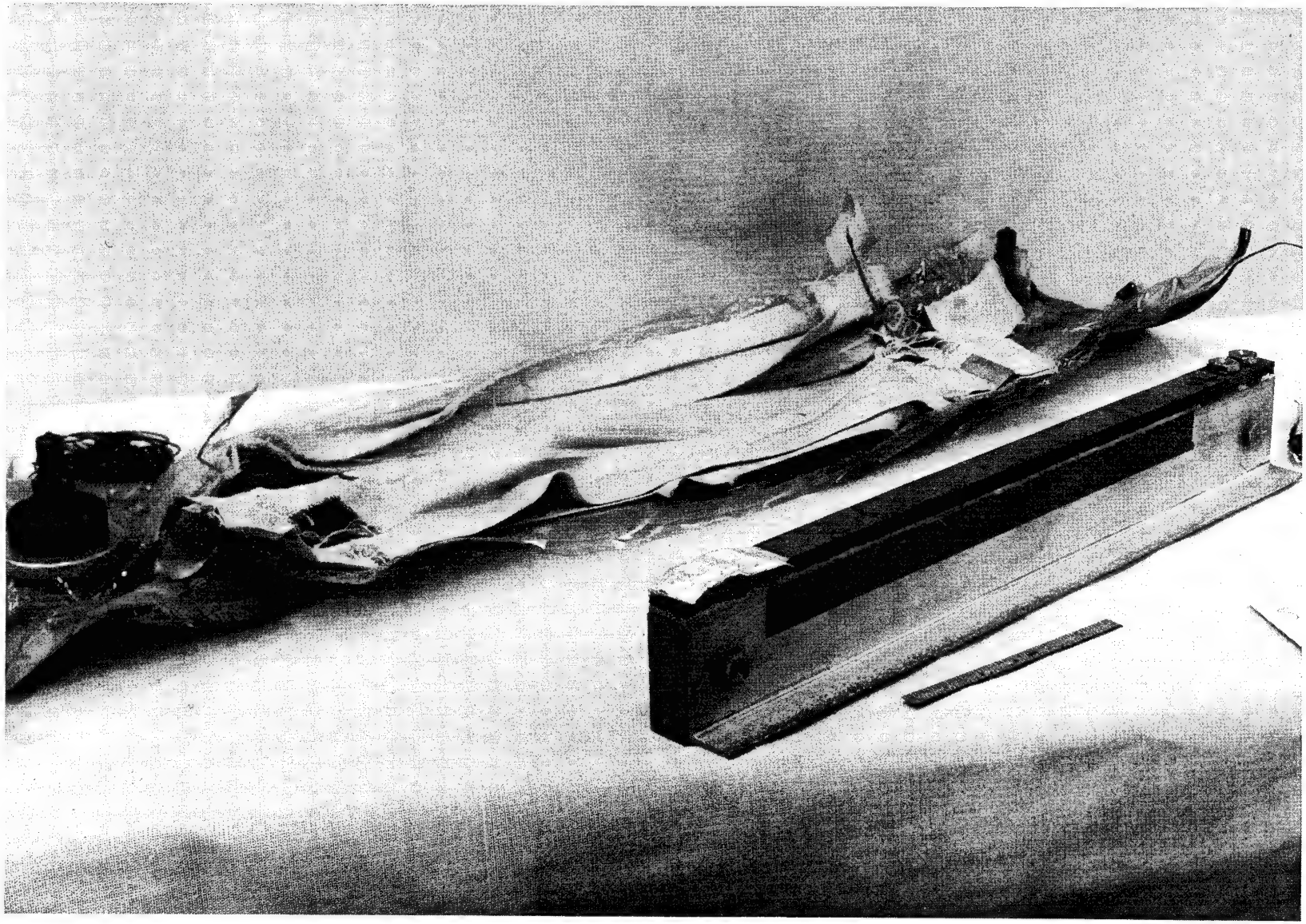

FIGURE 35.—ZEE STIFFENER AND METHOD 3 STEEL TOOL

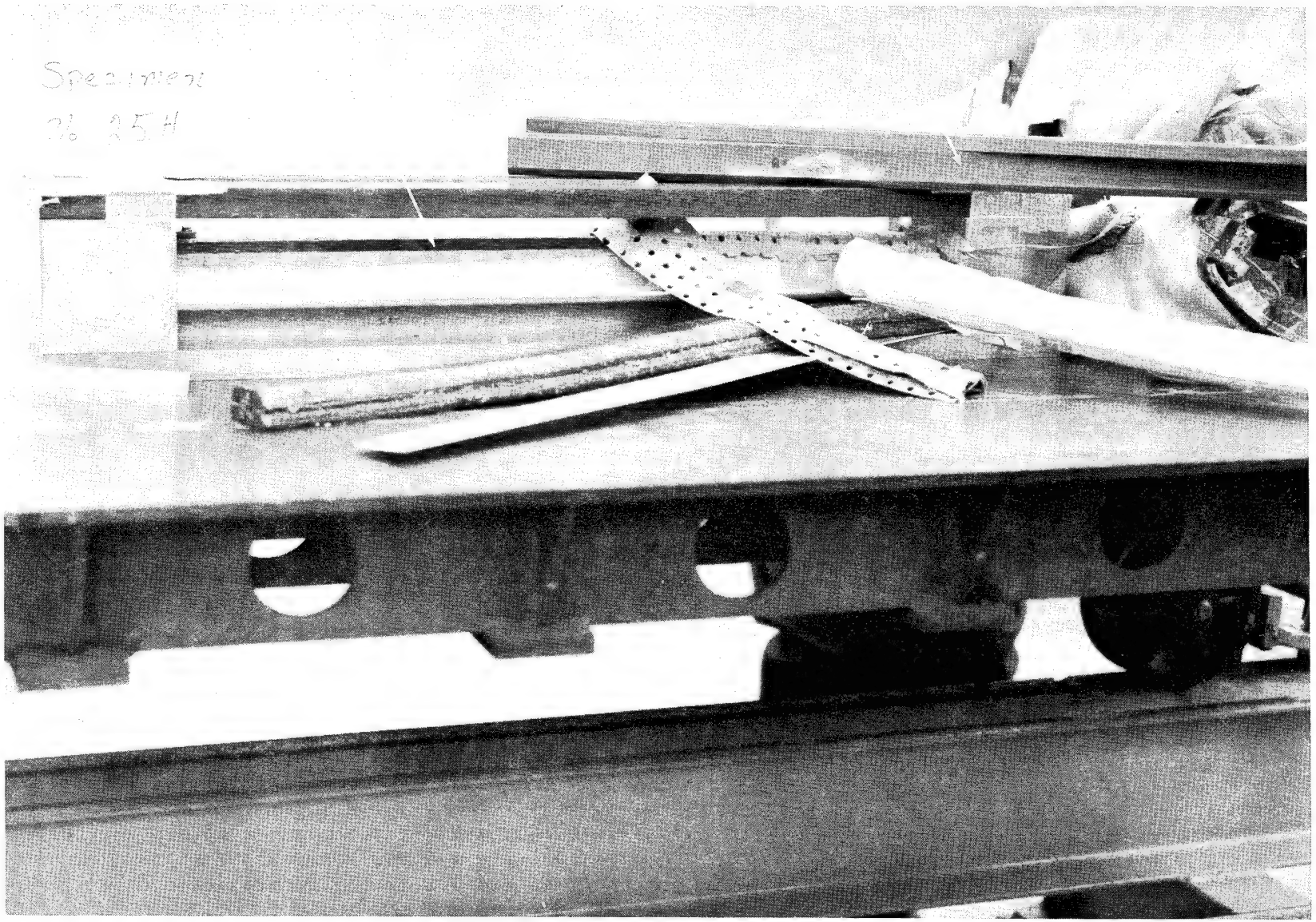

FIGURE 36.—BENDING-RESISTANT TOOL

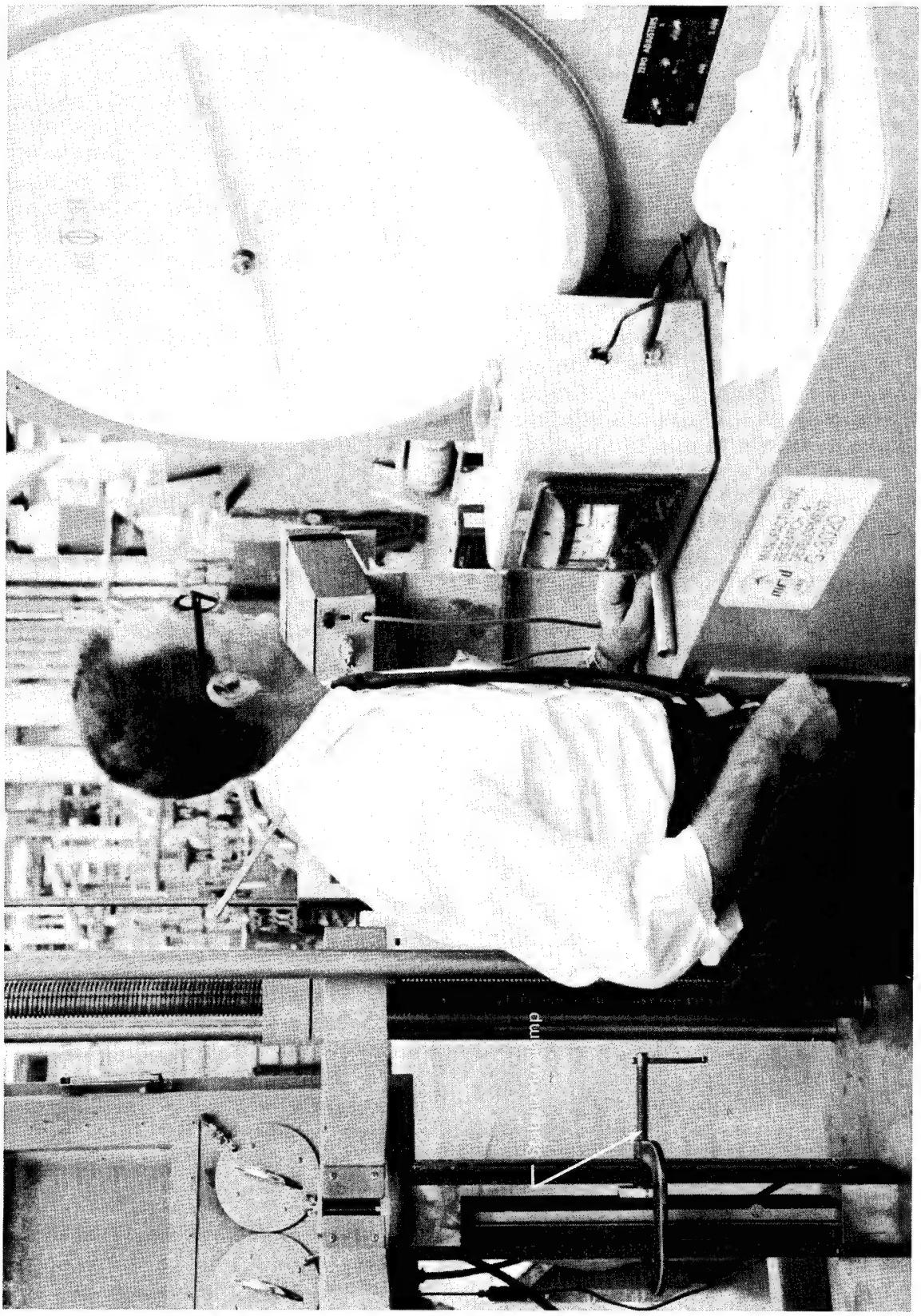

FIGURE 37.–PRELOADING HAT STIFFENER IN TOOL

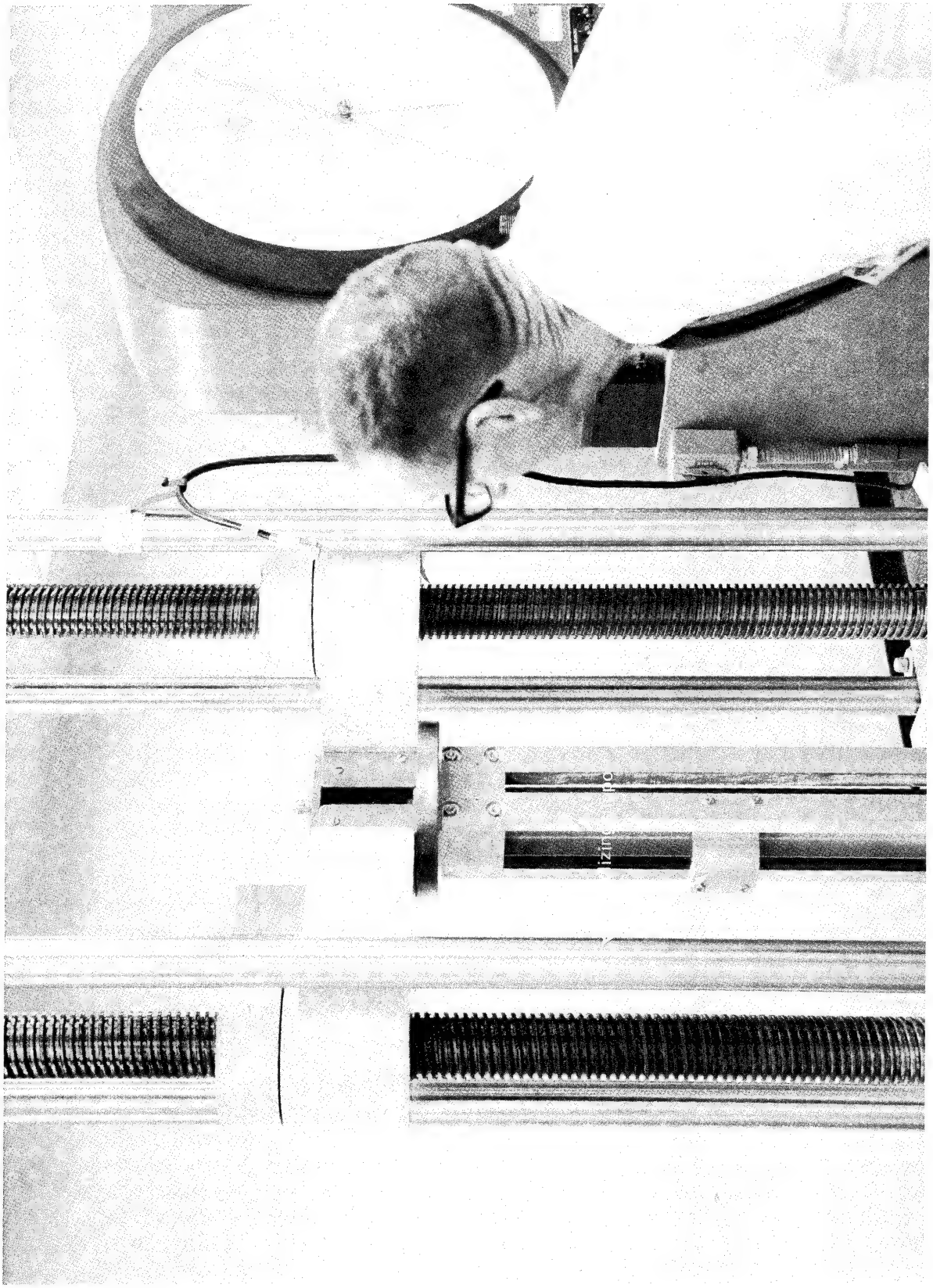

FIGURE 38.—PRELOADED ZEE SECTION SHOWING BUCKLING RESTRAINT

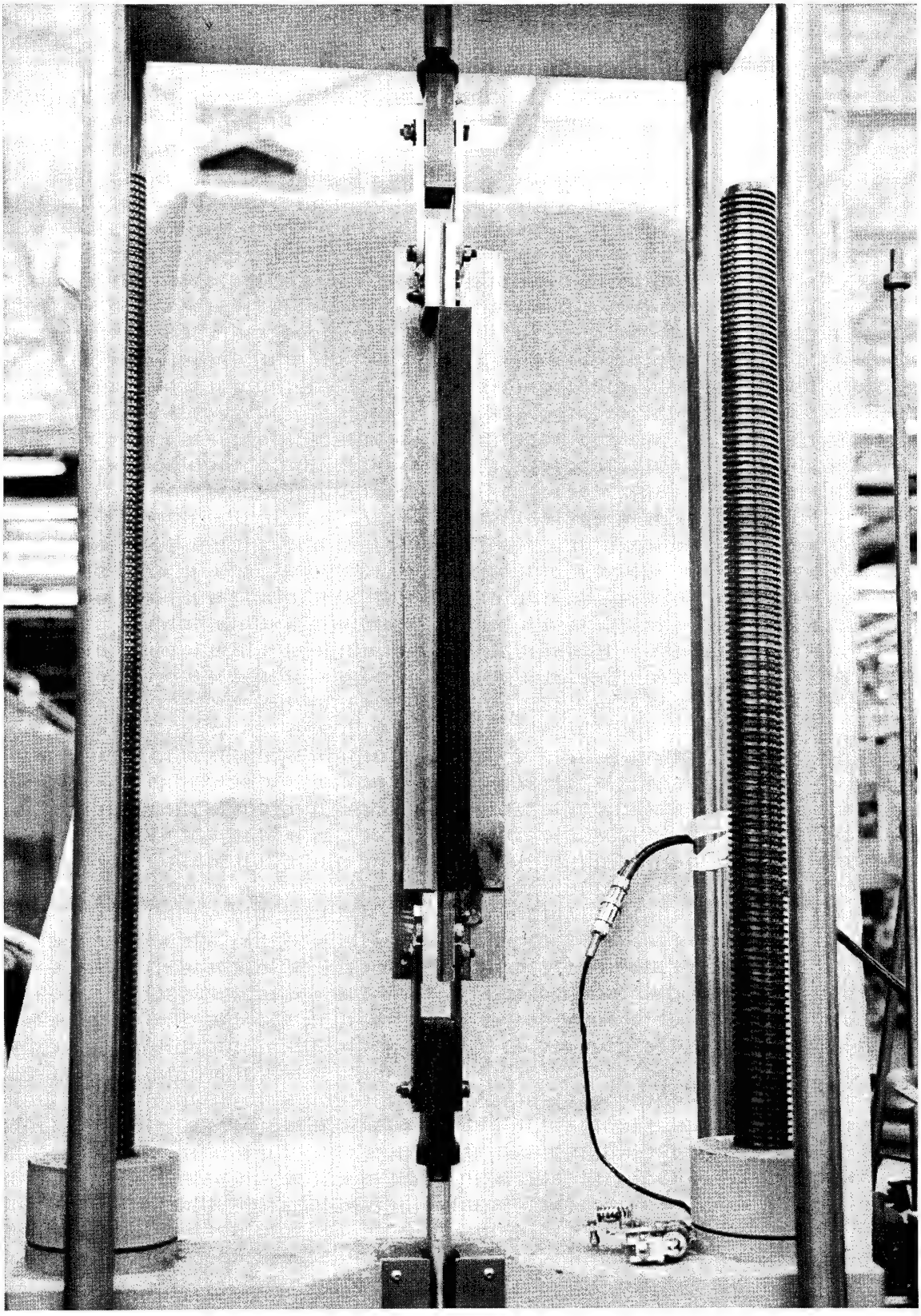

FIGURE 39.—PRELOADING ZEE SECTION IN TENSION

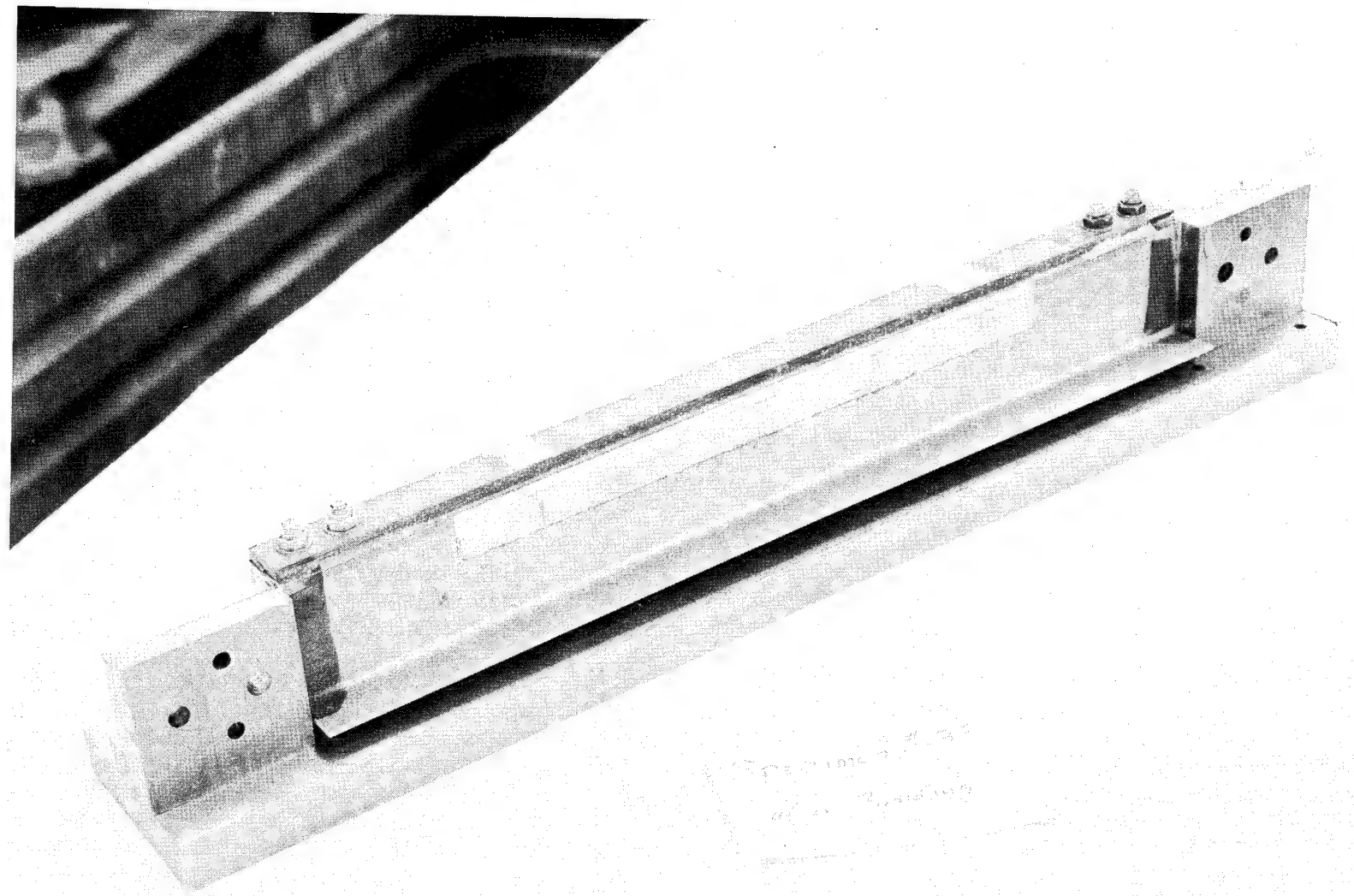

FIGURE 40.—COMPLETED ZEE SECTION IN TOOL

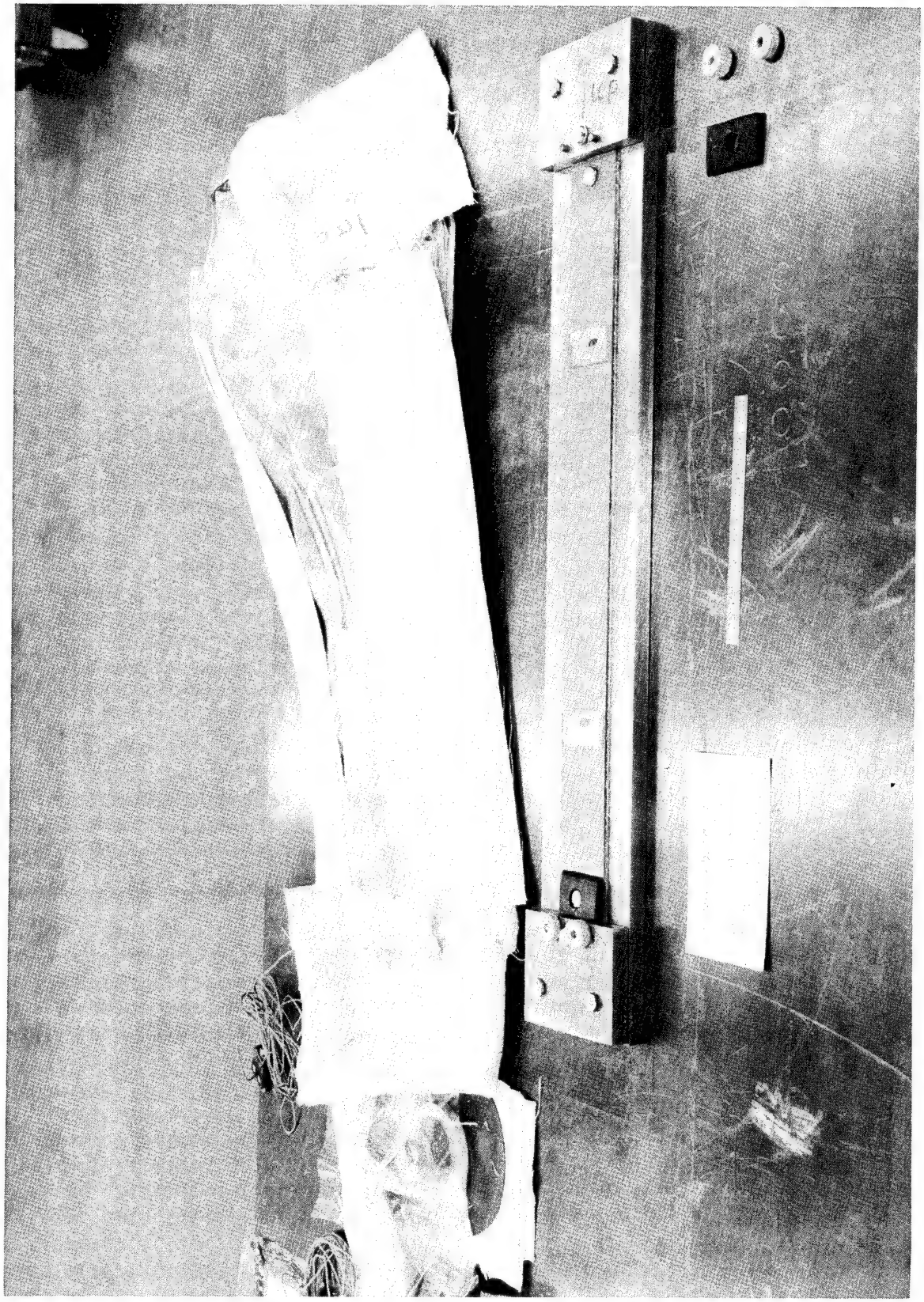

FIGURE 41.—COMPLETED SHEET SECTION IN TOOL

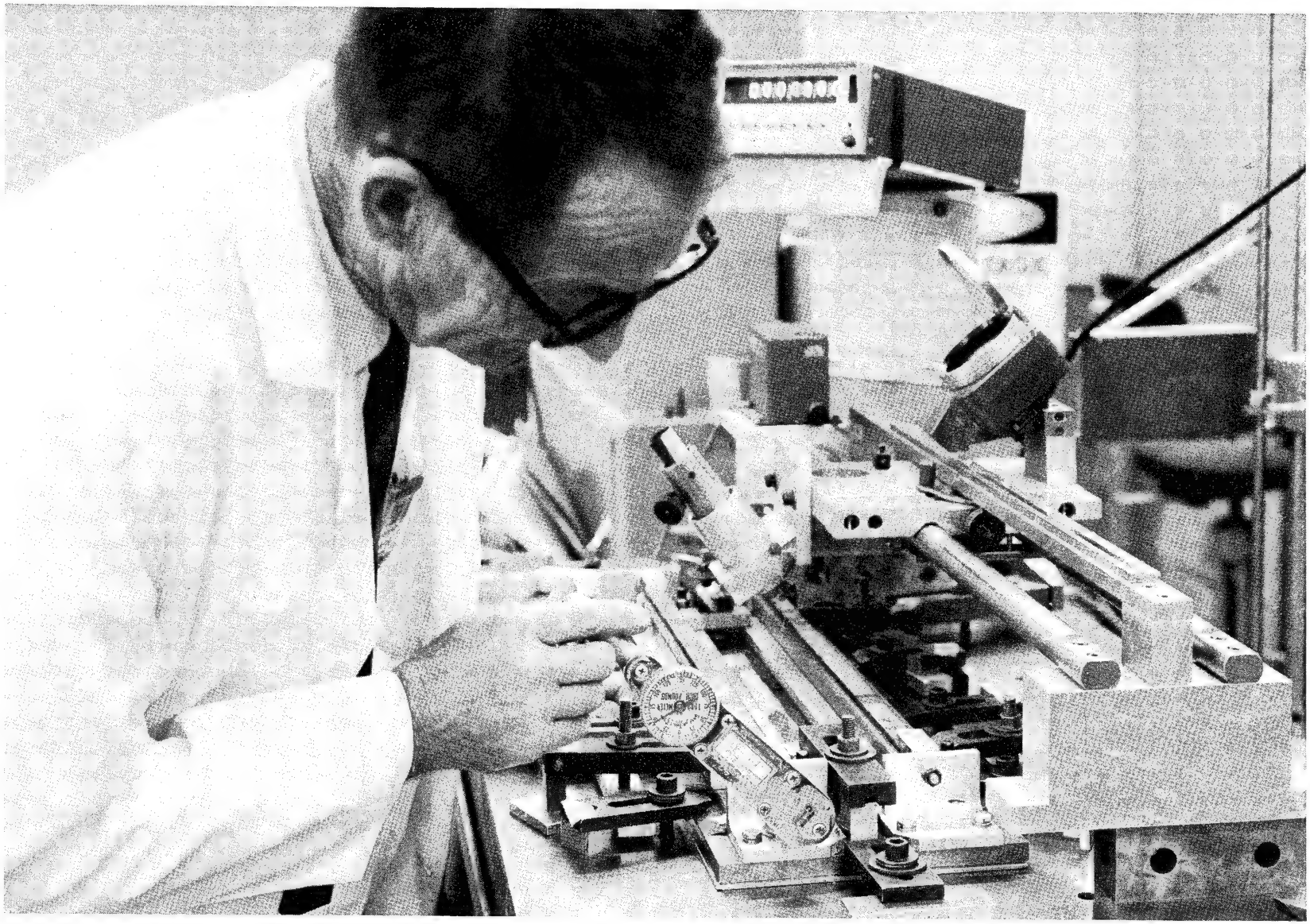

FIGURE 42.—PRELOADING HAT STIFFENERS FOR PANEL ASSEMBLY NUMBER 35

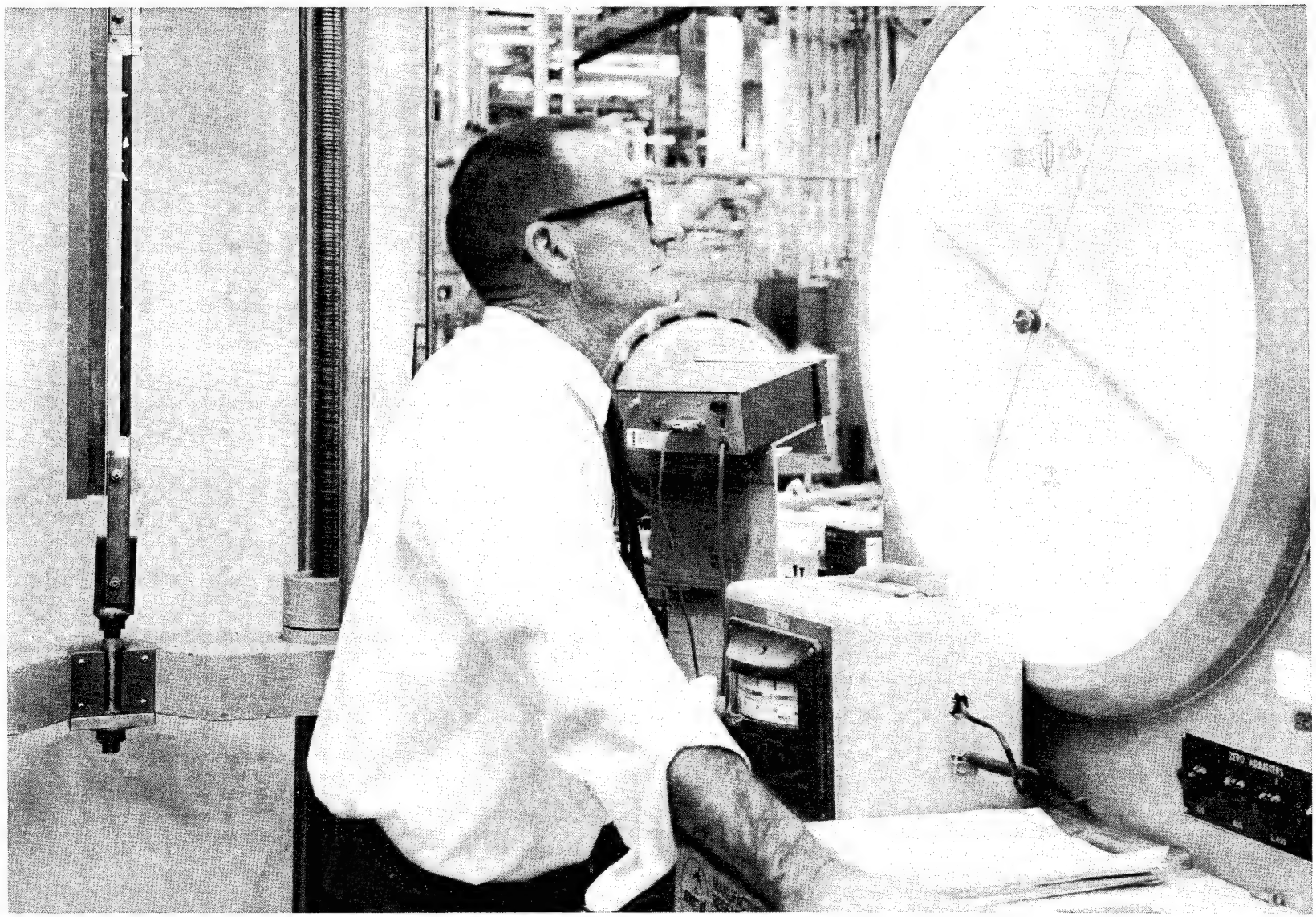

FIGURE 43.—PRELOADING HAT STIFFENER IN TENSION

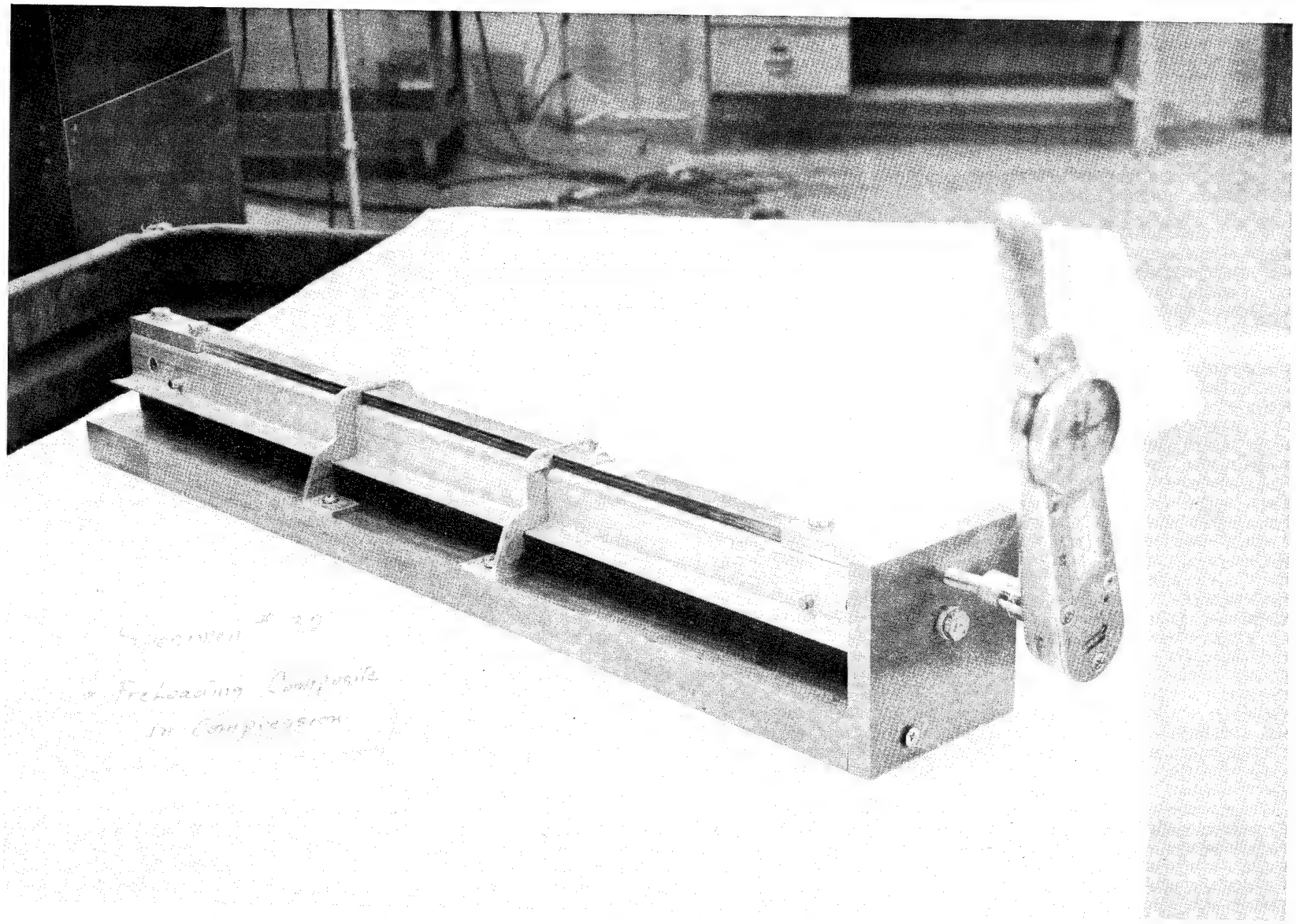

FIGURE 44.—PRELOADING COMPOSITE STRAP IN COMPRESSION, SHOWING STABILIZING ELEMENTS

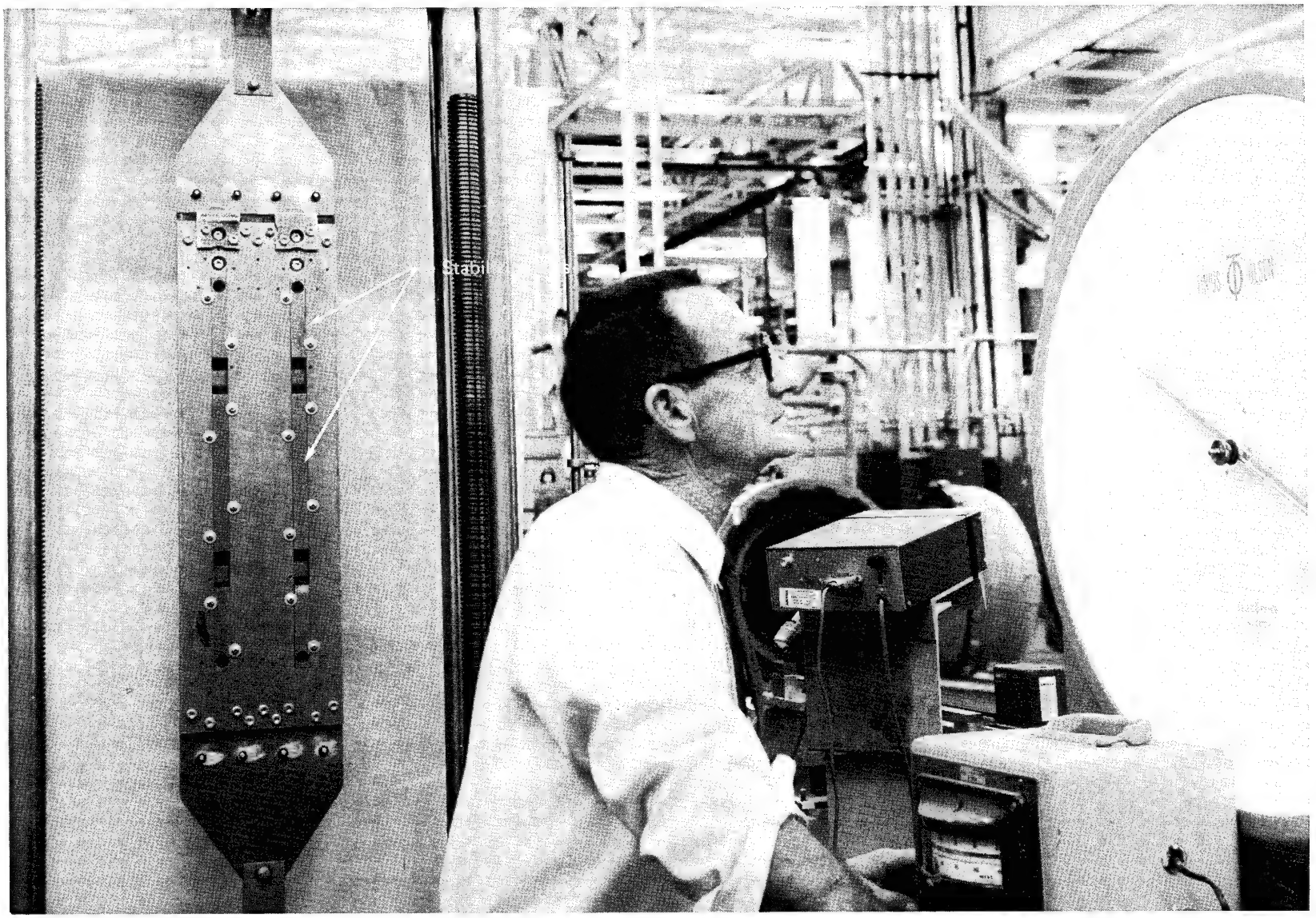

FIGURE 45.—PRELOADING SHEET IN TENSION

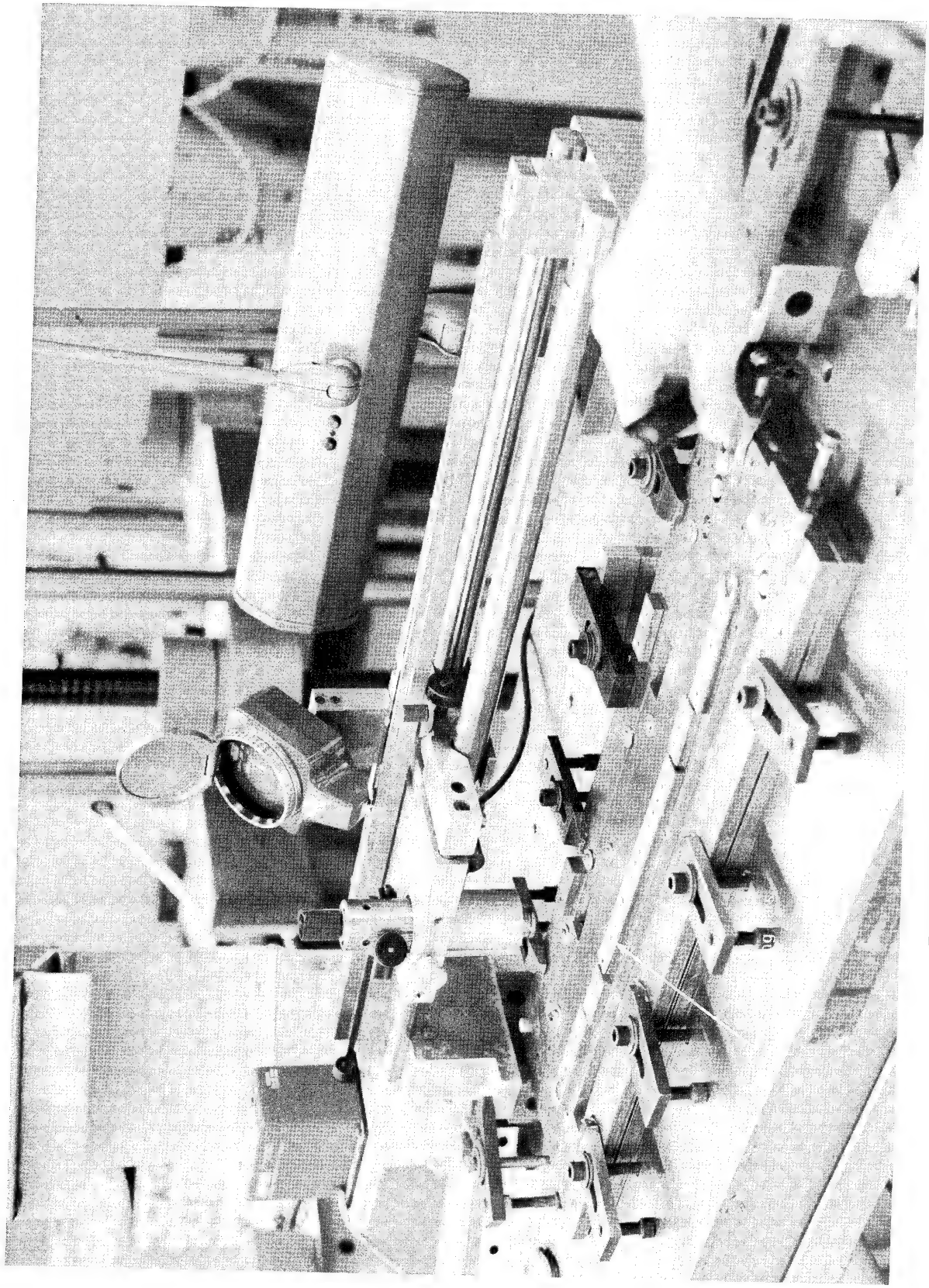

FIGURE 46.—PRELOADING STRAPS IN COMPRESSION

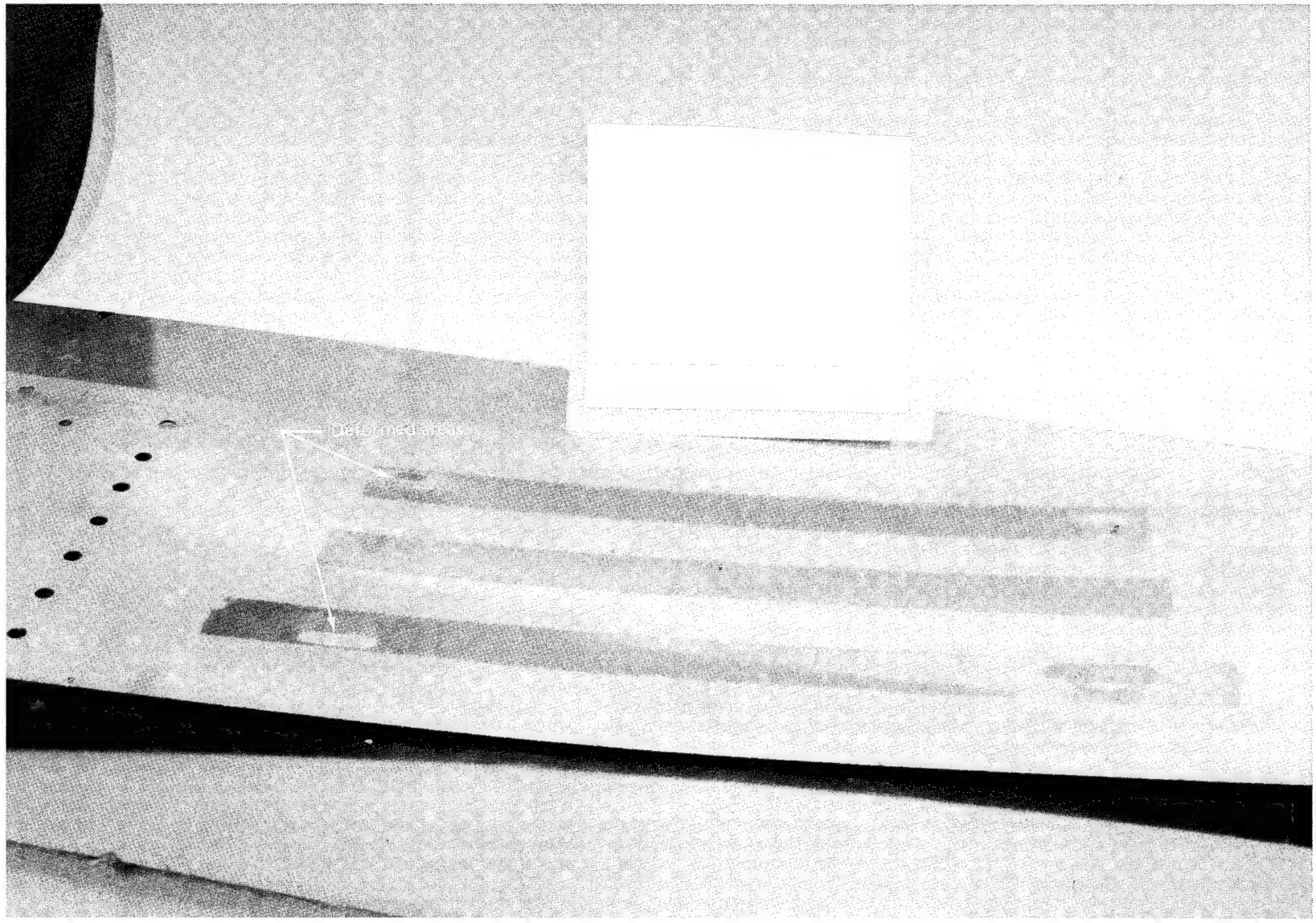

FIGURE 47.—SPECIMEN 30 SHOWING AREAS DEFORMED BY RUBBER PLUGS

FIGURE 48. LOADING COOLED ZEE STIFFENER IN TOOL

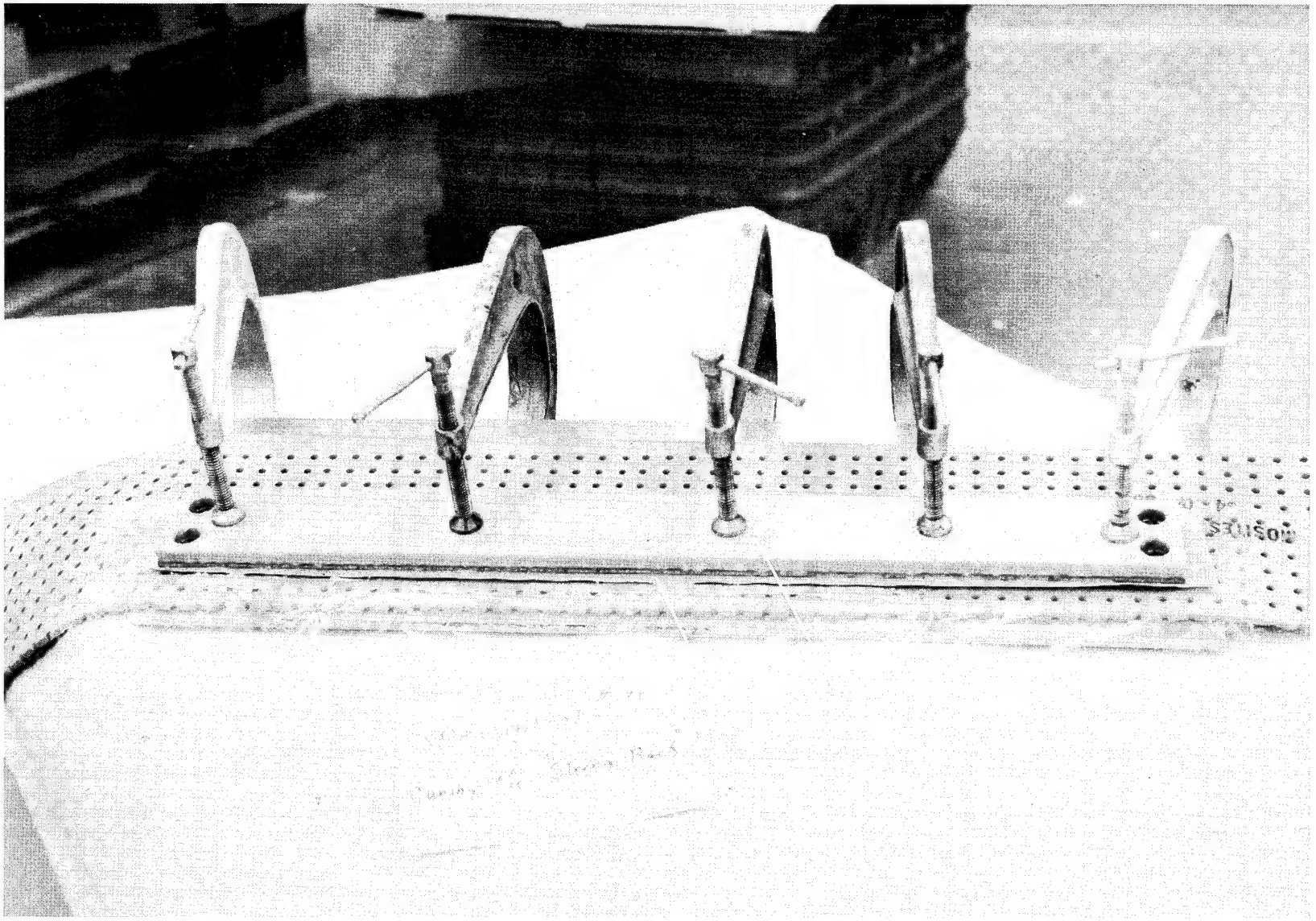

FIGURE 49.—ASSEMBLING FIBERGLASS TOOL TO SHEET

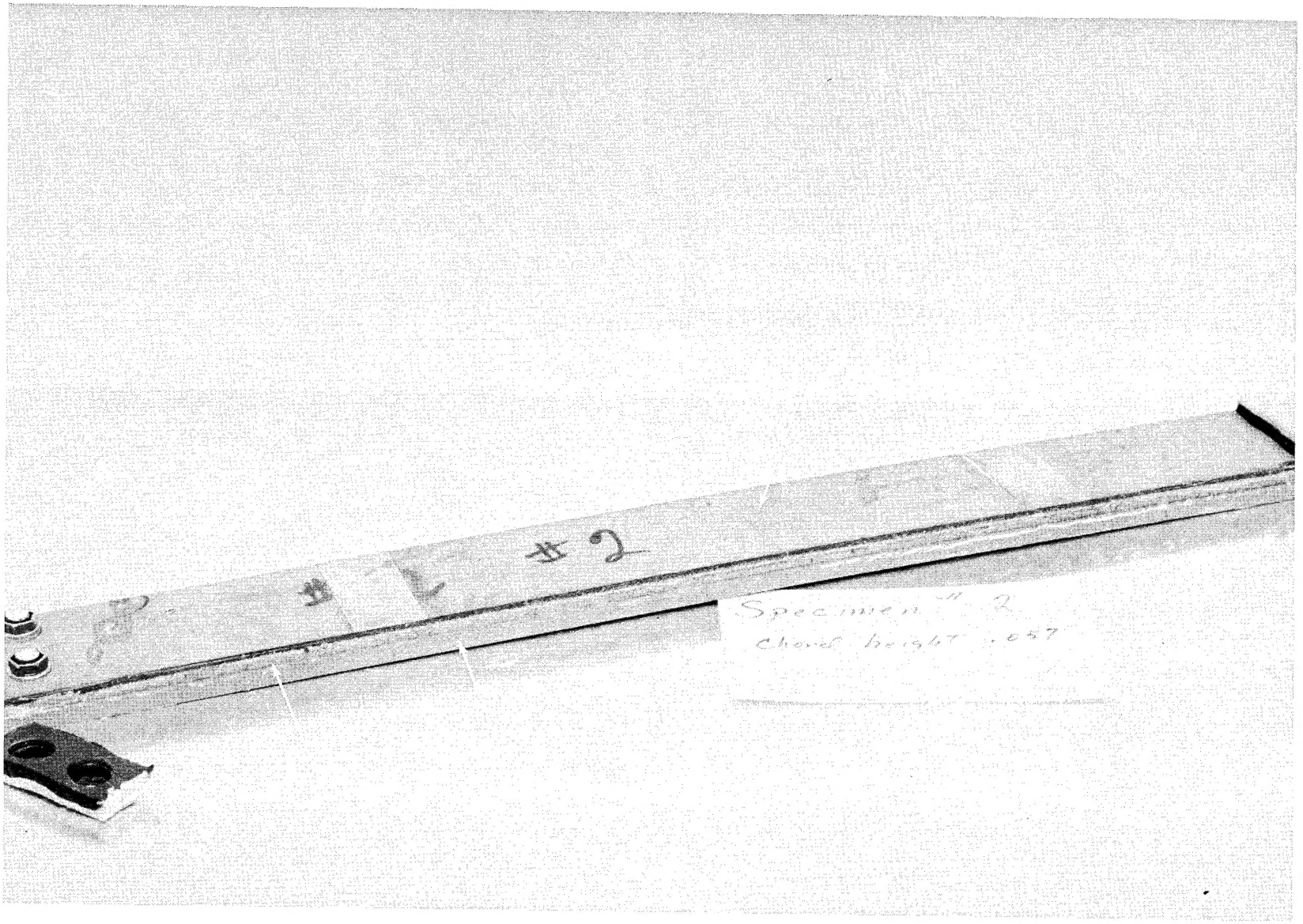

FIGURE 50.—COMPLETED SPECIMEN PRODUCED BY METHOD 9

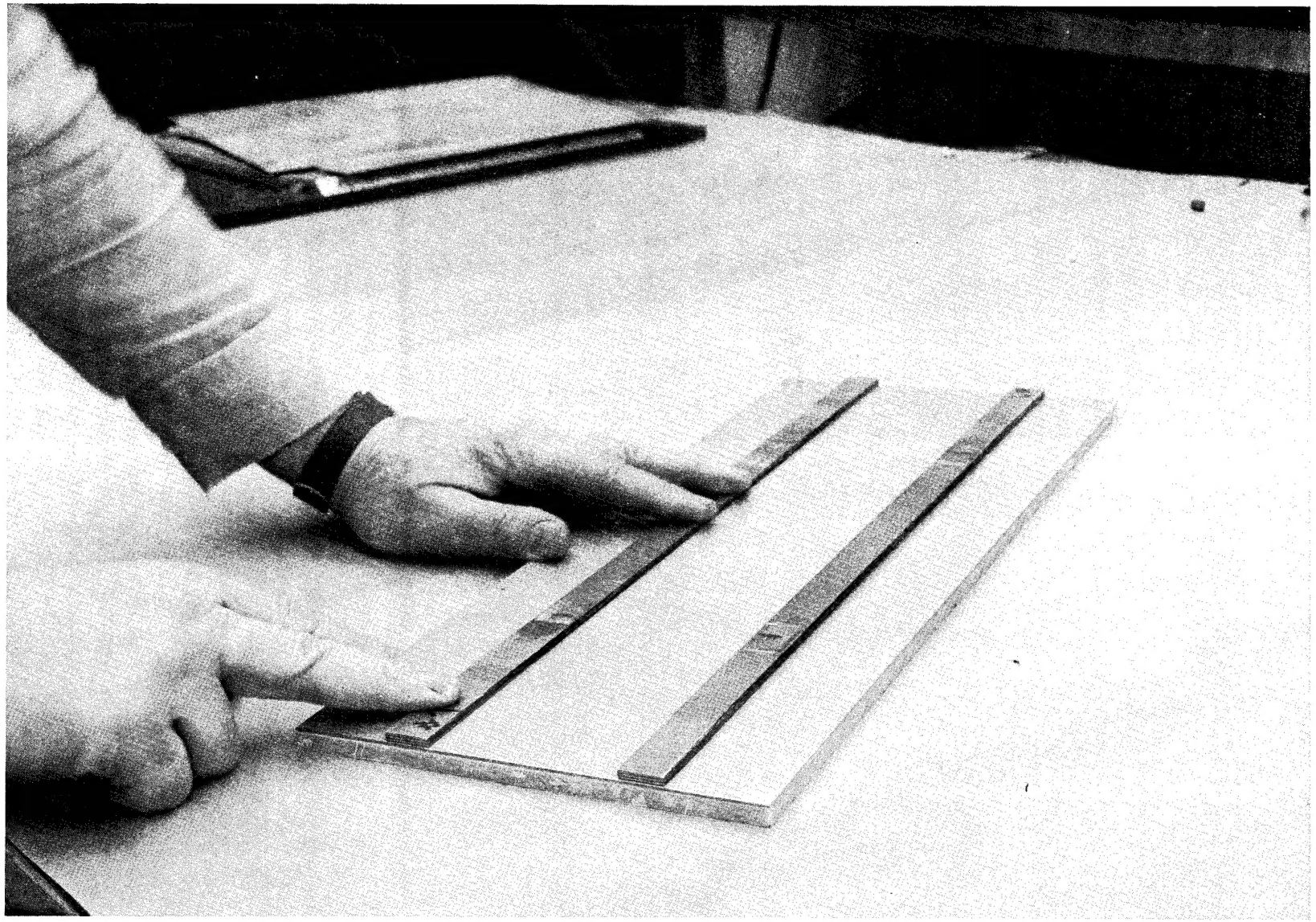

FIGURE 51.—ASSEMBLING STRAP REINFORCED SHEET BY METHOD 9

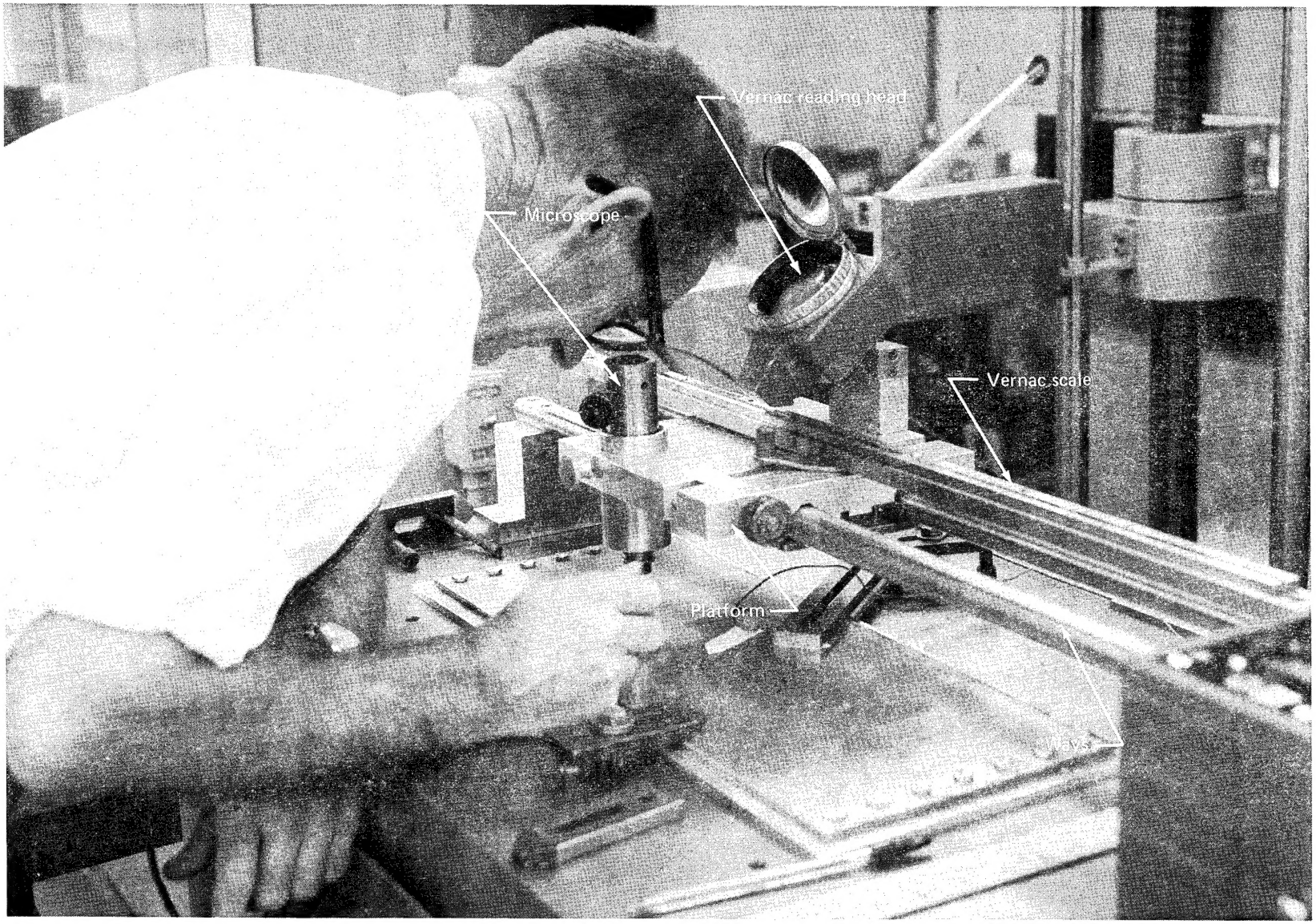

FIGURE 52.—MEASURING EQUIPMENT

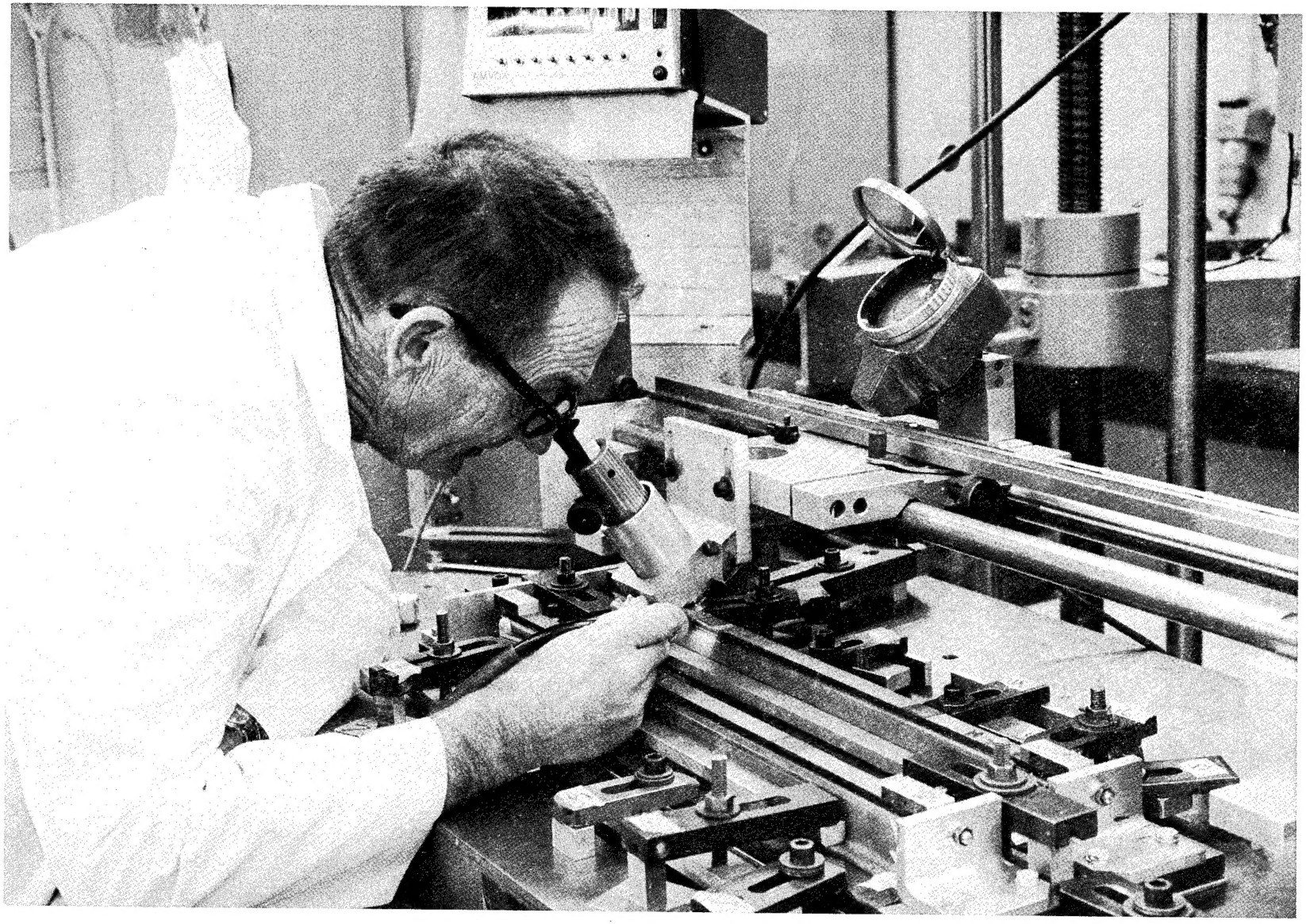

FIGURE 53.–CLAMPING FIXTURES REQUIRED FOR MEASUREMENT